ABSTRACT

Title of Dissertation:	MECHANISTIC STUDIES OF PHOTOCHEMICAL REACTIONS: PHOTOACID GENERATORS, PHOTORELEASEABLE PROTECTING GROUPS, AND DIARYLNITRENIUM IONS
	Andrea Nicole Zeppuhar, Doctor of Philosophy, 2021
Dissertation directed by:	Professor Daniel E. Falvey Department of Chemistry and Biochemistry

The use of light to drive chemical reactions is becoming increasingly popular due to the enhanced spatial and temporal control provided. Because of this, it is important to understand how these photochemical transformations occur from a mechanistic viewpoint in order to aid in the improvement of existing systems as well as in the development of new systems. The work presented in this dissertation will examine the mechanisms of several photochemical systems including photoacid generators, photoreleaseable protecting groups, and diarylnitrenium ions.

Chapter 1 will begin with an introduction to organic photochemistry and describe some of the excited state reactions that will be encountered throughout this text. It will also describe laser flash photolysis, a technique critical to studying the reactive intermediates generated in photochemical reactions. Chapter 2 will describe the design and synthesis of photoacid generators that are activated via sequential two-

photon absorption. The experiments conducted support a mechanism involving triplet re-excitation providing a more favorable bond scission. Chapter 3 will explore the applications of these newly developed photoacid generators, specifically for photopolymerization. It is shown that these compounds are capable of initiating both cationic and radical polymerizations depending on the intensity of visible light irradiation used. Chapter 4 will examine the 9-phenyl-9-tritylone photoreleaseable protecting group for alcohols to understand the details of its release mechanism. It is shown that the tritylone anion radical is required for alcohol photorelease. Chapters 5 and 6 will explore the behavior of diarylnitrenium ions in aqueous media. Chapter 5 will examine the reactivity of diarylnitrenium ions toward guanosine and it is shown that there is a rapid reaction to generate the C8 adduct, suggesting potential carcinogenicity. Chapter 6 will examine the reactivity of diarylnitrenium ions under acidic aqueous conditions. Under these conditions, a long-lived species is formed, and the experiments conducted indicate this species is the cation radical derived from the diarylnitrenium ion. Mechanistic analysis supports formation via a pathway separate from the nitrenium ion, suggestive of a triplet mechanism.

MECHANISTIC STUDIES OF PHOTOCHEMICAL REACTIONS: PHOTOACID GENERATORS, PHOTORELEASEABLE PROTECTING GROUPS, AND DIARYLNITRENIUM IONS

by

Andrea Nicole Zeppuhar

Dissertation submitted to the Faculty of the Graduate School of the
University of Maryland, College Park, in partial fulfillment
of the requirements for the degree of
Doctor of Philosophy
2021

Advisory Committee:
Professor Daniel Falvey, Chair
Professor Neil Blough
Professor Jeffery Davis
Professor Osvaldo Gutierrez
Professor Srinivasa Raghavan, Dean's Representative

Dedication

This dissertation is dedicated to my parents, who always remind me how proud they are of me. Thank you for your endless support.

Acknowledgements

First and foremost, none of this work would have been possible without the guidance of my advisor, Dr. Falvey. I am grateful for the knowledge that he shared with me. Even when I encountered struggles in my research, Dr. Falvey never made me feel discouraged and that gave me the confidence to push forward.

I would like to thank my committee members, Dr. Davis, Dr. Gutierrez, Dr. Blough, and Dr. Raghavan for their time and support. I am also grateful to the many faculty members who have mentored me as a teaching assistant including Dr. Falvey, Dr. DeShong, Dr. Davis, Dr. Gutierrez, Dr. Montague-Smith, Dr. Friedman, and Dr. Koppel.

Thank you to the analytical facilities staff including Dr. Fu Chen and Dr. Yinde Wang for training me to use the NMR instruments and maintaining the facility as well as Dr. Yue Li for help with mass spectrometry experiments.

Thank you to all my colleagues, past and present, in the department and especially the Falvey group members including Dr. Derek Denning, Dr. Steven Wolf, Dr. Matthew Thum, Donald Hong, and Edward Chinn. Thank you for all your help, feedback, and ideas throughout the years. I would also like to thank Abbie Svoysky, my undergraduate student, for letting me share my knowledge and for teaching me how to be a good mentor.

Finally, I would like to thank my friends, inside and outside the department, and my family for all the help, support, and encouragement throughout the years.

Table of Contents

List of Tables

List of Figures

Chapter 1: Organic Photochemistry

Chapter 2: Photoacid Generators Activated Through Sequential Two-Photon Excitation

List of Schemes

Chapter 1: Organic Photochemistry

Chapter 2: Photoacid Generators Activated Through Sequential Two-Photon Excitation

Chapter 3: Lamp vs. Laser: Visible Light Mediated Photopolymerizations with 1-tosyloxy-2-methoxy-9,10-anthraquinone

List of Abbreviations

B3LYP	Becke, three-parameter, Lee-Yang-Parr functional
BDE	Bond dissociation energy
CL	Caprolactone
CPADB	4-cyanopentanoic acid dithiobenzoate
CTA	Chain transfer agent
CW	Continuous wave
DCM	Dichloromethane
DFT	Density functional theory
dG	2'-deoxyguanosine
dGMP	2'-deoxyguanosine monophosphate
DMA	*N*,*N*-dimethylaniline
DMB	1,4-dimethoxybenzene
DMF	Dimethylformamide
DMSO	Dimethyl sulfoxide
DNA	Deoxyribonucleic acid
E_{00}	Excited state energy
E_{red}	Reduction potential
E_{ox}	Oxidation potential
ESI-TOF	Electrospray ionization time of flight
EVE	Ethyl vinyl ether
FID	Flame ionization detector
GC	Gas chromatography
GPC	Gel permeation chromatography
HEMA	2-hydroxyethyl methacrylate
ISC	Intersystem crossing
LFP	Laser flash photolysis
M06-2X	Minnesota 06 functional
MN12-SX	Minnesota 12 functional
MeCN	Acetonitrile
MeOH	Methanol
MMA	Methyl methacrylate
NaOH	Sodium hydroxide
NMR	Nuclear magnetic resonance
OD	Optical density
PAG	Photoacid generator
PDI	Polydispersity index
PET	Photoinduced electron transfer
PMT	Photomultiplier tube
PRPG	Photoreleaseable protecting group
PTO	9-Phenyl-9-tritylone
RAFT	Reversible addition-fragmentation chain transfer
ROP	Ring opening polymerization
RT	Room temperature
s-TPA	Sequential two-photon absorption

TEMPO	2,2,6,6-tetramethylpiperidine-1-oxyl
TfOH	Triflic acid
THF	Tetrahydrofuran
TMB	1,3,5-trimethoxybenzene
p-TsOH	*para*-toluenesulfonic acid
TD-DFT	Time-dependent density functional theory
UV	Ultraviolet
Vis	Visible
VL	Valerolactone

Chapter 1: Organic Photochemistry

1.1 Introduction to Organic Photochemistry

Photochemistry is a branch of chemistry associated with reactions initiated by the absorption of light. Contrary to thermal reactions where activation barriers are overcome through heating, photochemical reactions overcome these barriers using energy provided by light. This allows reactions to occur at ambient temperature on reasonable timescales. Photochemistry is becoming increasingly popular in areas including organic synthesis,[1-6] nanofabrication,[7-9] and photodynamic therapy.[10, 11] The use of light to drive chemical reactions is of considerable interest as it is considered a "green" resource and it reduces the necessity of other reagents which aids in reduction of by-products as well as providing simple work-up procedures.[12] Another attractive feature of photochemical reactions is the energy supplied by photons can only be accepted by molecules capable of absorbing the light, contrary to thermal reactions where the energy supplied by heat is distributed throughout the reaction mixture. This provides more spatial and temporal control over which reaction pathways can be activated, thus reducing unwanted side reactions.[13] In addition, reactive intermediates generated in photochemical transformations can be detected utilizing techniques such as transient absorption spectroscopy which substantially aids in the elucidation of reaction mechanisms. This text will focus on the generation of reactive intermediates in solution in order to elucidate the mechanisms of a variety of photochemical reactions. Mechanistic studies will be performed utilizing tools including nanosecond

transient absorption spectroscopy, photoproduct analysis, chemical yield determination, and computational analysis.

1.2 Excited State Reactions

In order for a photochemical reaction to occur, the molecule must absorb at the wavelength selected for irradiation. Upon absorption of a photon, an electron is promoted from an occupied molecular orbital to an unoccupied molecular orbital, generating an excited state molecule. Once in its excited state, the molecule can follow many pathways that lead to either a return to its ground state or to a chemical reaction. Radiative and non-radiative decay routes back to ground state are shown in the Jablonski diagram in Figure 1.1. Upon excitation, spin of the promoted electron is conserved, and the molecule is excited to a singlet state (S_n). In solution, non-radiative vibrational cooling rapidly relaxes the molecule to its first excited singlet state (S_1), typically on the timescale of 10^{-13} to 10^{-12} seconds. From S_1, several processes can occur. The excited molecule can undergo non-radiative decay in which the excess energy is dissipated in the form of heat to the solvent. Alternatively, it can undergo fluorescence (F), a form of radiative decay in which a lower energy photon is emitted. This process occurs on the timescale of 10^{-9} to 10^{-7} seconds. Another process that can occur from S_1 is intersystem crossing (ISC) in which the electron undergoes a spin flip, forming a lower energy triplet state (T_1). Relaxation to the ground state from T_1 occurs through either non-radiative decay or via radiative decay referred to as phosphorescence (P) which occurs on the timescale of 10^{-6} to 10^{-3} seconds.[14, 15]

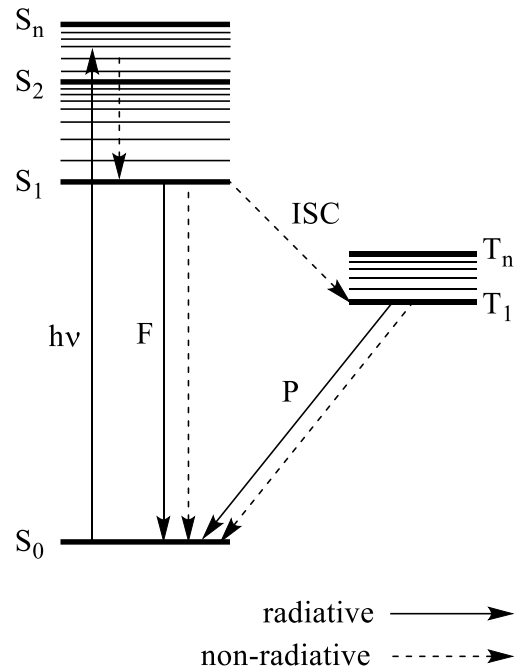

Figure 1.1. Jablonski diagram

When excited state reactions occur, the majority occur from the lowest excited state (S_1 or T_1) due to the extremely short lifetimes of the upper excited states. Some examples of excited state reactions include bond breaking, energy transfer, electron transfer, and hydrogen atom transfer.

Photoinduced energy transfer, described in Figure 1.2, is a transfer of excited state energy where an excited state donor molecule (D*) interacts with a ground state acceptor molecule (A). An electron exchange between the two species occurs, conserving spin, and this results in a transfer of excited state energy resulting in a ground state donor molecule (D) and an excited state acceptor molecule (A*). This process most commonly occurs via the triplet state of D and, since electron spin remains conserved, will produce the triplet state of A.

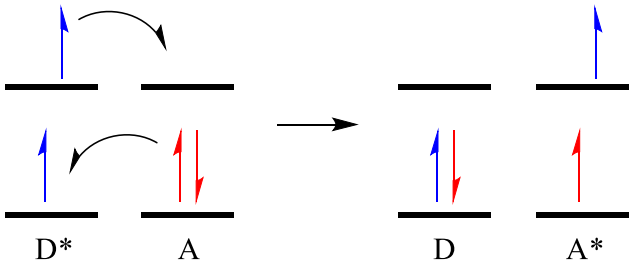

Figure 1.2. Simplified energy diagram describing photoinduced energy transfer

Photoinduced electron transfer (PET), described in Figure 1.3, is the transfer of a single electron to result in ion radical pairs and this can occur in two different ways. As Figure 1.3 (A) shows, an excited state donor can transfer an electron to a ground state acceptor. Alternatively, as described in Figure 1.3 (B), a ground state donor can transfer an electron to an excited state acceptor. Both cases result in oxidation of the donor to form a cation radical and reduction of the acceptor to form an anion radical.

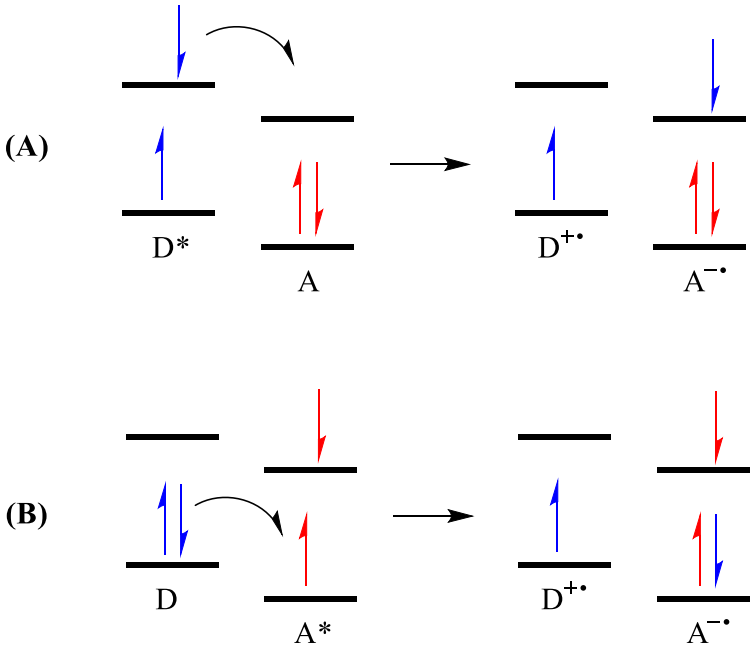

Figure 1.3. Simplified energy diagrams describing photoinduced electron transfer pathways. (A) electron transfer from an excited state donor to a ground state acceptor; (B) electron transfer from a ground state donor to an excited state acceptor

Based upon the work of Rehm and Weller,[16, 17] the feasibility of PET occurring can be predicted using Equation 1.

$$\Delta G_{PET} = 23.061 \frac{kcal}{V\ mol}(E_{ox} - E_{red}) - E_{00} - \omega \qquad \textbf{(1)}$$

The thermodynamics depends on the oxidation potential of the donor (E_{ox}) and the reduction potential of the acceptor (E_{red}), both measured in volts. In addition, it is also dependent on the excited state energy of the species being excited (E_{00}), measured in kcal/mol. Finally, there is a correction for the influence of the solvent (ω) however in polar solvents such as methanol and acetonitrile, this term is negligible.

Another common photochemical process observed, especially in carbonyl compounds, is hydrogen atom transfer. This occurs when an excited state carbonyl compound abstracts a hydrogen atom from a suitable donor.[14, 15] An example of this process is shown in Scheme 1.1 with benzophenone. The first excited triplet state of benzophenone is typically represented as a diradical. This diradical can abstract a hydrogen atom to form a ketyl radical which can undergo additional secondary reactions.[18]

Scheme 1.1. Hydrogen atom transfer to the first excited triplet state of benzophenone

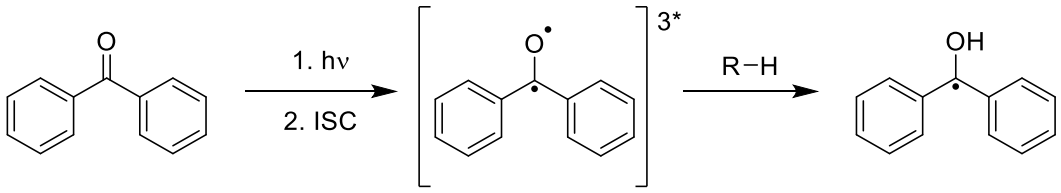

1.3 Laser Flash Photolysis

As mentioned in Section 1.1, transient absorption spectroscopy, also referred to as laser flash photolysis (LFP), is paramount when it comes to elucidating the mechanisms of photochemical reactions and will be used extensively throughout this

text. LFP is a time-resolved spectroscopic technique that allows for identification and characterization of short-lived, reactive intermediates such as excited states, ions, radicals, and radical ions.

The laser setup used to acquire LFP data is shown in Figure 1.4. The excitation source is a neodymium-doped yttrium aluminum garnet (Nd:$Y_3Al_5O_{12}$, Nd:YAG) laser which is capable of emitting light at 1064 nm, 532 nm, 355 nm, and 266 nm and has a pulse duration of 4-6 nanoseconds. Before reaching the sample, the light from the laser is passed through a cylindrical lens to evenly distribute the light across the sample. The probe beam used is a 350 W xenon-arc lamp and this provides a continuous broad spectrum of light and is used to generate the absorption spectrum of the transient species. The laser and the probe beam are positioned perpendicular to each other to minimize light scattering from the laser to the monochromator. A shutter is positioned in front of the probe beam and is in sync with the laser pulses in order to minimize excess light exposure to the sample. The probe beam is focused through two lenses before reaching the monochromator. After passing through the monochromator, the light reaches a photomultiplier tube (PMT) which amplifies the signal which is then measured using an oscilloscope. The raw signal measured by the oscilloscope is converted to a change in optical density (ΔOD) by computer software. A positive ΔOD indicates the transient species has a greater absorbance than the ground state species being excited and a negative ΔOD indicates a decrease in absorbance relative to the ground state species. The ΔOD at a given wavelength can be measured as a function of time to produce a kinetic trace. The kinetic traces can be collected at multiple wavelengths and, when combined, generate a transient absorption spectrum. The

experimental spectrum can be compared with those found in literature and/or calculated by time-dependent density functional theory (TD-DFT) to determine the identity of the transient species. The reactivity of the transient species can be studied by monitoring the spectral changes upon addition of oxygen, nucleophiles, electron donors/acceptors, and other quenchers.

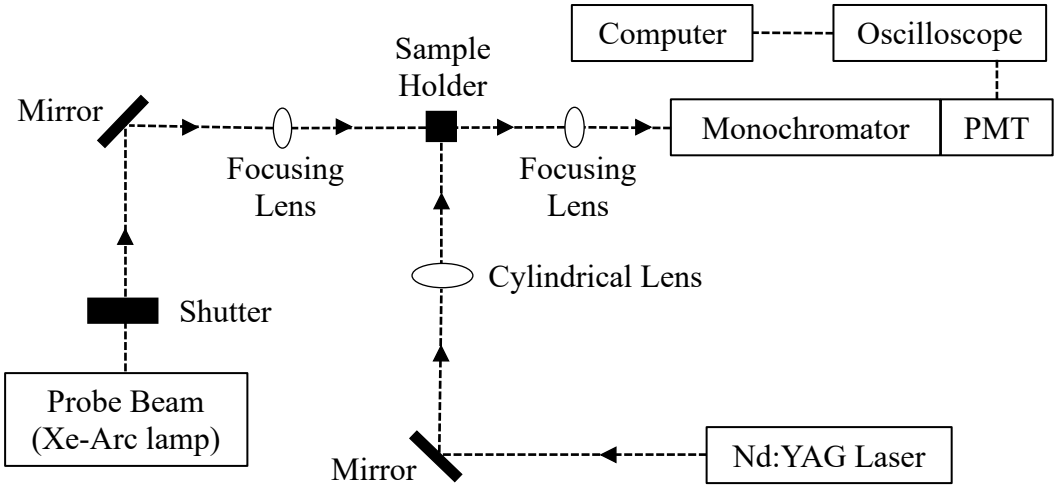

Figure 1.4. Block diagram of the laser flash photolysis apparatus

Chapter 2: Photoacid Generators Activated Through Sequential Two-Photon Absorption

The majority of the work in this chapter has been published:[19]

Zeppuhar, A. N.; Wolf, S. M.; Falvey, D. E., Photoacid Generators Activated through Sequential Two-Photon Excitation: 1-Sulfonatoxy-2-alkoxyanthraquinone Derivatives. *The Journal of Physical Chemistry A* **2021,** *125* (24), 5227-5236

2.1 Photoacid Generators

Photoacid generators (PAGs) are compounds that, upon irradiation, undergo reactions or dissociations which generate acid as one of the photoproducts.[20] PAGs find applications in areas such as biological probing,[21] photodynamic therapy,[22, 23] and polymerization initiation.[24-26]

PAGs are divided into two classes: ionic and non-ionic. The most common ionic PAGs are derivatives of onium salts,[27] such as diarylhalonium salts[24, 28, 29] and sulfonium salts,[25, 30, 31] which include an anionic counterion. Generally, the cationic onium moiety is the photochemically activatable species while the anion determines the strength of the acid formed. Due to increasing interest for polymerization initiation, attention is becoming drawn away from ionic PAGs due to their limited solubility in monomer mixtures. In recent years, non-ionic PAGs have become more popular as they have higher solubility in a broad range of monomers.[32] Non-ionic PAGs are most commonly derivatives of aryl sulfonate esters,[33-36] iminosulfonates,[37] imidosulfonates,[38-40] and spiropyrans.[41] Of increasing interest are PAGs that can be activated via two-photon absorption.

2.2 Two-Photon Absorption

In recent years, photochemical systems have been developed to utilize two-photon absorption. In contrast to a conventional one-photon absorption process, two-photon absorption processes possess a quadratic dependence on the reaction rate with respect to light intensity which provides enhanced spatial control.[42, 43] Two-photon absorption processes find applications in areas including photolithography,[7, 44-46] optical storage,[47, 48] and photodynamic therapy.[49, 50]

Two-photon absorption processes can be divided into two categories: simultaneous and stepwise. In a simultaneous process, two photons, which individually lack the energy required to populate the targeted excited state, are absorbed simultaneously by the substrate producing an excited state via a virtual state. This allows for the use of low energy photons to promote photochemical reactions that would otherwise require high energy, UV photons. However, achievement of simultaneous two-photon absorption requires the use of expensive femtosecond lasers. To reduce the expenses associated with simultaneous two-photon absorption, many groups are exploring two-photon processes in which the two photons are absorbed in a stepwise manner.[51-55]

In a stepwise, two-photon absorption (s-TPA) process, the second photon is absorbed by a photogenerated transient state. As Scheme 2.1 describes, initial excitation of a substrate (S) will lead to generation of a reversibly formed intermediate (I). This intermediate either reverts back to S or it can absorb a second photon to undergo a reaction or dissociation generating the product of interest (P).

Scheme 2.1. Idealized scheme of a stepwise, two-photon process

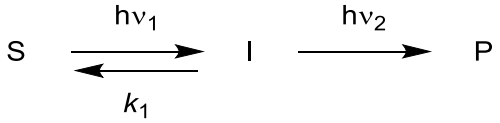

The intermediate species in this scheme could be an excited singlet state (S_1), an excited triplet state (T_1), or a reversibly formed photoisomer of the substrate. The probability of the intermediate absorbing a second photon is dependent on both its lifetime as well as the nature of the light source used. If the intermediate lives for microseconds to milliseconds, then s-TPA can occur using nanosecond lasers or less expensive continuous wave (CW) lasers.[43]

This chapter will discuss the design and synthesis of non-ionic, sulfonate ester PAGs that can be activated via s-TPA. Because of the enhanced spatial control provided by s-TPA, this type of PAG would be beneficial in improving resolution in the field of photolithography.

2.3 Design of Two-Photon Absorbing Photoacid Generators

An example of a sequential two-photon photoacid generating system to generate sulfonic acid was reported by Turro and coworkers[54] in 2008, and is outlined in Scheme 2.2. In this system, the first photon activates a latent photosensitizer which a dimer of the active sensitizer, 2-methoxynaphthalene. The active sensitizer absorbs a second photon, exciting it to its singlet state. The latter then undergoes electron transfer to a photochemically inactive acid generator causing an acid generating reaction.

Scheme 2.2. Sequential two-photon photoacid generation developed by Turro and coworkers[54]

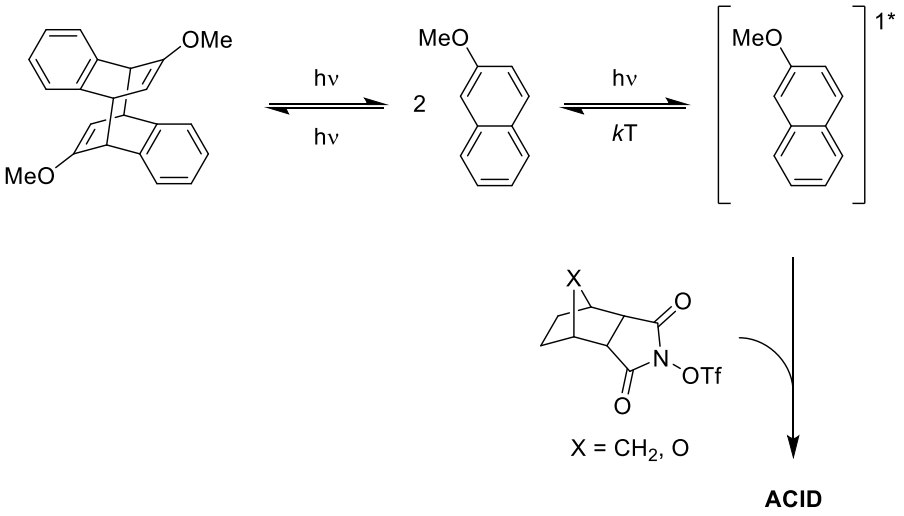

The drawback to this system is that the sensitizer and acid generating species are separate molecules which adds complexity to the system, and it requires an intermolecular reaction to occur with a molecule in its excited singlet state. The aim of this chapter is to design a s-TPA PAG in which the chromophore is covalently linked to the acid generating species. For this, aryl sulfonate esters based upon the anthraquinone chromophore were investigated, specifically 1-tosyloxy-2-methoxy-9,10-anthraquinone **2.1a** and 1-(trifluoromethylsulfonoxy)-2-methoxy-9,10-anthraquinone **2.1b**, which are expected to generate *p*-toluenesulfonic acid (*p*-TsOH) and triflic acid (TfOH), respectively (Figure 2.1).

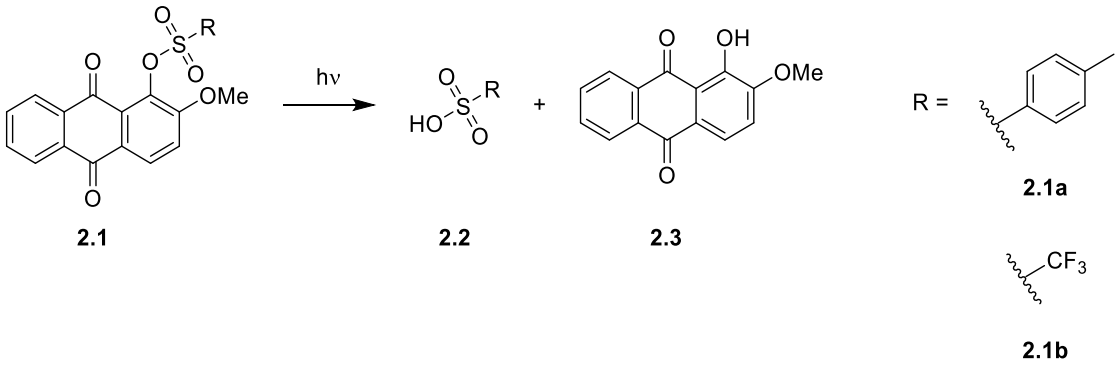

Figure 2.1. Photoacid generators studied in this chapter. Photolysis of **2.1a** and **2.1b** will generate *p*-TsOH and TfOH, respectively

Previous studies have demonstrated that aryl sulfonate esters can generate sulfonic acids via a 1-photon photohomolytic pathway.[34, 36] However, the desired bond scission was achieved via high energy excited states which required the use of high energy, low wavelength UV excitation, as described in Scheme 2.3. In addition, photo-Fries rearrangement products were observed thus reducing the yield of acid generated. These rearrangement products are believed to arise via the excited singlet state.

Scheme 2.3. Mechanism of 1-photon photoacid generation from aryl sulfonate esters

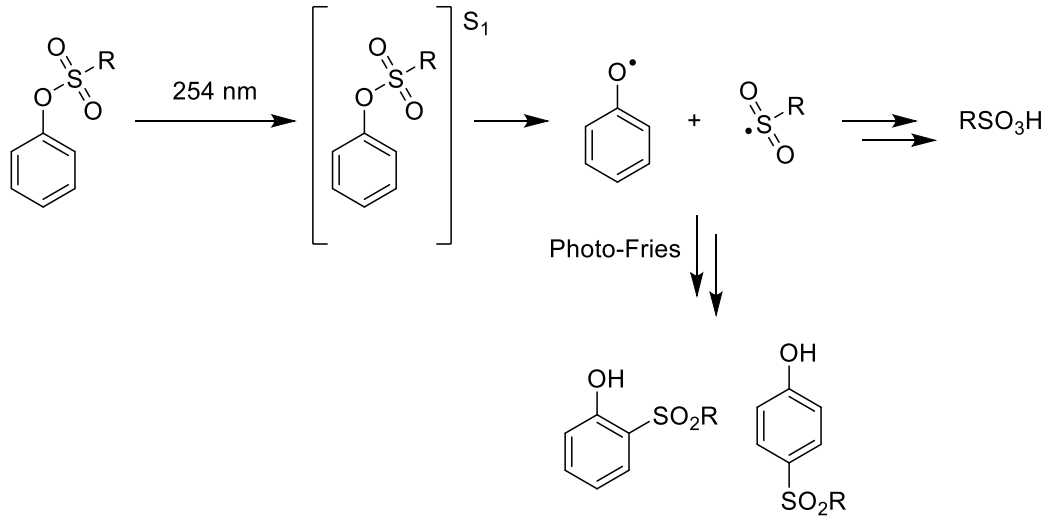

The use of anthraquinone derivatives should allow photoacid generation via lower energy photons and also allow for s-TPA. Anthraquinone derivatives absorb in

the high wavelength UV to low wavelength visible region, depending on substitution. In addition, many derivatives intersystem cross with high efficiency to generate their lower energy triplet state, T_1.[56, 57] Scheme 2.4 outlines the proposed pathway for two-photon photoacid generation from anthraquinone sulfonate ester derivatives. The hypothesis is that T_1 of the anthraquinone sulfonate esters would not possess sufficient energy for efficient S—O bond homolysis and that T_1 would possess sufficient lifetime and visible light absorption that would allow for re-excitation to a higher energy triplet state where bond scission would become more favorable.

Scheme 2.4. Proposed mechanism of two-photon photoacid generation from anthraquinone sulfonate esters

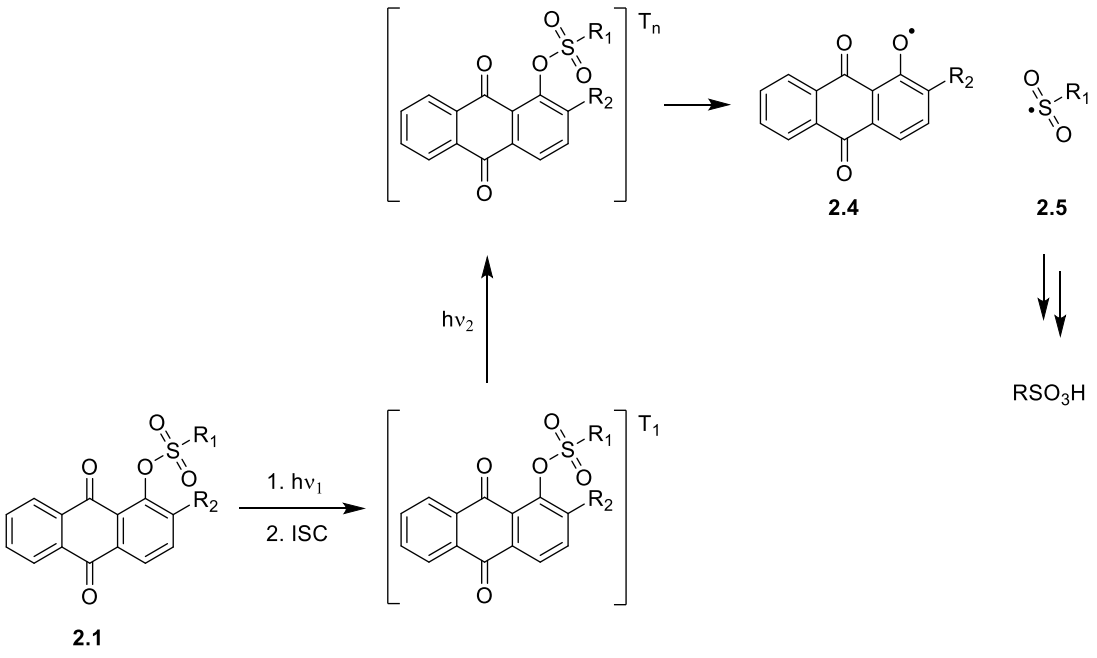

2.4 DFT Calculations

In order for s-TPA to be achieved, the substrate must possess a bond dissociation energy (BDE) that is higher than, or nearly equal to, T_1. However, if the BDE is too high, dissociation may not occur even upon re-excitation. In order to assess

the feasibility of **2.1a** and **2.1b** as two-photon PAGs, density functional theory (DFT) calculations were carried out to determine the energy of T_1, the BDE for S—O homolysis, and the barriers for bond homolysis. These results are summarized in Figure 2.2.

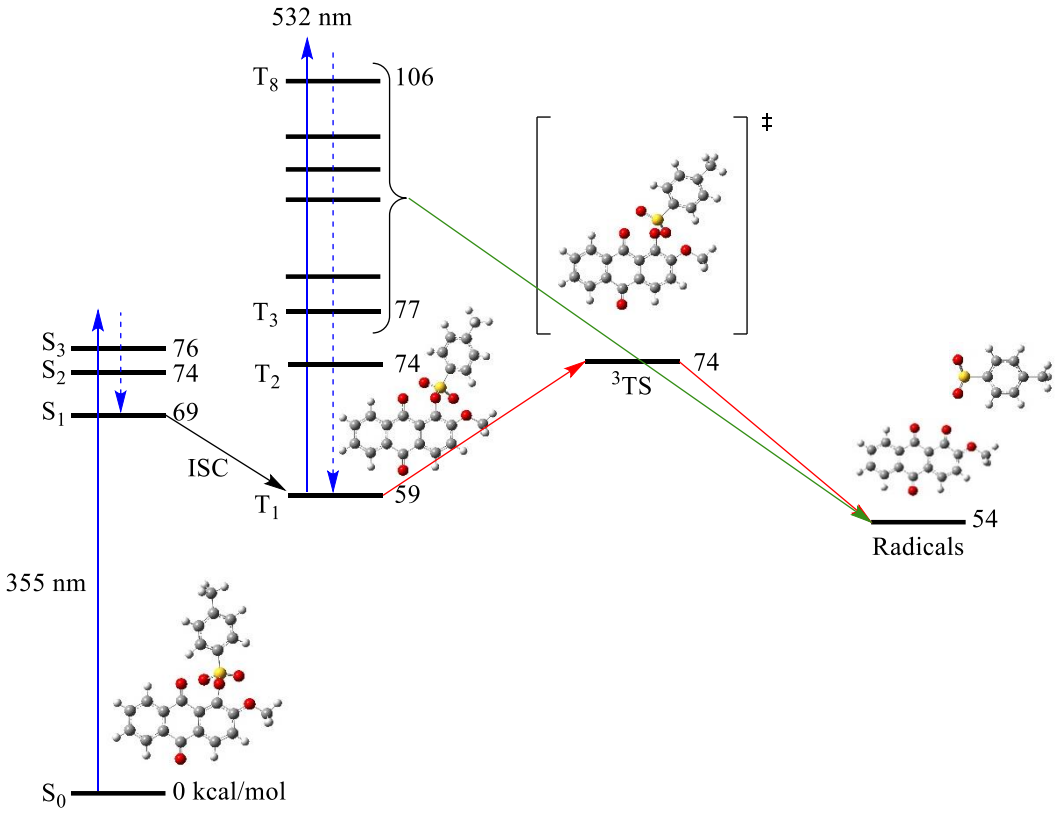

Figure 2.2. Energy level diagram for photolysis of **2.1a**. Energies of T_1, the transition state (TS), and the radical pair are derived from DFT calculations. Higher excited singlet and triplet states are vertical excitation energies derived from TD-DFT calculations. Calculations performed on **2.1b** provided similar results

The energy of T_1 was calculated by optimizing the geometries of the ground state (S_0) and T_1 for **2.1a** at the (u)B3LYP/6-311G(d) level and single point energies were calculated using (u)M06-2X/6-311G(2d, 3p). This combination of functional and basis set was shown to give good agreement for singlet-triplet energy gaps in similar

systems where experimental data was available. The calculations predict that T_1 lies 59 kcal/mol above the ground state.

To determine the BDE, the geometry for S_0 for **2.1a** optimized at the (u)B3LYP/6-311G(d) level was used and the single point energy was calculated using (u)MN12-SX/6-311G(3d). Similar calculations were performed on the presumed radical products, the anthraquinone based radical **2.4** and the sulfonyl radical **2.5a**. These calculations predict a BDE of 54 kcal/mol. This value is reasonably consistent with experimental values of similar systems. For example, HO—SO_2CH_3 has a BDE of 87 kcal/mol.[58] Due to the increased steric strain of the reactant **2.1a** and the additional resonance stabilization of the anthraquinone based radical **2.4**, 54 kcal/mol is a plausible estimate.

The triplet energy and BDE calculations predict that S—O bond dissociation from T_1 is weakly exothermic which indicates bond scission could occur from T_1 without re-excitation. To further determine the possibility of bond scission from T_1, the transition state for dissociation was located on the B3LYP surface and its energy was calculated at the MN12-SX level. The calculations predict that this barrier lies 14 kcal/mol above T_1 and thus is unlikely to be kinetically feasible without re-excitation. The calculations carried out on **2.1b** provided similar results.

2.5 Sequential Two-Photon Absorption Experiments

A solution of PAG **2.1a** in CD_3CN was photolyzed using pulsed (10 Hz, 10 ns) 355 nm irradiation at varying intensities and formation of *p*-TsOH was monitored via ^{1}H NMR as displayed in Figure 2.3. For a s-TPA process, the yield should be dependent on both the total dose of light applied and the intensity whereas a one-photon process

would depend on the dose but be independent of the intensity. When **2.1a** is photolyzed for 6.67 minutes at 15 mJ/pulse, 79% of the substrate is converted and 48% yield of *p*-TsOH is generated. When an identical solution is photolyzed for 20 minutes at 5 mJ/pulse, which provides a constant dose at a lower intensity, only 53% of the substrate is converted with 15% yield of *p*-TsOH.

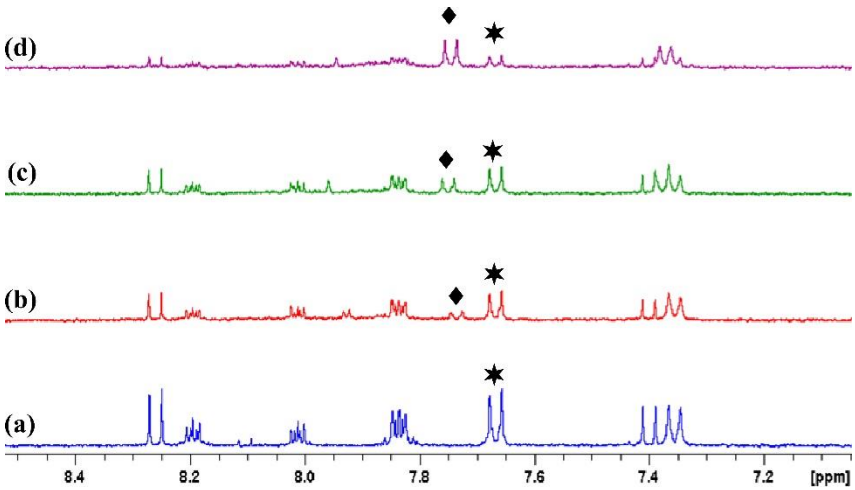

Figure 2.3. ^{1}H NMR monitoring formation of *p*-TsOH (♦) during the 355 nm pulsed photolysis of **2.1a** (✶) with constant dose of irradiation but varying power. (a) **2.1a**, no photolysis; (b) 20 mins of irradiation at 5 mJ/pulse; (c) 10 mins of irradiation at 10 mJ/pulse; (d) 6.67 mins of irradiation at 15 mJ/pulse

Another method of analyzing the effect of intensity on photolysis rates is done by varying the area of irradiation. For this, samples of **2.1a** in CD_3CN were photolyzed with pulsed 355 nm irradiation with a constant dose but the intensity was varied by using a focused (2.08×10^{9} mW cm^{-2}) or an unfocused (1.14×10^{9} mW cm^{-2}) laser beam. As displayed in Table 2.1, irradiating the sample with a focused laser beam significantly increases substrate conversion as well as the yield of *p*-TsOH.

Table 2.1. Pulsed 355 nm photolysis of **2.1a** in CD_3CN with and without defocusing the laser beam

Laser Beam	Photolysis Time (min)	355 Power (mJ/pulse)	% Conversion[a]	% Yield *p*-TsOH[a]
Focused	10	7-9	67	26
Unfocused	10	7-9	39	12

[a] Determined by ^{1}H NMR

Additional evidence for s-TPA is provided from two-color irradiation experiments. The DFT calculations predict that several higher triplet states should be accessible with visible light irradiation of T_1 and possess sufficient energy to overcome the kinetic barrier for S—O homolysis. Therefore, solutions of **2.1a** were photolyzed with the pulsed laser at 355 nm, 532 nm, and both wavelengths simultaneously and these results are summarized in Table 2.2. When comparing Entries 1 & 2, the addition of 532 nm irradiation dramatically increases the rate of conversion of **2.1a** as well as the yield of *p*-TsOH. It should be noted that the ground state of **2.1a** does not absorb at 532 nm and indeed irradiation with 532 nm alone does not result in conversion nor generation of acid (Table 2.2, Entry 3). A control where a sample was not exposed to irradiation (Table 2.2, Entry 4) also resulted in lack of conversion.

Table 2.2. Yields of *p*-TsOH from pulsed photolysis of **2.1a** in CD_3CN with varying wavelengths of irradiation

Entry	Photolysis Time (min)	355 Power (mJ/pulse)	532 Power (mJ/pulse)	% Conversion[a, b]	% Yield *p*-TsOH[a, b]
1	10	8-10	87-89	94 ± 3	77 ± 10
2	10	9-11	0	58 ± 7	34 ± 10
3	10	0	87-90	0	0

4	10	0	0	0	0

[a]Determined by [1]H NMR, [b]Error bars are the result of triplicate experiments

The rate of acid production at low conversions using the different irradiation wavelengths was assessed by comparing the yield of acid as a function of photolysis time and acid generation was assessed using malachite green carbinol base as a pH indicator. In the presence of acid, malachite green carbinol base is converted to malachite green which has a maximum absorption at 618 nm. As displayed in Figure 2.4, addition of 532 nm pulsed irradiation increases the rate of conversion by a factor of 4 relative to 355 nm pulsed irradiation alone.

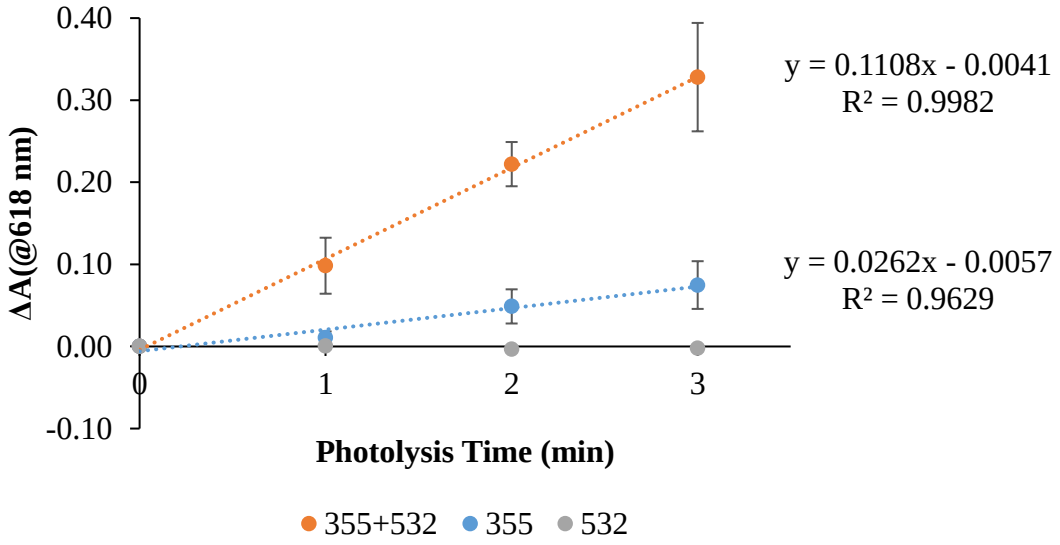

Figure 2.4. Monitoring formation of *p*-TsOH from the pulsed photolysis of **2.1a** in acetonitrile using malachite green carbinol base as a pH indicator. Orange line: 355 nm + 532 nm irradiation. Blue line: 355 nm irradiation. Gray line: 532 nm irradiation. Error bars are the result of triplicate experiments

When the lifetime of the species absorbing the second photon is on the microsecond to millisecond timescale, s-TPA may also be achieved with CW irradiation from diode lasers.[43] To determine the effect of CW irradiation on photoacid generation, acetonitrile solutions of **2.1a** were photolyzed using 447 nm CW irradiation

(**2.1a** has an absorption tail at this wavelength) and the *p*-TsOH generation was monitored using malachite green carbinol base as a pH indicator. The dependence of acid generation on laser intensity was measured at a constant irradiation time. At modest laser powers and substrate conversions, a one-photon process would show a linear dependance whereas a two-photon process should show a quadratic dependence. As displayed in Figure 2.5, the yield of acid as a function of laser power shows a nonlinear dependence that fits to an order of 2.07.

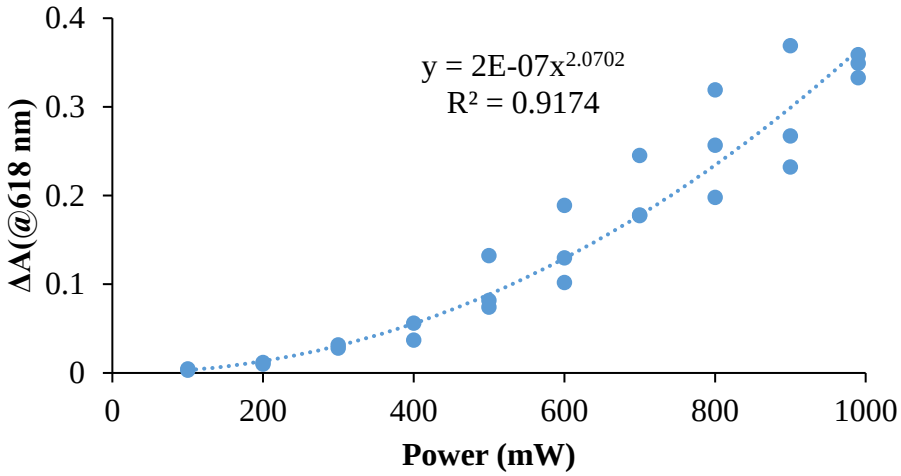

Figure 2.5. Monitoring formation of *p*-TsOH from photolysis of **2.1a** with 447 nm CW irradiation at a fixed irradiation time but with varying power. Formation of *p*-TsOH monitored with malachite green carbinol base pH indicator

In order to generate a stronger sulfonic acid, high intensity photolysis experiments were carried out on the trifluoromethanesulfonyl derivative, **2.1b**, and these results are summarized in Table 2.3.

Table 2.3. Yields of TfOH from pulsed photolysis of **2.1b** in CD_3CN with varying wavelengths of irradiation

Entry	Photolysis Time (min)	355 Power (mJ/pulse)	532 Power (mJ/pulse)	% Conversion[a, b]	% Yield TfOH[a, b]
1	20	8-10	88-91	81 ± 1	10 ± 1
2	20	8-10	0	48 ± 0	21 ± 2
3	20	0	88-91	8	0
4	20	0	0	8	0

[a]Determined by ^{19}F NMR, [b]Error bars are the result of triplicate experiments

In this case, substrate conversion is still enhanced by the addition of 532 nm irradiation however, the yields of the corresponding sulfonic acid (TfOH) are significantly lower. However, this result is consistent with the formation of the trifluoromethanesulfonyl radical **2.5b** which would form via S—O bond homolysis, as predicted in Scheme 2.4. The trifluoromethanesulfonyl radical has been shown to undergo rapid loss of SO_2 and generate the trifluoromethyl radical.[59] These decomposition products can undergo secondary reactions that can lead to an overall stoichiometric excess of acid as outlined in Scheme 2.5. The trifluoromethyl radical can react with oxygen to generate trifluoromethanol which decomposes to generate HF and fluorophosgene. The latter further hydrolyzes into carbon dioxide and two more equivalents of HF. Additionally, the SO_2 expelled from the decomposition can react with water to form sulfurous acid.

Scheme 2.5. Secondary reactions from the decomposition of the trifluoromethanesulfonyl radical **2.5b**

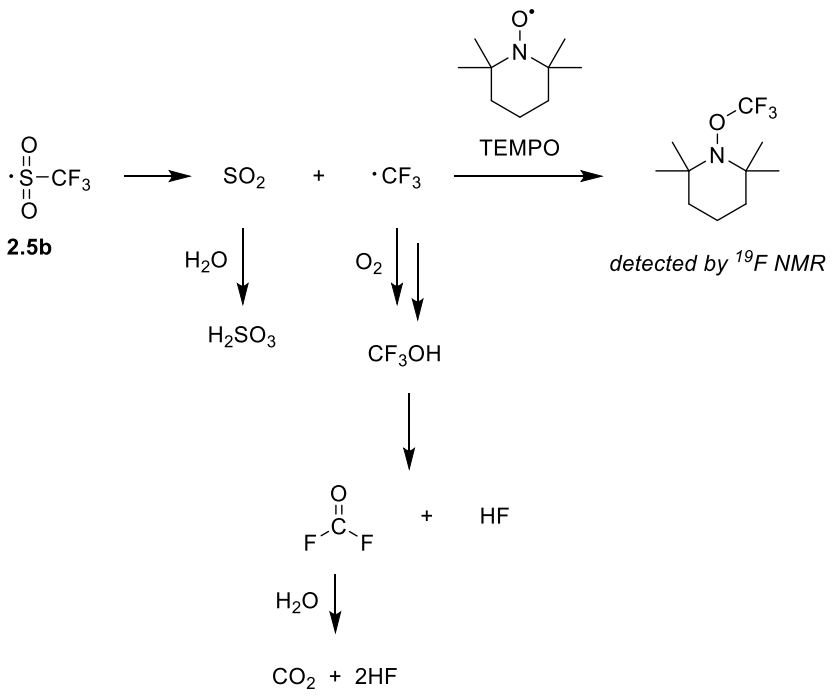

Evidence of these secondary reactions come from total acid determination, fluoride ion analysis, and TEMPO trapping experiments. To determine the total yield of acid generated, solutions of **2.1b** were subjected to high intensity photolysis and the yield of acid was quantified via acid-base titration. As seen in Table 2.4, despite the low yields of TfOH, pulsed photolysis of **2.1b** with 355+532 nm irradiation (Table 2.4, Entry 1) generates more than three equivalents of acid and 355 nm irradiation (Table 2.4, Entry 2) providing less, analogous to the s-TPA behavior of **2.1a**. As expected, irradiation with 532 nm alone (Table 2.4, Entry 3) provides no acid as the ground state of **2.1b** does not absorb at that wavelength.

Table 2.4. Overall yields of acid resulting from the pulsed photolysis of **2.1b** in CH_3CN

Entry	Photolysis Time (min)	355 Power (mJ/pulse)	532 Power (mJ/pulse)	% Yield Acid[a]
1	20	9-10	89-91	332 ± 13
2	20	9-10	0	208 ± 20
3	20	0	89-91	0
4	20	0	0	0

[a]Error bars are the result of triplicate experiments

In order to confirm that much of this yield of acid is from the formation of HF, as predicted in Scheme 2.5, the same pulsed photolysis experiments were performed, and the samples were analyzed using a colorimetric fluoride test. Indeed, combined 355+532 nm irradiation (Table 2.5, Entry 1) provided the highest yield of fluoride and 355 nm alone (Table 2.5, Entry 2) yielding less. There appears to be some intrinsic error in the fluoride test given the nonzero fluoride yields for 532 nm irradiation and the dark control (Table 2.5, Entries 3 & 4), however the results obtained are still consistent with a s-TPA process.

Table 2.5. Yields of F^- resulting from the pulsed photolysis of **2.1b** in CH_3CN

Entry	Photolysis Time (min)	355 Power (mJ/pulse)	532 Power (mJ/pulse)	% Yield F^{-a}
1	20	8-10	86-88	171 ± 16
2	20	8-10	0	66 ± 6
3	20	0	86-88	25
4	20	0	0	23

[a]Error bars are the result of triplicate experiments

Additional support for the pathways described in Scheme 2.5 comes from radical trapping experiments. A solution of **2.1b** and 2,2,6,6-tetramethylpiperidine-1-oxyl (TEMPO) was subjected to pulsed 355 nm irradiation and the TEMPO-CF_3 adduct was detected by its characteristic ^{19}F NMR resonance.[60]

The experiments carried out on the trifluoromethanesulfonyl derivative, **2.1b**, provide evidence of the homolysis mechanism predicted in Scheme 2.4. In order to generate sulfonic acid from the sulfonyl radical **2.5**, the predicted mechanism involves a reaction with oxygen as outlined in Scheme 2.6.

Scheme 2.6. Sulfonic acid generation from O_2 trapping of sulfonyl radical **2.5**

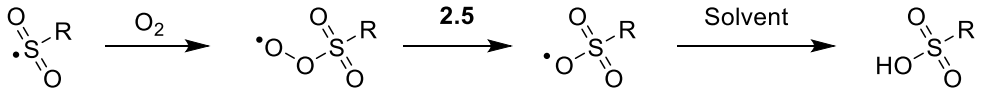

2.5 **2.6** **2.7** **2.2**

As Table 2.6 describes, solutions of **2.1a** in acetonitrile were purged with nitrogen, oxygen, or air-equilibrated and then photolyzed with pulsed 355+532 nm irradiation. All samples resulted in similar photoconversions however, the nitrogen atmosphere suppresses the yield of *p*-TsOH significantly indicating that oxygen is necessary for acid generation.

Table 2.6. Pulsed photolysis of **2.1a** in CD_3CN with varying atmospheres

Atmosphere	Photolysis Time (min)	355 Power (mJ/pulse)	532 Power (mJ/pulse)	% Conversion[a]	% Yield *p*-TsOH[a]
Air	10	8-10	88-90	89	64
Nitrogen	10	8-10	88-90	72	11
Oxygen	10	8-10	88-90	88	63

[a]Determined by ^1H NMR

The reaction of the sulfonyl radical **2.5** with oxygen produces a sulfonyl peroxyl radical **2.6** which can react with another molecule of **2.5** to generate the sulfonyloxy radical **2.7**. The latter abstracts a hydrogen atom, presumably from the solvent, to yield the sulfonic acid product.

2.6 Laser Flash Photolysis Studies

Based upon the results of the experiments conducted thus far, the intermediate that absorbs the second photon is assigned to the triplet state (T_1) of **2.1**. This is further supported by LFP studies. Figures 2.6 and 2.7 display the transient absorption spectra from pulsed 355 nm photolysis of **2.1a** and **2.1b**, respectively, in acetonitrile.

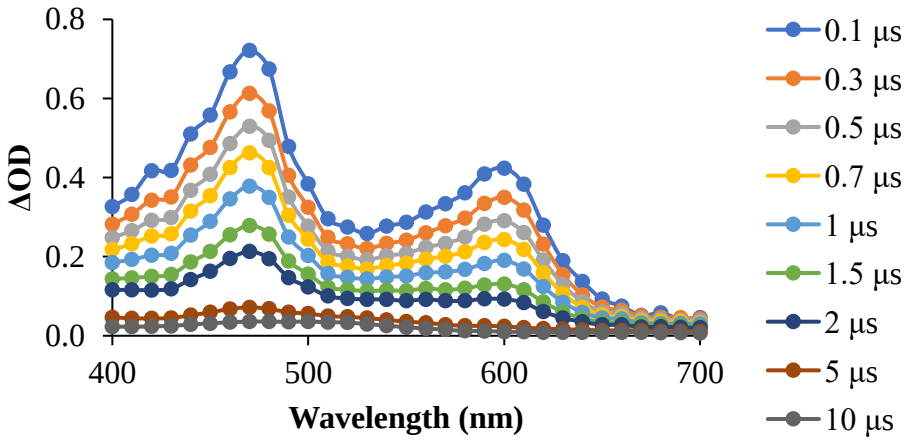

Figure 2.6. Transient absorption spectrum from the 355 nm pulsed photolysis of **2.1a** in acetonitrile

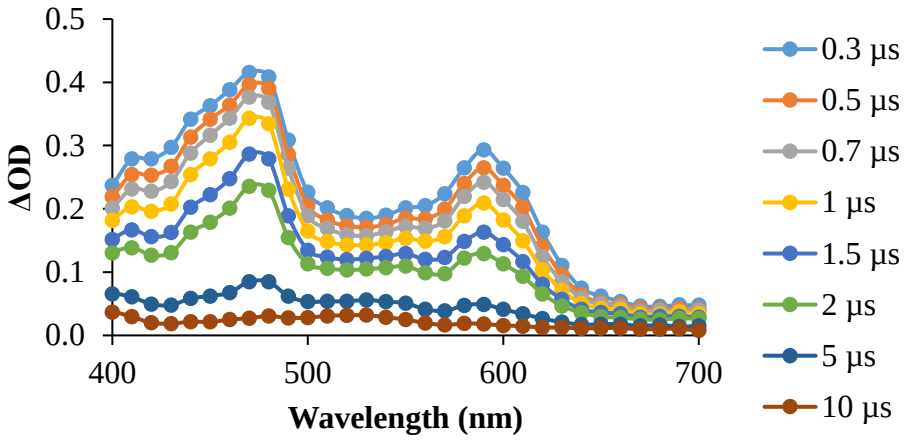

Figure 2.7. Transient absorption spectrum from the 355 nm pulsed photolysis of **2.1b** in acetonitrile

Immediately following the excitation pulse, two absorption bands with maxima at 470 nm and 600 nm are observed. Both bands decay with first-order kinetics and have lifetimes of 1.2 ± 0.1 µs. These spectra are assigned to the triplet spectrum of **2.1** based on the following considerations: (1) The spectra are consistent with triplet spectra of similar anthraquinone derivatives;[61, 62] (2) the lifetime of the bands decreases when the sample is purged with oxygen, which is typical for excited triplet states; (3) the TD-DFT calculated triplet-triplet spectrum (Figure 2.8) shows good agreement with the experimental spectrum.

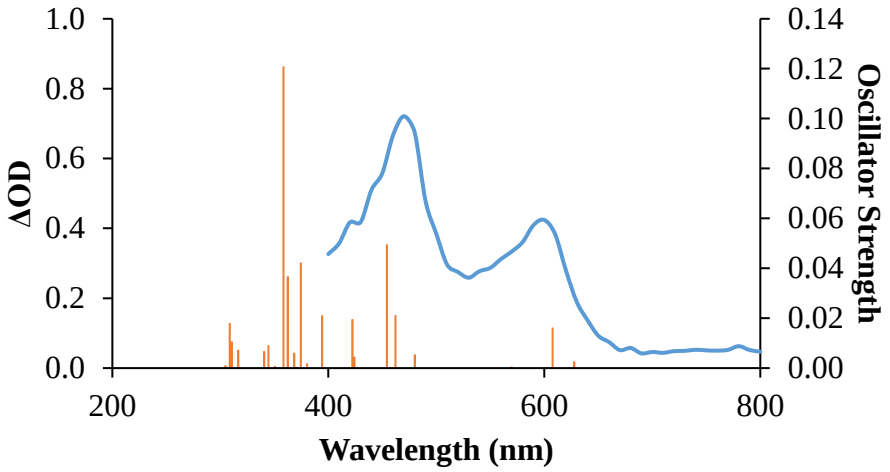

Figure 2.8. Orange bars: TD-DFT calculated triplet-triplet spectrum for **2.1a**. Blue curve: experimental transient absorption spectrum from pulsed 355 nm photolysis of **2.1a** at 0.1 μs

The triplet absorption spectrum of **2.1** is consistent with the s-TPA results. Even though 532 nm is at a local minimum on the spectrum, the absorption at this wavelength is still sufficient to allow re-excitation, consistent with the two-color (pulsed 355+532 nm) results. Additionally, the triplet has significant absorption at 447 nm, consistent with the results in Figure 2.5. Due to the ground state absorption at 355 nm, it is not possible to accurately verify the experimental triplet absorption at this wavelength however, the TD-DFT calculations shown in Figure 2.8 predict a strong absorption near this wavelength, consistent with the 355 nm pulsed photolysis results.

2.7 Effect of Structure on Sequential Two-Photon Absorption

To further demonstrate that it is T_1 that absorbs the second photon, structural modifications were investigated. Compound **2.8**, which lacks the 2-methoxy group, was synthesized and examined. As Scheme 2.7 shows, this compound, like **2.1a**, is expected to generate *p*-TsOH upon photolysis.

Scheme 2.7. Photolysis of **2.8** to generate *p*-TsOH

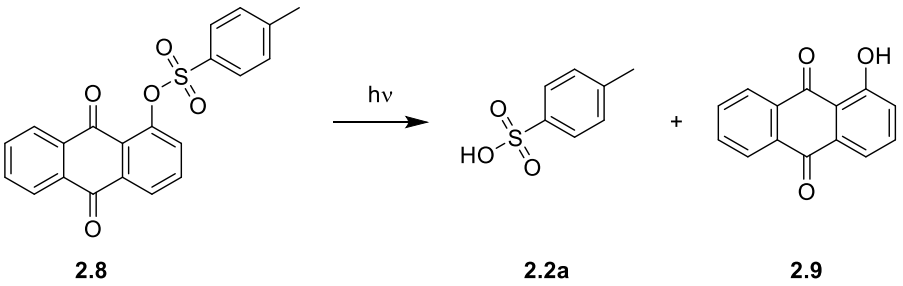

2.8 **2.2a** **2.9**

A transient absorption spectrum was obtained and is displayed in Figure 2.9. There is an absorption band with a maximum at 380 nm and a very weak tail that extends from 400-700 nm. This spectrum is assigned to the triplet state (T_1) of **2.8** as it is quenched by oxygen and it has a lifetime similar to that of **2.1a** and **2.1b**.

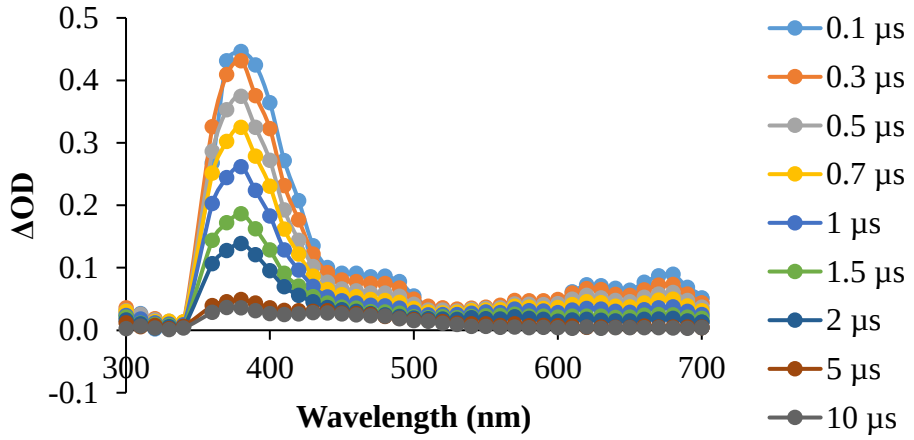

Figure 2.9. Transient absorption spectrum from the 355 nm pulsed photolysis of **2.8** in acetonitrile

Upon observing the lack of significant triplet absorption at 532 nm, **2.8** was photolyzed under the same two-color conditions as **2.1a** and these results are shown in Table 2.7. Not surprisingly, pulsed photolysis with combined 355+532 nm irradiation (Table 2.7, Entry 1) did not provide any noticeable enhancement as compared to 355 nm irradiation alone (Table 2.7, Entry 2). These results are consistent with re-excitation occurring from the triplet. If T_1 has significant absorption at 532 nm, a two-color effect

is observed but if the absorption is weak or absent at that wavelength, no enhancement is observed.

Table 2.7. Yields of *p*-TsOH from pulsed photolysis of **2.8** in CD_3CN with varying wavelengths of irradiation

Entry	Photolysis Time (min)	355 Power (mJ/pulse)	532 Power (mJ/pulse)	% Conversion[a, b]	% Yield *p*-TsOH[a, b]
1	10	8-9	87-88	43 ± 3	15 ± 1
2	10	8-9	0	36 ± 6	17 ± 2
3	10	0	87-98	0	0
4	10	0	0	0	0

[a]Determined by ^{1}H NMR, [b]Error bars are the result of triplicate experiments

It is important to note that the absorption spectra for S_1 of compounds **2.1a** and **2.8** have yet to be characterized and therefore a singlet mechanism cannot be completely ruled out. There is a possibility that S_1 of **2.1a** absorbs at 532 nm and S_1 of **2.8** does not which would leave re-excitation from S_1 as a possible mechanism. However, given the expected short lifetimes of S_1, this pathway seems extremely unlikely.

2.8 Cationic Polymerization

To demonstrate the utility of **2.1a** and **2.1b** as s-TPA photoinitiators, these compounds were applied to the cationic polymerization of ethyl vinyl ether (EVE) as outlined in Scheme 2.8. For this, 0.05 mol% of **2.1a** or **2.1b** was combined with EVE and the mixtures were then subjected to pulsed two-color photolysis. Figure 2.10 displays the ^{1}H NMR analysis of these experiments as well as control experiments. Both PAGs were able to initiate polymerization and reach 100% monomer conversion

as assessed by the absence of the signals corresponding to the vinylic protons. Formation of poly(ethyl vinyl ether) was observed based upon the observation of new, broad signals at 1.2 ppm and 3.5 ppm. Control experiments were performed where photolysis was applied but photoinitiator was omitted or where photoinitiator was included but the sample was not irradiated. In these cases, insignificant monomer conversion was observed indicating irradiation of the PAG is necessary for polymerization to occur.

Scheme 2.8. Cationic photopolymerization of EVE with **2.1a** or **2.1b**

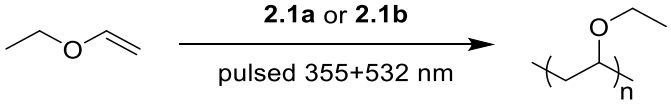

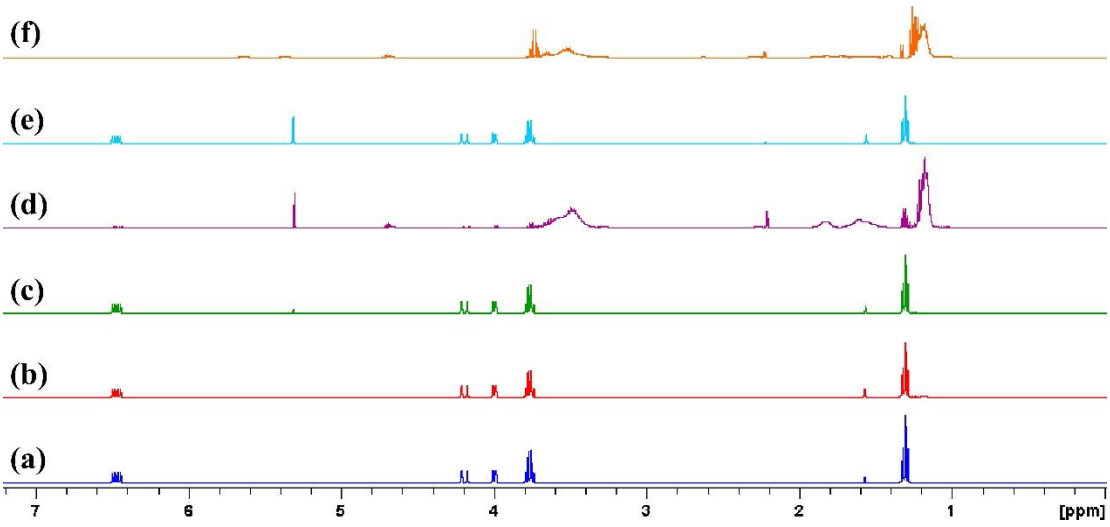

Figure 2.10. ^{1}H NMR resulting from the cationic photopolymerization of EVE with PAGs **2.1a** and **2.1b**. (a) EVE only, no photolysis; (b) EVE only, 10 minutes of irradiation; (c) EVE+**2.1b**, 24 hour dark control; (d) EVE+**2.1b**, 10 minutes of irradiation; (e) EVE+**2.1a**, 24 hour dark control; (f) EVE+**2.1a**, 2 hours of irradiation

2.9 Conclusions & Future Directions

The calculations and experiments in this chapter have demonstrated the ability to design photoacid generators that can be activated with sequential two-photon

absorption. Anthraquinone sulfonate esters **2.1a** and **2.1b** can be excited using UV or visible light and they rapidly form their triplet state. Under high intensity photolysis conditions, the triplet state can be re-excited which causes S—O bond homolysis. Subsequent reactions of the resulting radicals lead to the generation of strong acids in excellent yields. These acids were shown to initiate the polymerization of ethyl vinyl ether.

In order to expand the applicability of the photoacid generator, attempts were made to synthesize water soluble derivatives. The derivatives shown in Figure 2.11 were predicted to show improved water solubility.

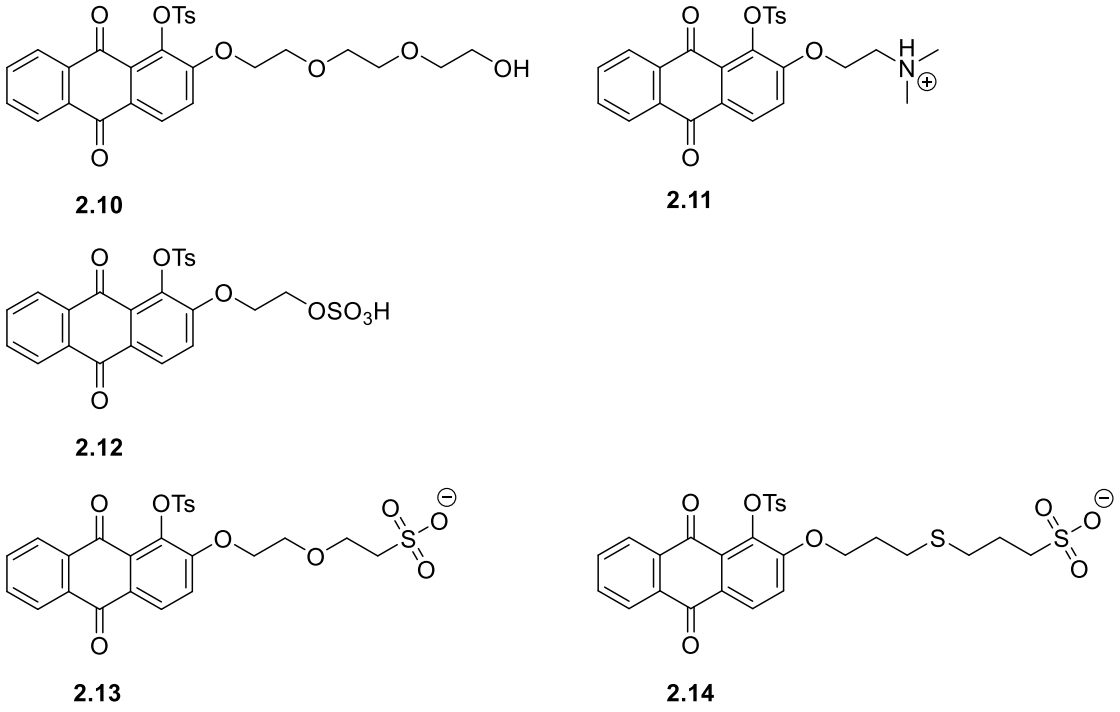

Figure 2.11. PAG derivatives predicted to be water soluble

Of the derivatives listed, only derivatives **2.10** and **2.11** were successfully synthesized whereas derivatives **2.12**, **2.13**, and **2.14** were a synthetic challenge. Unfortunately, derivatives **2.10** and **2.11** only showed minimal solubility in water.

Derivatives **2.12**, **2.13**, and **2.14** remain to be promising candidates if they could be successfully synthesized.

There are still improvements that could be made to this system. The ideal two-photon PAG would be unreactive under low intensity irradiation however, prolonged irradiation of **2.1a** and **2.1b** under such conditions leads to significant photoconversion where acid is only a minor component of a complex mixture of products. This photoconversion is most likely due to other triplet decomposition pathways. To avoid this, it is possible that a chromophore with a lower triplet energy could promote faster relaxation from T_1 back to ground state and minimize unwanted reactions from T_1. Of course, T_1 must still possess a sufficient lifetime to allow for re-excitation to occur. This hypothesis has been investigated by switching the chromophore from 9,10-anthraquinone (E_T = 63 kcal/mol[57]) to 5,12-naphthacenequinone (E_T = 56 kcal/mol[63]). As Scheme 2.9 describes, derivative **2.15** was synthesized and its ability to photogenerate *p*-TsOH was studied. This derivative differs from **2.1a** by having an extended pi-system but lacking the methoxy group.

Scheme 2.9. Photolysis of **2.15** to generate *p*-TsOH

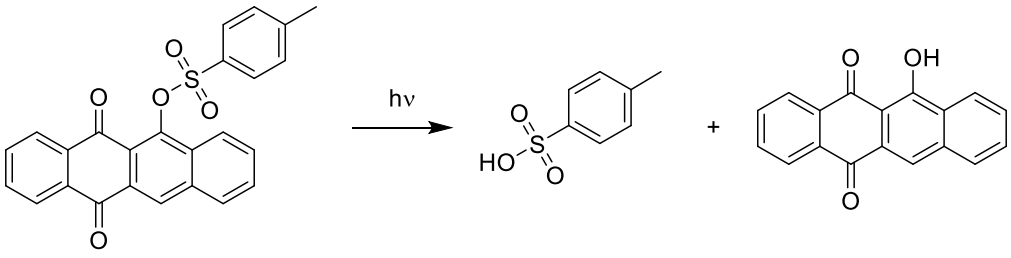

2.15 **2.2a** **2.16**

However, photolysis of **2.15** under low intensity irradiation resulted in full substrate conversion and an 86% yield of *p*-TsOH indicating this compound efficiently dissociates under one-photon conditions. It is possible that simply reducing the triplet

energy is not sufficient to eliminate one-photon decomposition. Alternatively, the methoxy group may have a more significant impact than previously anticipated and a more careful computational investigation should be conducted.

Currently being investigated is 1-hydroxy-2-tosyloxyanthraquinone **2.17** which releases *p*-TsOH upon photolysis, as described in Scheme 2.10.

Scheme 2.10. Photolysis of **2.17** to generate *p*-TsOH

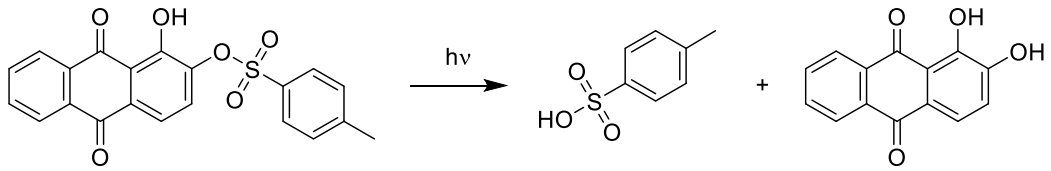

2.17 **2.2a** **2.18**

1-hydroxyanthraquinone derivatives have been found to undergo excited state intramolecular proton transfer (ESIPT) via the singlet manifold, as described in Figure 2.12.[64-67] Upon absorption of a photon, 1-hydroxyanthraquinone **2.9** undergoes ESIPT to its tautomer **2.19** which, in its excited state, is lower in energy than the excited state of **2.9**. The excited state of **2.19** relaxes to its ground state, which is higher in energy than the ground state of **2.9**. The ground state of **2.19** then thermally relaxes back to the ground state of **2.9**. It would be interesting to know if this process has any influence on the photoacid generation from the tosylated derivative **2.17**.

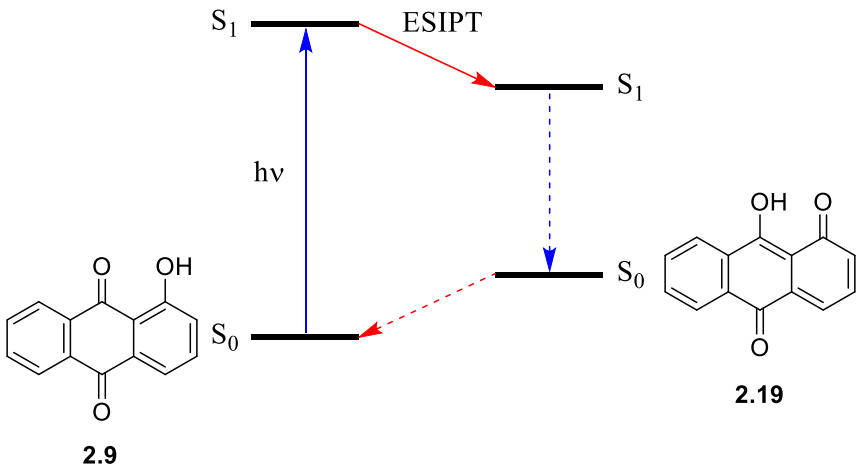

Figure 2.12. Excited state intramolecular proton transfer in 1-hydroxyanthraquinone

Preliminary results found a profound solvent effect on the two-photon photoacid generation from **2.17**. In polar aprotic solvents (e.g., acetonitrile), low intensity irradiation of **2.17** does not lead to substrate decomposition however, high intensity, pulsed irradiation leads to acid generation that is nonlinear with respect to laser power. In contrast, in polar protic solvents (e.g., methanol), low intensity irradiation leads to substrate decomposition accompanied by acid generation. It is hypothesized that the proticity of the solvent affects the ground state equilibrium of the tautomers with polar protic solvents providing a higher concentration of the proton transfer tautomer **2.19** in the ground state than in polar aprotic solvents. However, the reason that this would affect the two-photon photoacid generation is unclear at this time. Future studies will include nanosecond transient absorption spectroscopy, photoproduct analysis, fluorescence spectroscopy, and computational analysis in order to understand the details of acid generation.

Chapter 3: Lamp vs. Laser: Visible Light Mediated Photopolymerizations with 1-tosyloxy-2-methoxyanthraquinone

3.1 Photopolymerization

Photopolymerization is the use of light to trigger polymerization. As the demand for the synthesis of more complex polymeric materials increases, the need for controlled polymerization processes also increases. With the spatial and temporal control that light provides, photopolymerization has become extensively explored.[13, 68-73] Depending on the polymerization method, light can even act as an "on/off" switch for polymerization reactions.

Photopolymerization processes can either be photoinitiated or photocontrolled. Photoinitiated polymerization occurs when the initiating species (e.g., radicals, ions) are generated upon irradiation. In this case once the initiating species are formed, there is no control over chain growth. More recently, due to progress in the field of photoredox catalysis, methods of photocontrolled polymerization have emerged. Photocontrolled methods utilize reversible initiation and termination regulated by irradiation. In this case, the initiating species is activated by light and deactivated in the absence of light allowing control over chain growth.[70]

Photopolymerization reaction rates can be adjusted by varying the intensity of light used. The output of photons from a given light source increases in proportion with increasing light intensity. Because the rate of polymerization depends on the concentration of initiating and propagating species, controlling the intensity of irradiation allows precise control over the concentration of active species.[74]

This chapter will demonstrate the ability of 1-tosyloxy-2-methoxy-9,10-anthraquinone **3.1**, which was introduced in the previous chapter, to photoinitiate both cationic ring opening polymerization of cyclic lactones as well as mediate radical polymerization of acrylates depending on the intensity of visible light irradiation used. As Scheme 3.1 describes, irradiation of **3.1** will generate its first excited triplet state (T_1). Under high intensity irradiation, the triplet state will be re-excited causing bond dissociation to generate acid, as described in the previous chapter. The resulting acid can go on to initiate cationic polymerization. In contrast, under low intensity irradiation, the triplet state of **3.1** will act as a photosensitizer to lead to the formation of radicals which can initiate radical polymerization. In addition, copolymers can be synthesized utilizing both radical and cationic polymerizations in a one-pot mixture. Having a photosensitizer that is capable of mediating more than one type of polymerization allows for the preparation of more complex materials yet maintains the simplicity of the reaction mixture.

Scheme 3.1. Using 1-tosyloxy-2-methoxyanthraquinone **3.1** to mediate cationic or radical photopolymerizations depending on the intensity of visible light irradiation

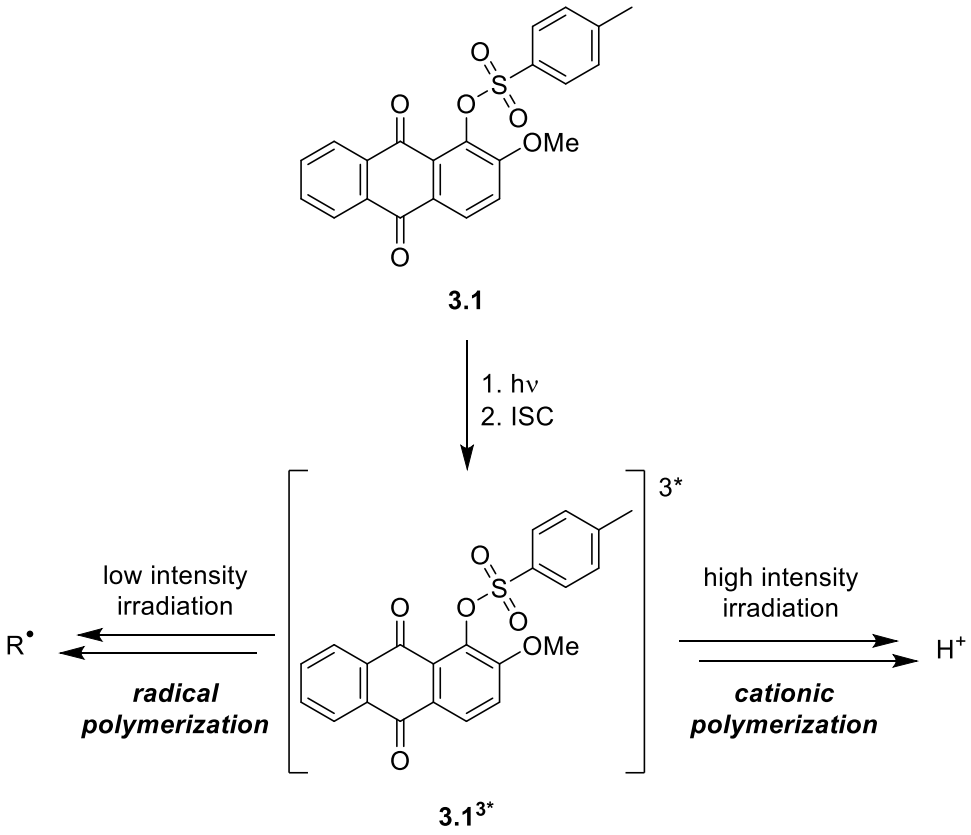

3.2 Ring Opening Polymerization

Ring opening polymerization (ROP) is a type of chain growth polymerization in which a cyclic monomer is opened by the terminal end of the growing polymer chain. The driving force of the ring opening of cyclic monomers is the relief of bond angle ring strain or strain due to steric repulsions between atoms. Some examples of cyclic monomers that can be polymerized via ROP include epoxides, lactones, and lactams. ROP mechanisms generally proceed under cationic or anionic pathways but there are also examples of radical pathways.

The ROP of lactones is a prominent technique for preparing polyesters however, only in recent years has it been mediated by light.[75-81] In 2013, Dove and

coworkers demonstrated that, upon UV irradiation, triarylsulfonium PAGs can act as effective photoinitiators for the cationic ROP of lactones and carbonates.[76] Then in 2016, Boyer and coworkers provided the first example of cationic ROP of lactones with visible light. They demonstrated that a reversible merocyanine-based photoacid can be activated using visible light and the resulting acid is capable of initiating polymerization to form well-defined polymers.[77]

This chapter will demonstrate the utility of the PAG, 1-tosyloxy-2-methoxy-9,10-anthraquinone **3.1**, from the previous chapter for the ROP of lactones using high intensity, visible light irradiation. The two-photon behavior of **3.1** allows for combination of ROP with other photomediated polymerization techniques.

3.3 RAFT Polymerization

Reversible addition-fragmentation chain transfer (RAFT) polymerization is one type of controlled radical polymerization. This type of polymerization allows the synthesis of polymers with predictable molecular weights and narrow polydispersities. RAFT polymerization proceeds through use of a chain transfer agent (CTA), also referred to as a RAFT agent. CTAs used in RAFT processes are typically a thiocarbonylthio group, with dithiobenzoates being very effective RAFT agents due to the radical stabilizing ability of the phenyl group. A general mechanism of the RAFT polymerization process is described in Scheme 3.2. Initiating radicals are generated and react with monomer to generate a propagating radical $P_n^{\bullet}$ (Steps 1 & 2). This radical is rapidly captured by the CTA to form a new radical intermediate which has an equal probability of eliminating the propagating radical $P_n^{\bullet}$ or the end group $R_2^{\bullet}$ (Step 3). When the end group is eliminated, it can react with monomer to generate a new

propagating radical chain $P_m^{\bullet}$ (Step 4). These steps are referred to as the pre-equilibrium. Once all of the initial CTA has been consumed, the main equilibrium occurs by propagating radical chains reacting with the now polymeric CTA (Step 5). As with any other radical polymerization, termination occurs by two radical species reacting with each other.[82, 83]

Scheme 3.2. Mechanism of RAFT polymerization adapted from Reference 82

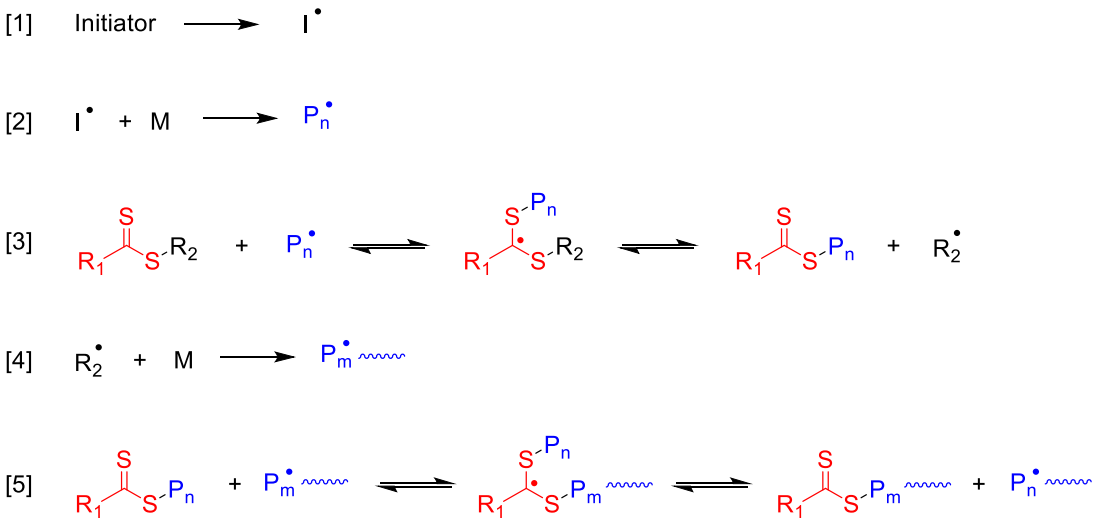

Photoinitiated RAFT polymerization can occur either by direct irradiation and subsequent dissociation of the RAFT agent[84] or via a photoinduced electron transfer (PET-RAFT) process.[85-89] Direct irradiation of the RAFT agent, also referred to as the photoinifertor method, typically requires high energy, UV irradiation. While this reduces complexity of the system, UV irradiation poses the possibility of competing absorption of other substrates as well as degradation of the CTA end groups.[90] In contrast, the PET-RAFT process can use visible light absorbing photocatalysts to activate the RAFT agent and begin the polymerization process. As described in Scheme 3.3, the light is absorbed by the photocatalyst which, in its excited state, will undergo

electron transfer to the RAFT agent. The reduced RAFT agent can fragment to generate propagating radicals.

Scheme 3.3. Activation of a RAFT agent via photoinduced electron transfer from an excited state photocatalyst

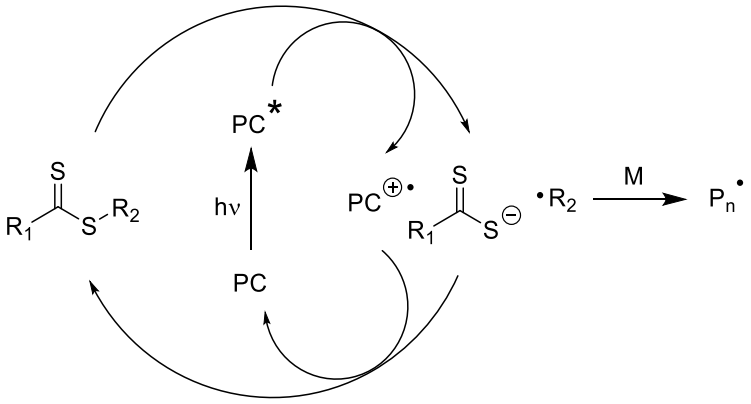

In addition to using visible light absorbing photosensitizers to undergo electron or energy transfer to the RAFT agent, an alternate approach is to use the photosensitizer in order to generate initiating radicals. In 2016, Boyer and coworkers demonstrated that excitation of metal phthalocyanines leads to oxidation of the solvent, *N*-methyl-2-pyrrolidone, which then undergoes deprotonation and rearrangement to generate a radical capable of initiating polymerization of acrylate monomers (Scheme 3.4). Upon addition of a RAFT agent, the polymerizations became controlled and narrow polydispersities were achieved.[91]

Scheme 3.4. Generation of initiating radicals via photooxidation of *N*-methyl-2-pyrrolidone

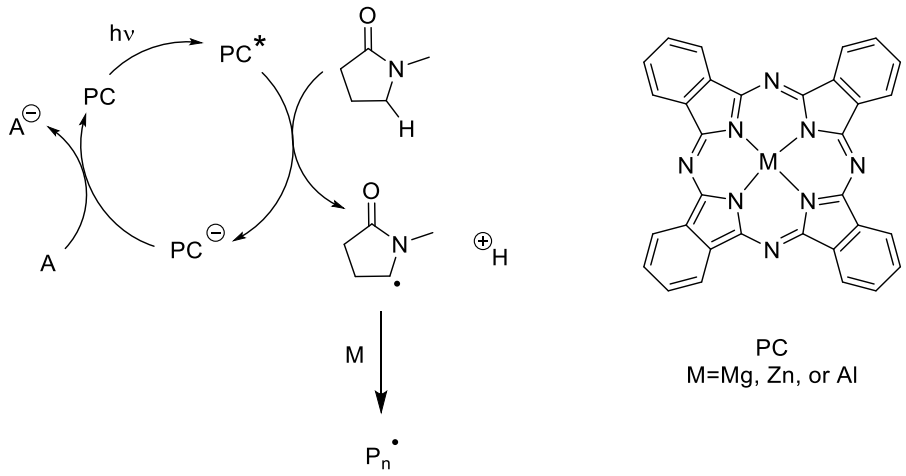

Using a similar approach, Falvey and coworkers demonstrated generation of initiating radicals via photooxidation of DMSO.[92] DMSO is a commonly used solvent for RAFT polymerizations due to its ability to solubilize both reactants and products, and it generally functions as an inert medium. However, under highly oxidizing conditions, it has been shown that DMSO can undergo one electron oxidation.[93] The resulting cation radical further reacts with water, leading to formation of methyl radicals. This approach has been used for free radical methylation of 2'-deoxyguanosine.[94]

As discussed in the previous chapter, many anthraquinone derivatives intersystem cross with high efficiency to their lower energy triplet state. In addition, the triplet state of anthraquinone is a strong oxidant and therefore, could be capable of oxidizing DMSO.[3, 95] Indeed, using LFP, Görner demonstrated that the triplet state of anthraquinone is quenched by DMSO near the diffusion limit and this quenching is the result of one electron transfer from DMSO to the excited state anthraquinone.[96]

The work of Falvey and coworkers demonstrated that, in its excited state, a visible light absorbing anthraquinone derivative is capable of oxidizing DMSO which leads to the generation of initiating methyl radicals, as outlined in Scheme 3.5. By the addition of a RAFT agent, the polymerization can be controlled to yield well-defined polymers.

Scheme 3.5. Generation of initiating methyl radicals via photooxidation of DMSO

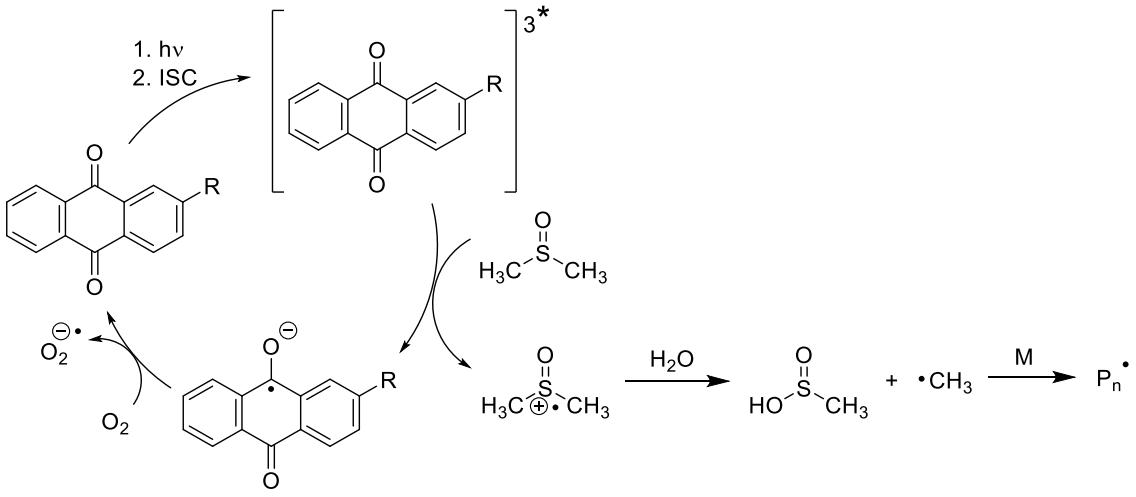

This chapter will demonstrate that, under low intensity, visible light irradiation, 1-tosyloxy-2-methoxy-9,10-anthraquinone **3.1** can act as a sensitizer for the photooxidation of DMSO to initiate RAFT polymerization. This process, in addition to cationic polymerization under high intensity irradiation, will demonstrate a dual capability of one sensitizer.

*3.4 Ring Opening Polymerization with **3.1***

As Scheme 3.6 describes, a series of polymers from the ROP of ε-caprolactone (ε-CL) and δ-valerolactone (δ-VL) catalyzed by the 447 nm CW photolysis of **3.1** were synthesized. Varying degrees of polymerization were targeted and the results are

summarized in Table 3.1. In all cases, benzyl alcohol was used as the initiator due to its distinct ^{1}H NMR resonance which allowed for ease of analysis.

Scheme 3.6. ROP of ε-CL and δ-VL catalyzed by photolysis of **3.1**

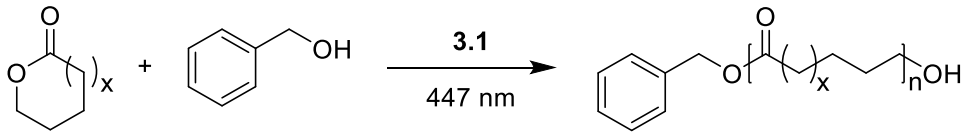

x = 1: δ-VL
x = 2: ε-CL

Initially, the concentration of **3.1** relative to initiator was set to 0.1 (Table 3.1, Entries 2 & 8) and the targeted degree of polymerization was 50. The targeted degree of polymerization is determined by the initial ratio of monomer to initiator ($[M]_0/[I]_0$). With both lactones, high monomer conversion was observed and the resulting polymers showed good agreement between the theoretical molecular weight and the measured molecular weight. Additionally, both polymers displayed a narrow polydispersity index (PDI) indicating a controlled polymerization. Increasing the concentration of **3.1** from 0.1 to 0.25 (Table 3.1, Entries 3 & 9) did not have a significant effect on the outcome of the polymerization reaction. In both cases, high conversions were still achieved and there was no significant difference in the polydispersities. Omitting **3.1** from the reaction mixture resulted in lack of monomer conversion (Table 3.1, Entries 1 & 7). Additionally, including **3.1** but not irradiating the sample also resulted in a lack of monomer conversion (Table 3.1, Entries 6 & 12). These control experiments indicate that irradiation of **3.1** is necessary to catalyze the polymerization reaction. Various degrees of polymerization were targeted (Table 3.1, Entries 4-5, 10-11) and in all cases the theoretical and experimental molecular weights were in good agreement with narrow polydispersities.

Table 3.1. Ring opening polymerization of ε-CL and δ-VL with varying concentrations of **3.1** and varying targeted degrees of polymerization

Entry	Monomer	[**3.1**][a]	$[M]_0/[I]_0$	Irradiation Time (min)	Polymerization Time (hr)	% Monomer Conversion[b]	$M_{n,\ theo}$[c]	$M_{n,\ GPC}$[d]	PDI[d]
1	ε-CL	0	50	60	24	0	--	--	--
2	ε-CL	0.10	50	30	48	88	5130	5606	1.25
3	ε-CL	0.25	50	90	48	71	4160	5110	1.19
4	ε-CL	0.10	25	30	24	86	2562	3336	1.24
5	ε-CL	0.10	100	30	96	73	8440	6846	1.19
6	ε-CL	0.10	50	0	24	0	--	--	--
7	δ-VL	0	50	60	24	0	--	--	--
8	δ-VL	0.10	50	30	5	73	3612	4899	1.17
9	δ-VL	0.25	50	90	2	83	4263	5224	1.22
10	δ-VL	0.10	25	30	0.75	86	2261	3729	1.19
11	δ-VL	0.10	100	30	18	97	9820	10836	1.28
12	δ-VL	0.10	50	0	24	0	--	--	--

[a]Molar equivalents relative to the amount of initiator, [b]Determined by ^{1}H NMR, [c]Calculated by the equation: $M_{n,\ theo} = MW_{initiator} + (\%\ conv. \times [M]_0/[I]_0 \times MW_{monomer})$, [d]Determined by GPC using THF as a solvent and calibrated using polystyrene standards

3.5 Power Dependence on Ring Opening Polymerization

To understand how laser power affects the rate of polymerization, the polymerization of ε-CL was monitored over time with varying powers of 447 nm irradiation. Figure 3.1 shows that the most pronounced effect is during the first 15 minutes of irradiation and after that, the rate of polymerization is relatively linear with time. When plotted, the monomer conversion after 15 minutes of photolysis as a

function of laser power displays a nonlinear trend which is consistent with a nonlinear generation of acid (Figure 3.2). The slow polymerization rate at low laser powers opens the possibility of combining ROP with other photomediated polymerizations.

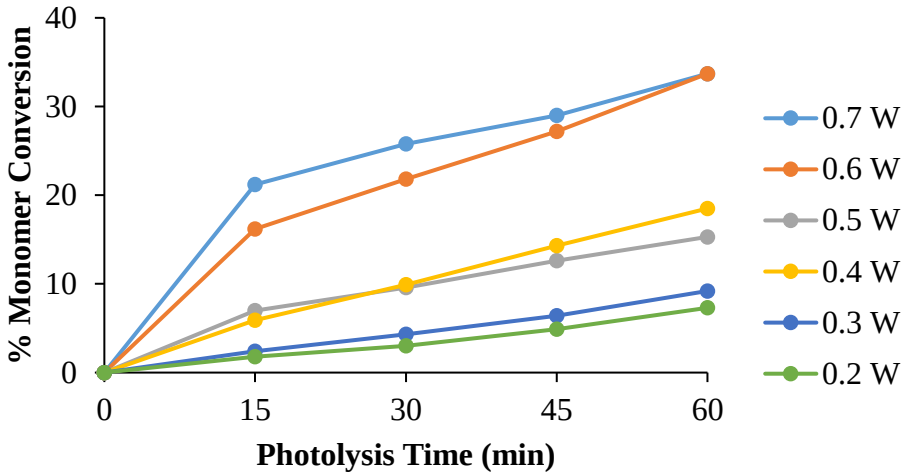

Figure 3.1. Monitoring conversion of ε-CL over time at varying powers of 447 nm irradiation

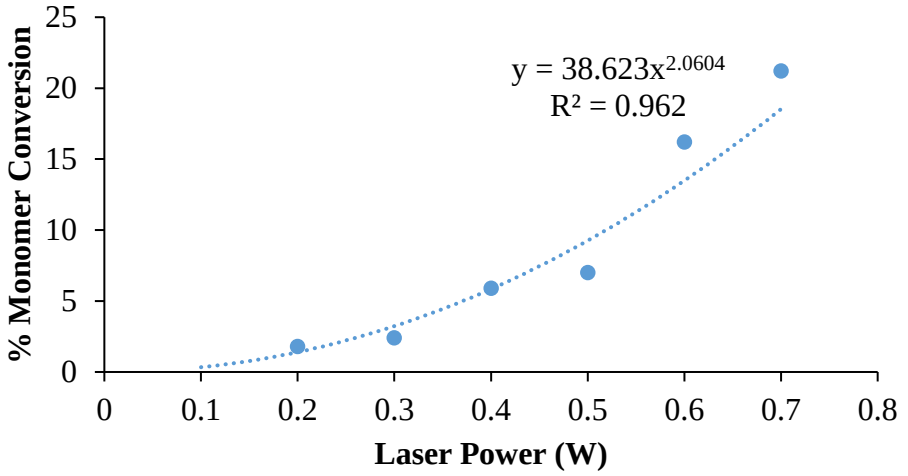

Figure 3.2. Conversion of ε-CL after 15 minutes of irradiation as a function of 447 nm laser power

*3.6 RAFT Polymerization with **3.1***

As described in Section 3.3, anthraquinone derivatives are capable of producing initiating radicals through photooxidation of DMSO. Because **3.1** is an anthraquinone derivative, presumably it would have similar redox properties as other anthraquinone derivatives and would be capable of photooxidizing DMSO. The hypothesis is that under low intensity irradiation, acid generation would be a minor pathway and instead, **3.1** would act as an excited state oxidant to aid in the initiation of RAFT polymerization.

To demonstrate that **3.1** can photooxidize DMSO to initiate RAFT polymerization, polymerizations of acrylate monomers were carried out using 419 nm broadband irradiation, as described in Scheme 3.7. Using 4-cyanopentanoic acid dithiobenzoate (CPADB) as the chain transfer agent, the polymerizations of methyl methacrylate (MMA) and 2-hydroxyethyl methacrylate (HEMA) using were carried out in both the presence and absence of **3.1** and the results are summarized in Table 3.2. In all cases, monomer conversion was observed however the polymerization in the presence of **3.1** led to significantly higher monomer conversion, consistent with the results of previous work.[92] The polymerization that occurs in the absence of **3.1** is attributed to a photoiniferter mechanism caused by the UV emission of the 419 nm bulbs overlapping with the absorption tail of CPADB allowing direct absorption of the chain transfer agent.

Scheme 3.7. RAFT polymerization of acrylate monomers via photooxidation of DMSO with **3.1**

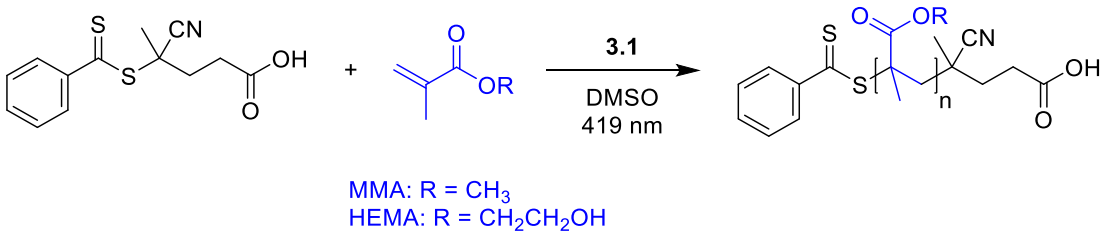

Table 3.2. RAFT polymerization of acrylate monomers in the presence and absence of **3.1**

Entry	Monomer	$[M]_0/[CTA]_0$	[**3.1**]/[CTA]	Photolysis Time (hr)	% Monomer Conversion[a]
1	MMA	100	0	18	46
2	MMA	100	0.1	18	76
3	MMA	100	0.5	18	63
4	HEMA	100	0	18	71
5	HEMA	100	0.1	18	97
6	HEMA	100	0.5	18	93

[a]Determined by ^{1}H NMR

3.7 Brush Copolymerization Using Varied Light Intensity

Knowing that **3.1** is capable of polymerizing acrylates under low intensity irradiation, a one-pot brush copolymerization, as outlined Scheme 3.8, was carried out. In a vial was combined HEMA and δ-VL monomers, CPADB as the RAFT agent, **3.1** as the photocatalyst/photoinitiator, and DMSO as the solvent. The hypothesis is that under low intensity irradiation (419 nm broadband lamps), polymerization of HEMA via RAFT polymerization should be the dominant reaction. Then, by switching to high

intensity irradiation (447 nm CW laser), **3.1** will generate acid and ROP should begin to take place.

Scheme 3.8. One-pot brush copolymerization

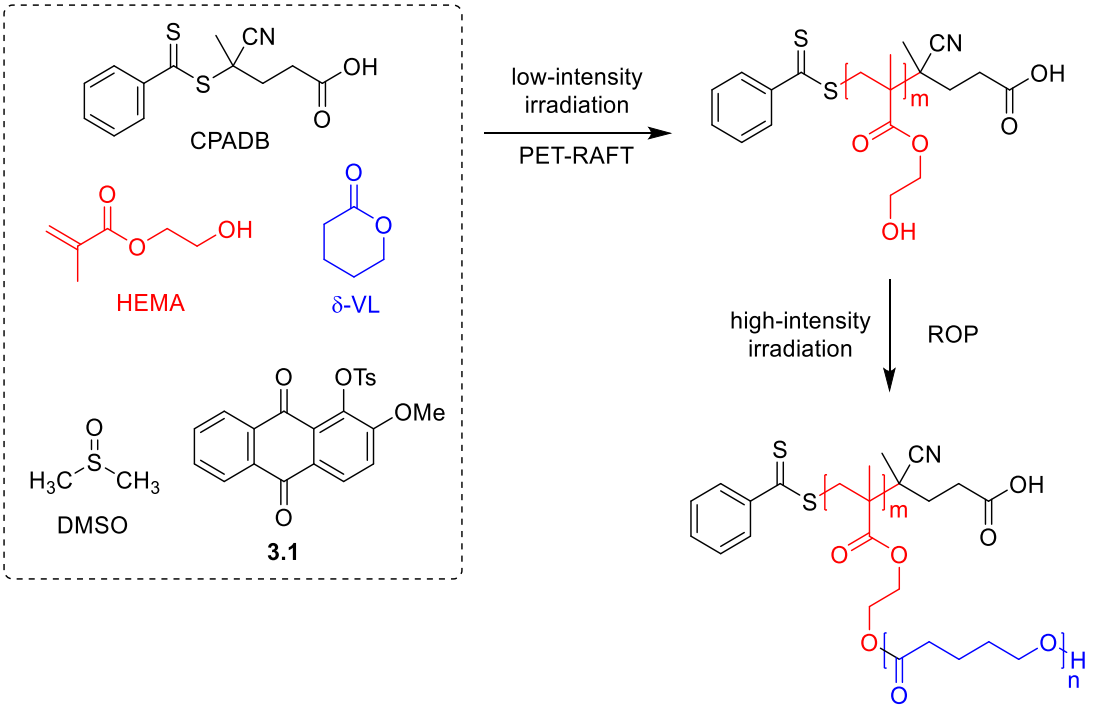

As Figure 3.3 shows, when the sample is irradiated with low intensity, broadband 419 nm irradiation, after 18 hours there is significant conversion of HEMA (80%) while the conversion of δ-VL is minimal (9%). When the light source is switched to the high intensity 447 nm CW laser, conversion of HEMA continues however there is a sharp increase in the conversion of δ-VL due to acid generation from **3.1**.

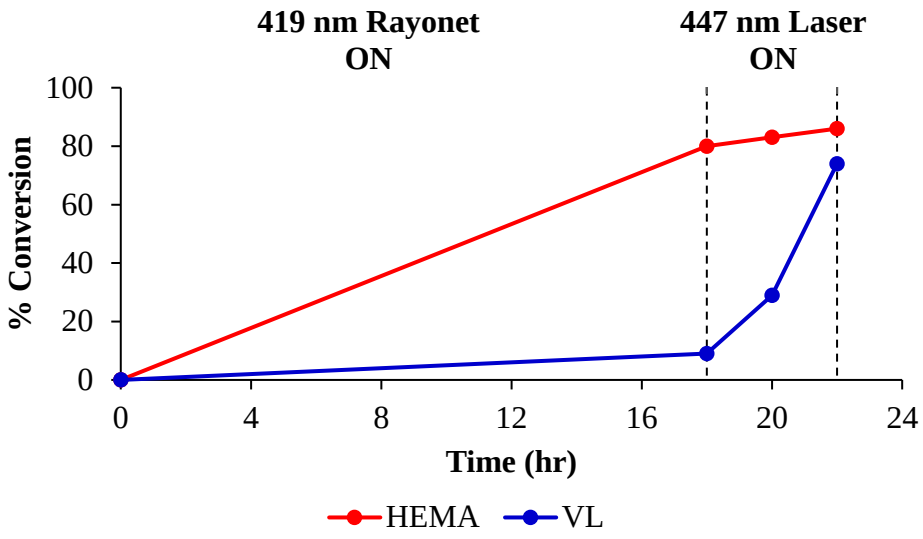

Figure 3.3. Monitoring conversion of HEMA and δ-VL under different intensities of visible light irradiation of **3.1** in DMSO. Monomer conversion monitored using ^{1}H NMR

Evidence for copolymer formation was provided through the use of gel permeation chromatography (GPC). Figure 3.4 displays the GPC trace for the isolated polymer from the copolymerization experiment described. The red line measures refractive index which indicates when a polymer has reached the detector and the purple line measures UV absorption. Because there is a measurable UV absorption when the polymer reaches the detector, this is evidence that the CTA end group is incorporated into the polymer. A single peak is indicative of a successful copolymerization rather than formation of two separate homopolymers. Additionally, a narrow molecular weight distribution (PDI = 1.26) was achieved.

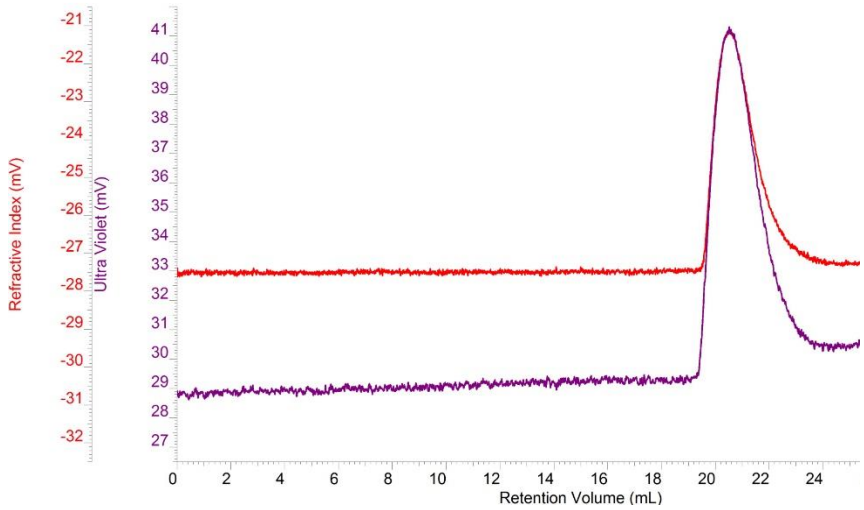

Figure 3.4. GPC trace of isolated brush copolymer. Red line: measuring refractive index. Purple line: measuring UV absorption

To ensure that the acrylate does not intrinsically polymerize more rapidly than the lactone, a similar sample was irradiated with only the high intensity 447 nm CW laser. In this case both monomers show immediate conversion however, δ-VL reached 60% conversion within 4 hours whereas HEMA only reached 20% conversion. (Figure 3.5).

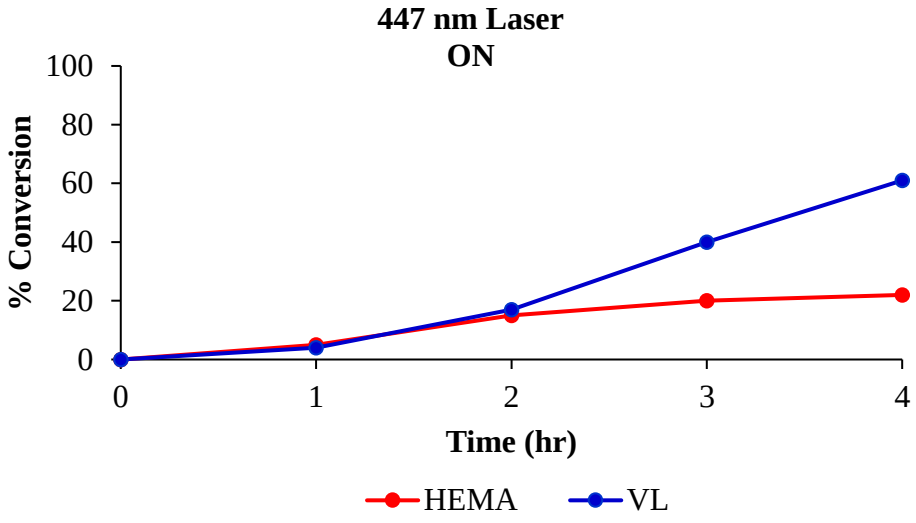

Figure 3.5. Monitoring conversion of HEMA and δ-VL during the 447 nm irradiation of **3.1** in DMSO. Monomer conversion monitored using ^{1}H NMR

3.8 Conclusions

The experiments described in this chapter demonstrate that 1-tosyloxy-2-methoxy-9,10-anthraquinone **3.1** is capable of mediating both cationic and radical polymerizations depending on the intensity of visible light irradiation. Under high intensity irradiation, photoacid generation occurs producing strong acid capable of catalyzing cationic ring opening polymerization of lactones. Under low intensity irradiation, **3.1** is able to photooxidize DMSO which leads to formation of methyl radicals capable of initiating RAFT polymerization. The dependence on light intensity allowed for the one-pot synthesis of a brush copolymer where a single photocatalyst can mediate two types of polymerizations.

Chapter 4: Mechanism of the Photorelease of Alcohols from the 9-Phenyl-9-tritylone Protecting Group

The majority of the work in this chapter has been published:[97]

Zeppuhar, A. N.; Hill-Byrne, K.; Falvey, D. E., Mechanism of the Photorelease of Alcohols from the 9-Phenyl-9-tritylone Protecting Group. *Photochemical & Photobiological Sciences* **2019,** *18* (8), 1990-1995

4.1 Photoreleaseable Protecting Groups

The use of protecting groups in organic synthesis is a necessity when it comes to the preparation of complex molecules.[98] When applied, protecting groups mask the reactivity of a certain functional group allowing reactions to occur at other sites on the molecule after which, the protecting group can then be removed. However, complications arise when multiple protecting groups are needed on one molecule. When this occurs, reaction conditions necessary for cleavage must be very specific for each group in order for the others to remain intact.

Photoreleaseable protecting groups (PRPGs) are an important subset and can overcome some of the challenges associated with conventional protecting groups. PRPGs generally do not require reagents for their removal, only light.[99] This is advantageous when working with molecules that are extremely sensitive to acids and/or bases. This feature also provides spatial and temporal control over the deprotection step. For a PRPG to be effective, most, if not all, of the following criteria must be met:[100, 101] (1) it should absorb at wavelengths greater than 300 nm to minimize absorption by other functional groups which could lead to undesired reactions; (2) it

should be stable in solution prior to photolysis; (3) the photochemical by-products should be transparent at the irradiation wavelength and unreactive; (4) deprotection should occur rapidly and quantitatively.

In addition to synthesis, PRPGs find applications in areas including controlled drug release,[102-104] photolithography,[105, 106] and optogenetics.[107] Because of this, there is continued interest in the design of new PRPGs with expanded capabilities. Some well-established PRPGs include the *o*-nitrobenzoyl group,[108-110] the coumaryl group,[111-113] and the phenacyl group.[114-116] These groups are excellent options when it comes to the photorelease of good leaving groups such as carboxylates, sulfonates, and phosphates. However, when it comes to less labile leaving groups, such as alcohols, there are fewer examples. One approach is to protect the alcohol as a mixed carbonate ester and then rely on spontaneous decarboxylation of the resulting alkoxy carbonate to release the alcohol.[117, 118] Other approaches include intramolecular cyclization of cinnamate esters,[119, 120] lactonization employed with a quinone trimethyl lock,[121] and direct photolysis of trityl ethers.[122] Recently, Falvey and coworkers adapted the 9-phenyl-9-tritylone (PTO) group to become a PRPG capable of cleanly and efficiently releasing primary and secondary alcohols.[123] The experiments described in this chapter will provide a deeper understanding of the photorelease mechanism in order to support further development of the group and similar PRPGs.

4.2 Introduction to the 9-Phenyl-9-tritylone Protecting Group

The 9-phenyl-9-tritylone group is a protecting group for alcohols that was first introduced in 1971 by Barnett and coworkers,[124, 125] whose aim was to develop a

protecting group for alcohols that retains the advantages of, but was complementary to, the well-established trityl protecting group (Figure 4.1).

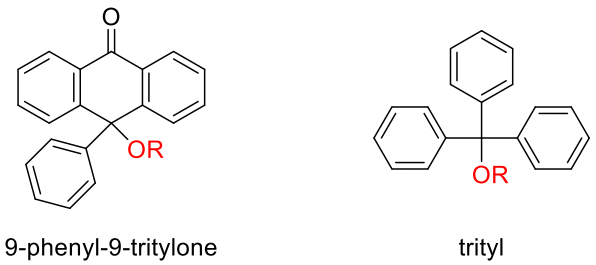

9-phenyl-9-tritylone trityl

Figure 4.1. The 9-phenyl-9-tritylone and trityl protecting groups

Trityl ethers are easily hydrolyzed with the use of dilute acid and are stable to a wide-variety of non-acidic reagents. In contrast, the PTO group is much more stable to acid hydrolysis. Instead, cleavage can be carried out with a base-catalyzed Wolff-Kishner reduction. While this is complementary to the trityl group, the disadvantage is that cleavage still requires the harsh conditions (high temperatures and strong bases) of the Wolff-Kishner reduction which many functional groups do not tolerate. To avoid the harsh conditions but still take advantage of reductive cleavage, Schäfer and coworkers demonstrated electrochemical reduction of the PTO group successfully deprotected alcohols at room temperature under neutral conditions.[126]

In 2015, Falvey and coworkers first reported alcohol deprotection from the PTO group by means of photochemical reduction.[123] Photoinduced electron transfer (PET) allowed for the clean and efficient release of primary and secondary alcohols. Excitation of PTO-ethers with UV irradiation in the presence of strong ground state electron donors, such as triethylamine, yielded the deprotected alcohol in good yields. Polar solvents, such as methanol and acetonitrile, provided better yields than nonpolar solvents, such as benzene. In addition, visible light driven photorelease was

accomplished by excitation of strong excited state electron donors including *fac*-(tris(2,2′-phenylpyridine))iridium(III) as well as tris(bipyridine)ruthenium(II) chloride in the presence of PTO-ethers. Using LFP, two key intermediates were identified under conditions in which photorelease was observed, as outlined in Scheme 4.1. When PTO-ether **4.1** is photolyzed in the presence of triethylamine, both the anion radical **4.2** and the ketyl radical **4.3** are observed. However, less clear was which of these intermediates is responsible for alcohol release.

Scheme 4.1. Proposed mechanism for the photorelease of alcohols from PTO-ethers under PET conditions

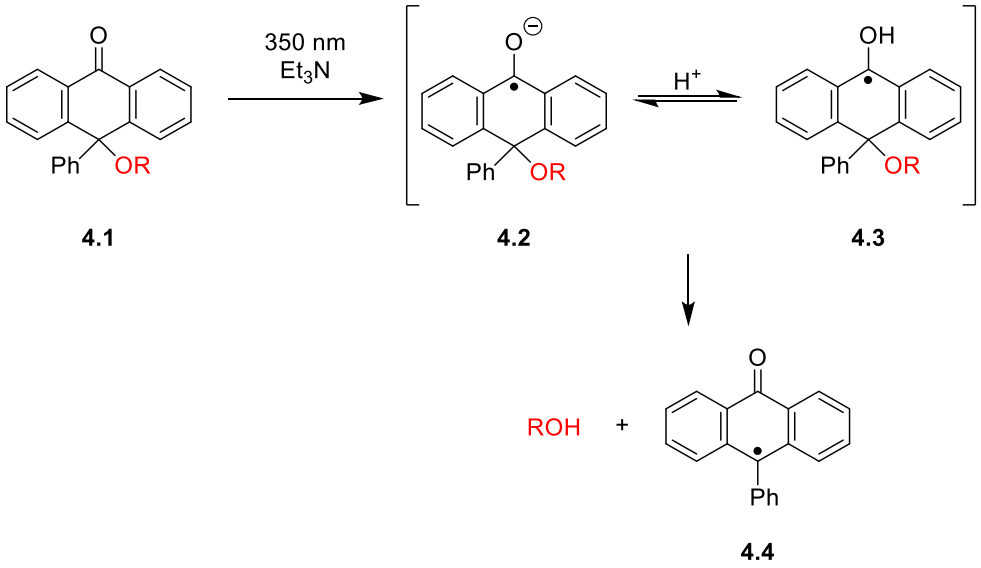

The experiments described in this chapter probe the behavior of PTO-ethers under direct photolysis conditions, i.e., in the absence of an electron donor, in order to understand the mechanistic details of photorelease.

4.3 Photorelease of Alcohols via Direct Photolysis

The PTO-ether selected for these studies, as outlined in Scheme 4.2, is benzyl ether **4.5** which, upon photolysis, releases benzyl alcohol **4.6**. This ether was chosen due to its ease of synthesis as well as ease of product analysis.

Scheme 4.2. Direct photolysis of benzyl ether **4.5** to generate benzyl alcohol **4.6**

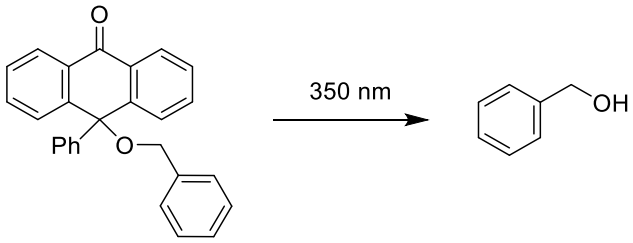

4.5 **4.6**

The first mechanistic aspect that was investigated was the role of the solvent. Benzyl ether **4.5** was photolyzed at 350 nm in various solvents and its depletion (Figure 4.2) as well as formation of benzyl alcohol **4.6** (Figure 4.3) was monitored by gas chromatography.

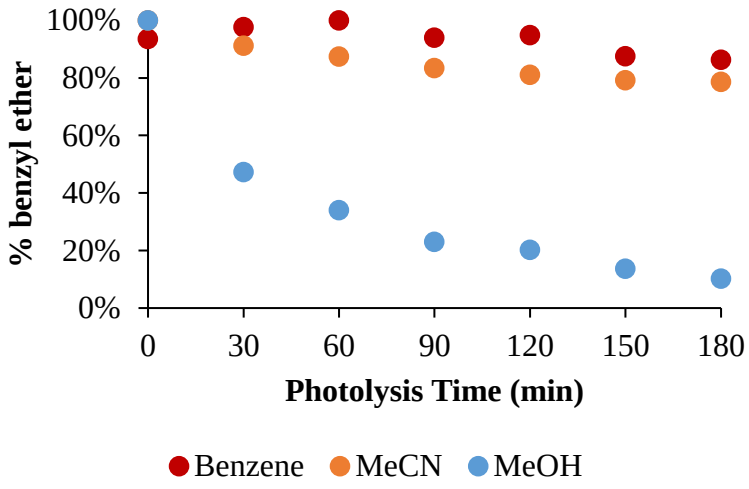

Figure 4.2. Monitoring conversion benzyl ether **4.5** from direct 350 nm photolysis in various solvents

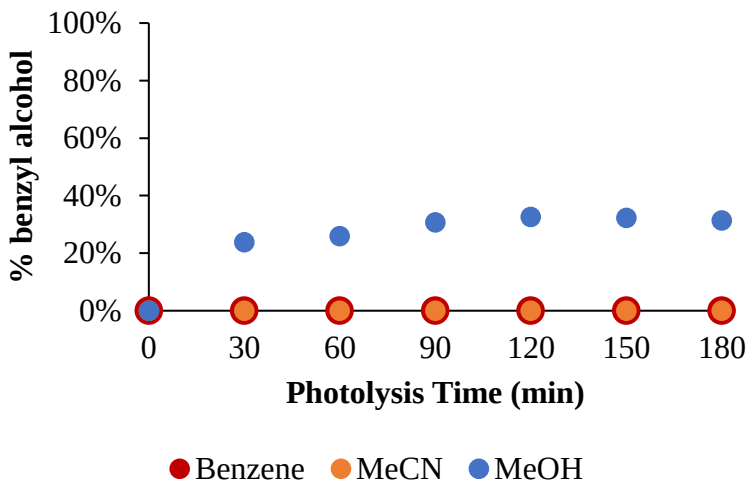

Figure 4.3. Monitoring yield of benzyl alcohol **4.6** during the direct 350 nm photolysis of benzyl ether **4.5** in various solvents

In benzene and acetonitrile, there is minimal depletion of **4.5** and no observable formation of **4.6**. This can be rationalized by the fact that these solvents are considered to be poor hydrogen atom donors, which is supported by the BDE for hydrogen atom abstraction. The C—H BDEs for these solvents are 112.9 kcal/mol[127] and 95.5 kcal/mol,[128] respectively. Due to its high BDE, benzene is considered inert as a hydrogen atom donor. Acetonitrile has a lower BDE and is therefore more thermodynamically favored for hydrogen atom transfer however, it is not kinetically favored due to the electron-withdrawing cyano group. The electron deficient C—H bond does not allow for a rapid reaction with the excited state triplet of **4.5**. Therefore, in these solvents, the excited state triplet is formed but then relaxes back to the ground state without releasing the alcohol. When switching to methanol, which is considered to be a good hydrogen atom donor, depletion of **4.5** is observed. Methanol has a BDE of 96.0 kcal/mol[129] and has a more electron rich C—H bond which allows for a more kinetically favorable hydrogen atom abstraction by the excited state triplet. The conversion of **4.5** is accompanied by formation of **4.6** but in poor yields. These results

suggest that in the presence of a good hydrogen atom donor, the excited state triplet abstracts a hydrogen atom to generate the ketyl radical **4.3**. From **4.3**, chemistry can begin to occur. However, since the yield of **4.6** is poor, it appears that alcohol release from **4.3** is a minor pathway and the depletion of **4.5** is due to other nonproductive pathways.

LFP experiments confirm that these intermediates are formed. Figure 4.4 displays the transient absorption spectrum resulting from 355 nm pulsed photolysis of **4.5** in benzene and Figure 4.5 displays the same experiment in methanol. In benzene, there is a short-lived peak with a maximum absorption at 540 nm that forms immediately following the laser pulse. Previous studies have assigned this peak as the triplet state of the PTO chromophore due to its resemblance to the structurally similar benzophenone chromophore.[123, 130] However, in methanol, the spectrum displays a longer-lived peak with a maximum absorption at 530 nm which has been previously assigned to the ketyl radical **4.3**.[123] The triplet and ketyl radical can be distinguished based upon the differences in lifetimes. Observation of **4.3** in methanol is consistent with the previous data that indicate **4.3** is necessary for chemistry to occur as depletion of **4.5** is observed in methanol but not in benzene.

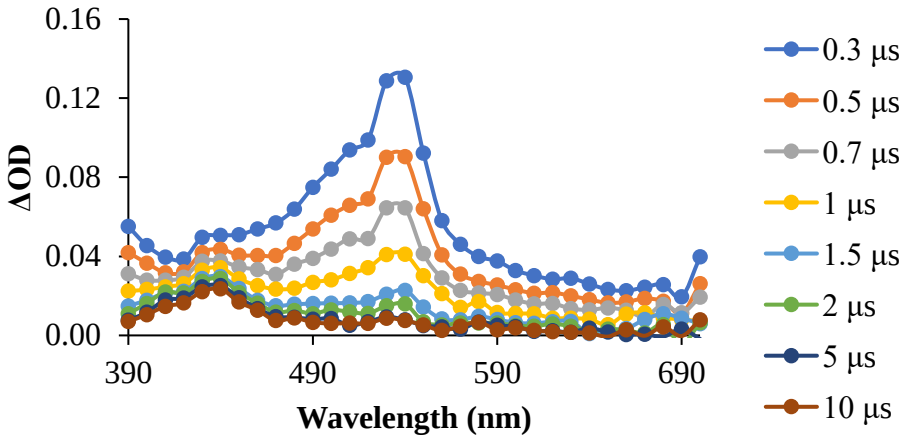

Figure 4.4. Transient absorption spectrum from the 355 nm pulsed photolysis of **4.5** in benzene

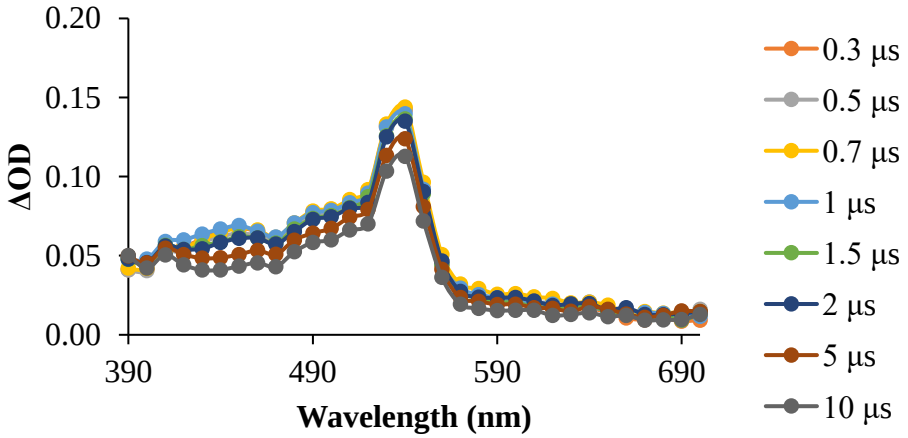

Figure 4.5. Transient absorption spectrum from the 355 nm pulsed photolysis of **4.5** in 3:1 MeOH: 1,4-dioxane

These data led to the hypothesis that alcohol release occurs predominantly through the anion radical intermediate **4.2**. To confirm this, studies were conducted in methanol with the addition of a base. Photolysis in methanol generates ketyl radical **4.3** which could then be deprotonated to generate **4.2**. From here, C—O bond scission is expected to occur and release the alcohol. When a strong base, such as hydroxide, is used, alcohol release is observed. As shown in Table 4.1, as the concentration of sodium hydroxide increases from 0-1 mM, the yield of **4.6** also increases. However,

for reasons that are unclear, when the hydroxide concentration is greater than 1.5 mM, the yields begin to drop.

Table 4.1. Yields of **4.6** generated during the 3-hour photolysis of **4.5** at 350 nm with varying concentrations of sodium hydroxide. Starting ether concentration is 9 mM

[NaOH] (mM)	% Yield Alcohol[a,b]
0.0	43.8 ± 0.96
0.1	68.4 ± 8.46
0.5	74.5 ± 6.51
1.0	77.5 ± 17.74
1.5	55.9 ± 11.73
2.0	46.7 ± 2.22
2.5	47.5 ± 2.81

[a]Error bars are the result of triplicate experiments. [b]Yields are corrected to reflect the amount of starting material that converted.

To ensure that complete deprotonation of ketyl radical **4.3** is necessary for release, experiments were performed by using a weaker base. Using previous estimates on similar radicals, the pK_a of **4.3** is estimated to be approximately 9.[131] Pyridine was selected because it can behave as a weak base that would not be strong enough to fully deprotonate **4.3**. Additionally, it a poor electron donor which means PET is unlikely to be a competing pathway. Under these conditions depletion of **4.3** is observed, as expected, but there was minimal release of alcohol.

To verify that addition of hydroxide is generating anion radical **4.2**, a transient absorption spectrum was obtained in methanol with the addition of sodium hydroxide, as displayed in Figure 4.6. Addition of sodium hydroxide leads to formation of a broad

band in the 550-650 nm region. Previous work has assigned this broad signal to be the anion radical **4.2**.[123]

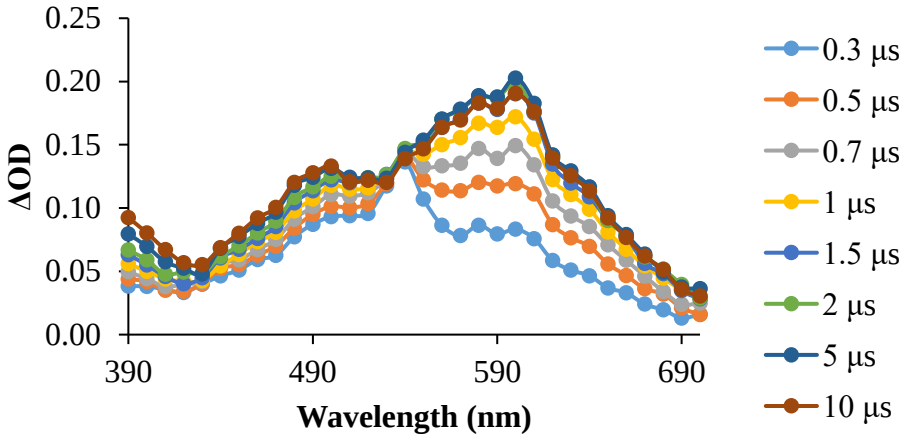

Figure 4.6. Transient absorption spectrum from the 355 nm pulsed photolysis of **4.5** in 3:1 methanol: 1,4-dioxane with the addition of 1 mM sodium hydroxide

Upon observing the increase in yields of **4.6** with increasing concentrations of sodium hydroxide, LFP experiments were performed to determine the effect of base concentration on formation of **4.2**. As seen in Figure 4.7, as the concentration of hydroxide increases, the rate at which **4.2** forms also increases. These data were used to perform a pseudo first-order analysis in order to determine the second-order rate constant for proton transfer between **4.3** and base. The rate constant was determined to be 1.84×10^{9} $M^{-1}s^{-1}$.

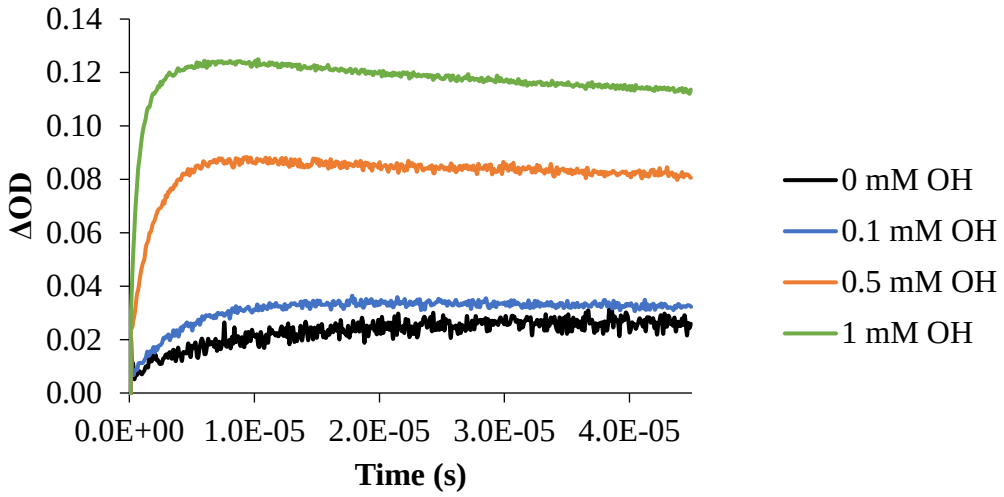

Figure 4.7. Kinetic traces taken at 620 nm to monitor the growth of anion radical **4.2** with increasing concentrations of sodium hydroxide. Starting ether concentration is 9 mM

4.4 Proposed Mechanism of Photorelease

The data in the previous section allow for a mechanism of photorelease to be proposed, as shown in Scheme 4.3. Upon excitation with 350 nm light, the PTO-ether is excited to its singlet state which rapidly undergoes intersystem crossing to form its triplet state. Because benzophenone generates its triplet state rapidly and with unit quantum yield,[132] it is believed that PTO-ethers behave similarly and the photochemistry that is observed is occurring exclusively from the triplet state. In the presence of a good hydrogen atom donor, the triplet state will abstract a hydrogen atom to generate ketyl radical **4.3**. From **4.3**, some alcohol release is observed but in poor yields and the remaining decomposition is due to formation of a complex mixture of by-products. The most likely by-products are the various isomers formed by dimerization of **4.3**. Similar products are observed where the structurally similar benzophenone ketyl radical is generated.[133] In the presence of a strong base, **4.3** is deprotonated to generate anion radical **4.2**. From **4.2**, C—O bond scission occurs to

cleanly release the alcohol. The absorption of **4.2** can be fitted to a first-order decay to derive a lifetime of ca. 1-2 ms. This value is the upper limit of lifetimes that can be accurately predicted with the LFP experimental setup.

Scheme 4.3. Proposed mechanism for the photorelease of alcohols under direct photolysis conditions

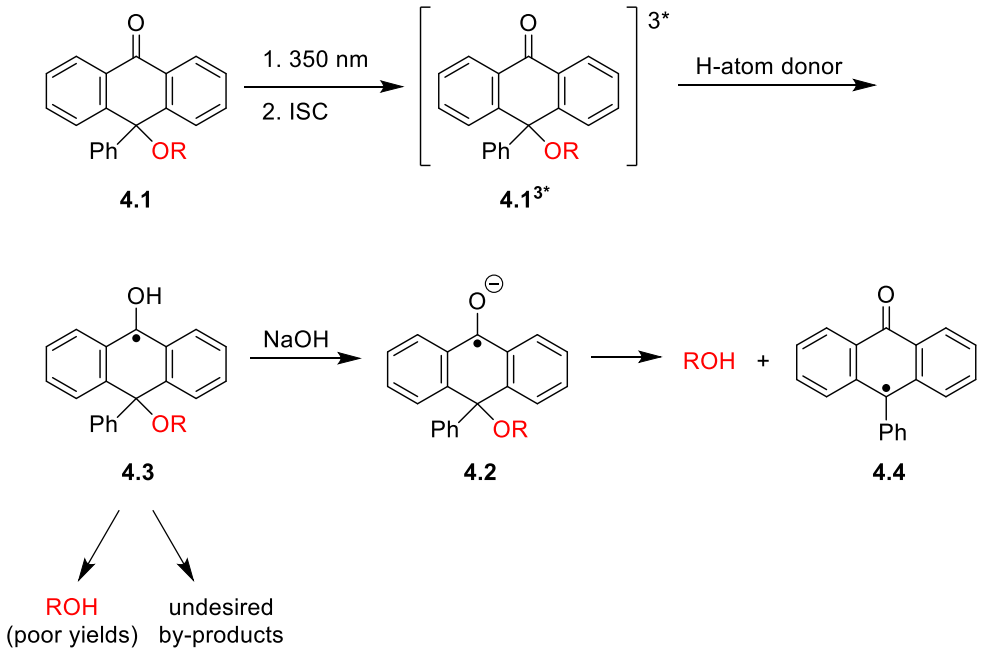

4.5 Modifications to the 9-Phenyl-9-tritylone Protecting Group

Upon determining that alcohol release occurs via the anion radical, attempts were made to improve the PTO group. Modifications were made in an effort to facilitate intramolecular electron transfer thus eliminating the need for an external electron donor. As outlined in Scheme 4.4, the phenyl group of the PTO-ether **4.1** was replaced with a with a 4-phenol group to make compound **4.7** which, upon photolysis, is expected to release 1-pentanol. With this design, it was anticipated that, upon deprotonation, the phenoxide anion would donate an electron to the tritylone moiety to generate the anion diradical **4.9**, which would subsequently release the alcohol.

Scheme 4.4. Proposed reaction for intramolecular electron transfer for alcohol release

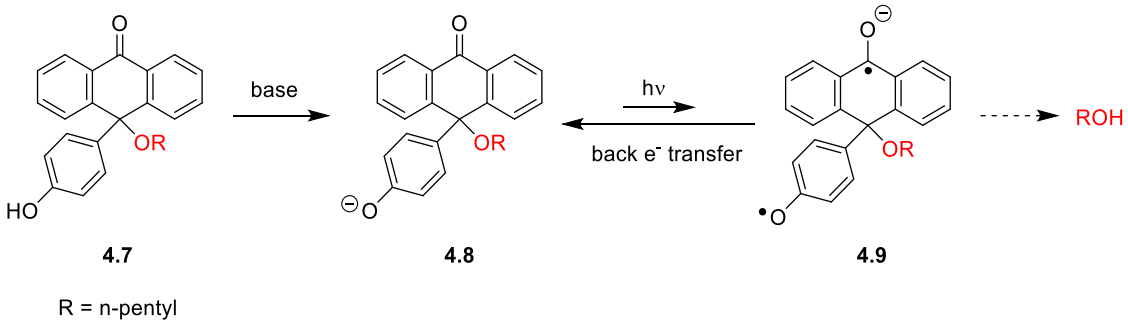

Figure 4.8 displays the UV-Vis absorption spectra of **4.7** at pH 7 and pH 14. Upon deprotonation, a new absorption band is observed with a maximum absorption at 362 nm and a tail extending out to approximately 500 nm. This band is not observed in neither the simple PTO group nor an isolated phenoxide ion (λ_{max} = 290 nm). Therefore, this band is attributed to a charge transfer absorption band from the phenoxide anion to the tritylone moiety.

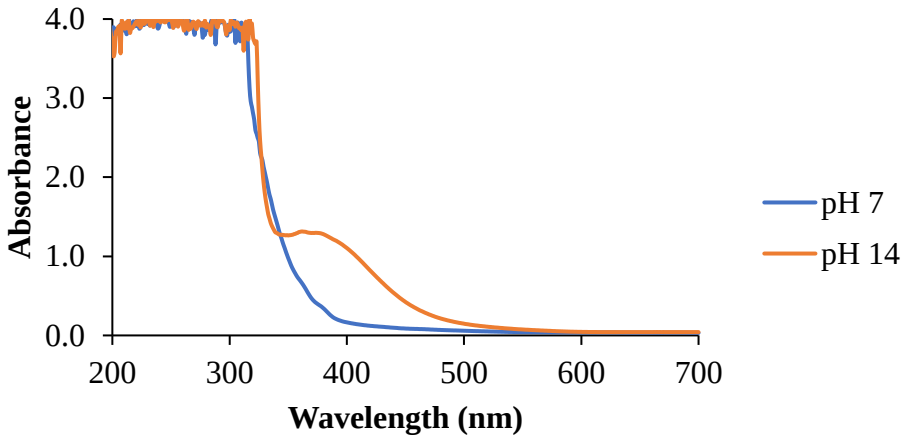

Figure 4.8. UV-Vis spectra of **4.7** in acetonitrile at pH 7 and pH 14

Unfortunately, prolonged photolysis (20 hours) of **4.7** in basic acetonitrile did not result in the release of 1-pentanol to any appreciable extent. The belief is that back electron transfer to return to the ground state occurs more rapidly than alcohol release. This can be further justified by LFP. The transient absorption spectrum of **4.7** in basic

acetonitrile, as shown in Figure 4.9, displays two absorption bands: one at 420 nm and the other at 510 nm. This spectrum is tentatively assigned as the triplet anion diradical **4.9**.

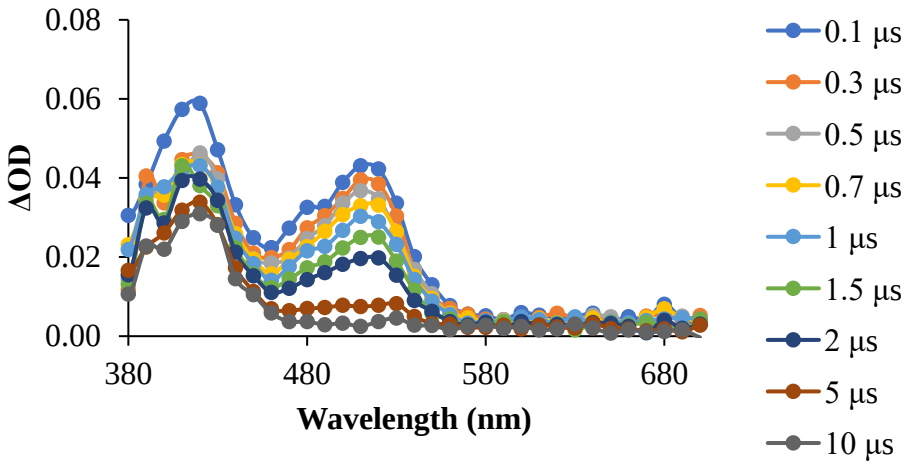

Figure 4.9. Transient absorption spectrum from the 355 nm pulsed photolysis of **4.7** in basic acetonitrile

This assignment is made on the basis of the following considerations: (1) extended photolysis of **4.7** in basic acetonitrile results in minimal decomposition suggesting that this spectrum is not due to radical or ionic fragmentation; (2) the spectrum differs in both position and shape from the spectra obtained from **4.5** (recall Figures 4.4, 4.5, and 4.6) indicating it is not a simple tritylone triplet, ketyl radical, or anion radical; (3) upon addition of oxygen, the band at 510 nm is quenched however the band at 420 nm is not. The 420 nm band is characteristic of a phenoxy radical which has an absorption at ca. 400 nm.[134] Further characterization of this intermediate can be done by computational modeling and ultrafast spectroscopy.

4.6 Conclusions

The experiments described in this chapter provide further insights into the mechanism of alcohol release from PTO-ethers. Through the use of laser flash photolysis as well as product analysis, it is confirmed that during photolysis both the ketyl radical and anion radical intermediates are generated but it is from the anion radical that C—O bond scission occurs to cleanly release the alcohol. However, under these conditions, alcohol release is relatively slow with the alcohol being released on the order of ca. 1 ms. Furthermore, the yield of alcohol under direct conditions is significantly less than those reported under PET conditions[123] indicating that, from a practical standpoint, direct photolysis is not the most beneficial route for alcohol deprotection from PTO-ethers.

Modifications were made to the PTO group to allow for intramolecular electron transfer in an attempt to eliminate the need for an external electron donor. Unfortunately, extended photolysis of this derivative did not demonstrate efficient alcohol release. The reason for inefficient photorelease is likely due to back electron transfer being more rapid than bond scission.

Chapter 5: Reactivity of Diarylnitrenium Ions Towards Guanosine

5.1 Introduction to Nitrenium Ions

Nitrenium ions are reactive intermediates which are classified as a divalent nitrogen species containing a lone pair of electrons and a formal positive charge.[135] They have properties similar to other electron deficient reactive intermediates including nitrenes, carbenes, and carbenium ions (Figure 5.1).

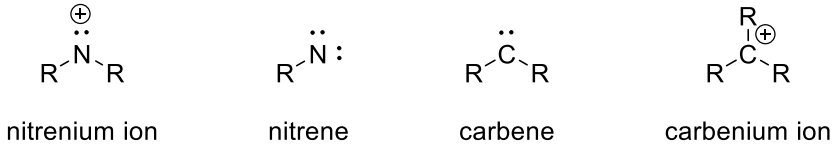

Figure 5.1. General structures of electron deficient reactive intermediates

Because nitrenium ions are divalent with two-nonbonding orbitals and two non-bonding electrons, they can exist in one of four possible electronic configurations as described in Figure 5.2. Due to differences in distribution of non-bonding electrons in the non-bonding orbitals, nitrenium ions can either exist in a singlet state or a triplet state. There are three possible configurations for the singlet state and one for the triplet state. For the singlet states, both electrons can be paired in the hybridized non-bonding n orbital (n^2 singlet), both electrons paired in the unhybridized non-bonding p orbital (p^2 singlet) or, one electron in each the n and p non-bonding orbitals with anti-parallel spins (n,p singlet). The triplet state forms when there is one electron in each the n and p non-bonding orbitals with parallel spins (n,p triplet). Singlet nitrenium ions exist as the n^2 singlet because the other configurations would require putting electrons into the higher energy p orbital. The differences in electronic configurations lead to differences

in reactivity. Typically, singlet nitrenium ions react with nucleophiles whereas triplet nitrenium ions behave as radicals and participate in hydrogen atom abstraction reactions.

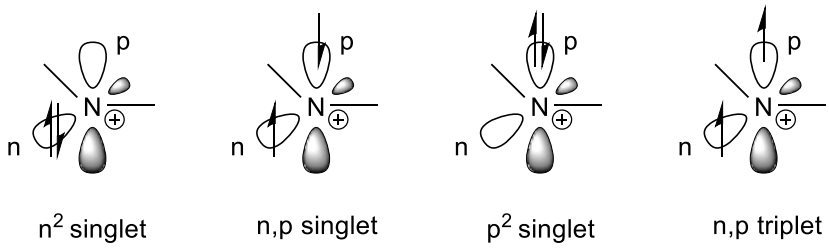

Figure 5.2. Possible electronic configurations for a nitrenium ion

Whether a nitrenium ion exists as a singlet or a triplet depends on the energy difference between the orbitals which is influenced by the ligands attached to the nitrogen. If the orbitals are close in energy, the triplet state will be the ground state due to Hund's rule. Structural changes that stabilize the n orbital or destabilize the p orbital will result in a larger energy gap and begin to favor the singlet state as the ground state. For example, the parent nitrenium ion, NH_2^+, is a ground state triplet whereas arylnitrenium ions are ground state singlets due to electron delocalization increasing the energy of the p orbital.[135-137]

5.2 Arylnitrenium Ions as Carcinogens

Arylnitrenium ions have received considerable attention due to their suspected involvement in DNA damaging reactions. Many aryl amines have been found to be known carcinogens and a few examples are shown in Figure 5.3.[138]

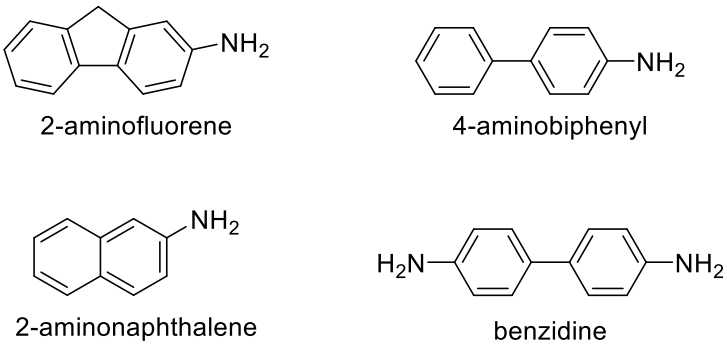

Figure 5.3. Examples of carcinogenic aryl amines

The most widely accepted mechanism for carcinogenesis involves metabolic generation of an arylnitrenium ion intermediate, as outlined in Scheme 5.1. *In vivo*, aryl amines are oxidized to the corresponding hydroxylamine followed by esterification to acetate esters or sulfate esters. The esters can readily undergo N—O heterolysis to generate the arylnitrenium ion which can then react with DNA.[139] Aryl amines predominately attach to the guanine residue of DNA and the major adduct is the nitrogen of the nitrenium ion attached to the C8 position of guanine.[140]

Scheme 5.1. Metabolic generation of arylnitrenium ions

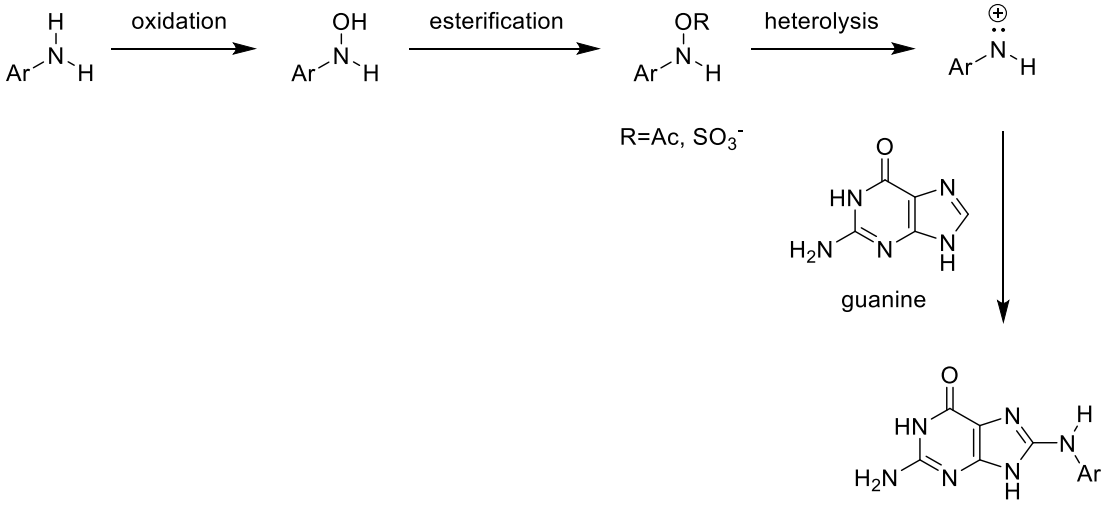

Further studies provide supporting evidence for the role of the nitrenium ion in DNA damaging reactions and extensive studies have been performed on the nitrenium

ions derived from 4-aminobiphenyl and 2-aminofluorene. With the ability to photochemically generate nitrenium ions and study them with LFP, their reactivity toward DNA can be studied and compared to their reactivity toward other nucleophiles.

One characteristic of some arylnitrenium ions that makes them viable intermediates in DNA damaging reactions is their relatively low reactivity towards water. For example, the 4-biphenylyl and 2-fluorenyl nitrenium ions decay in water with rate constants of 1.8×10^{6} s^{-1} and 3.4×10^{4} s^{-1}, respectively.[141] These rates suggest that arylnitrenium ions have sufficient aqueous lifetimes to allow for reactions with other nucleophiles. In addition to their low reactivity towards water, arylnitrenium ions also exhibit high reactivity towards guanosine. For example, the 4-biphenylyl and 2-fluorenyl nitrenium ions react with 2'-deoxyguanosine with rate constants of 2.0×10^{9} $M^{-1}s^{-1}$ and 7.6×10^{8} $M^{-1}s^{-1}$, respectively, which approaches the diffusion limit.[142]

The mechanism for the formation of the C8 adduct has been the subject of debate. Two different mechanisms have been proposed as described in Scheme 5.2. The first mechanism involves an initial addition to the N7 position, generating the N7 intermediate, followed by rearrangement to yield the C8 adduct. The second mechanism involves an initial addition directly to the C8 position, generating the C8 intermediate, followed by deprotonation to yield the C8 adduct.

Scheme 5.2. Proposed intermediates from the reaction of an arylnitrenium ion with guanine to yield the C8 adduct

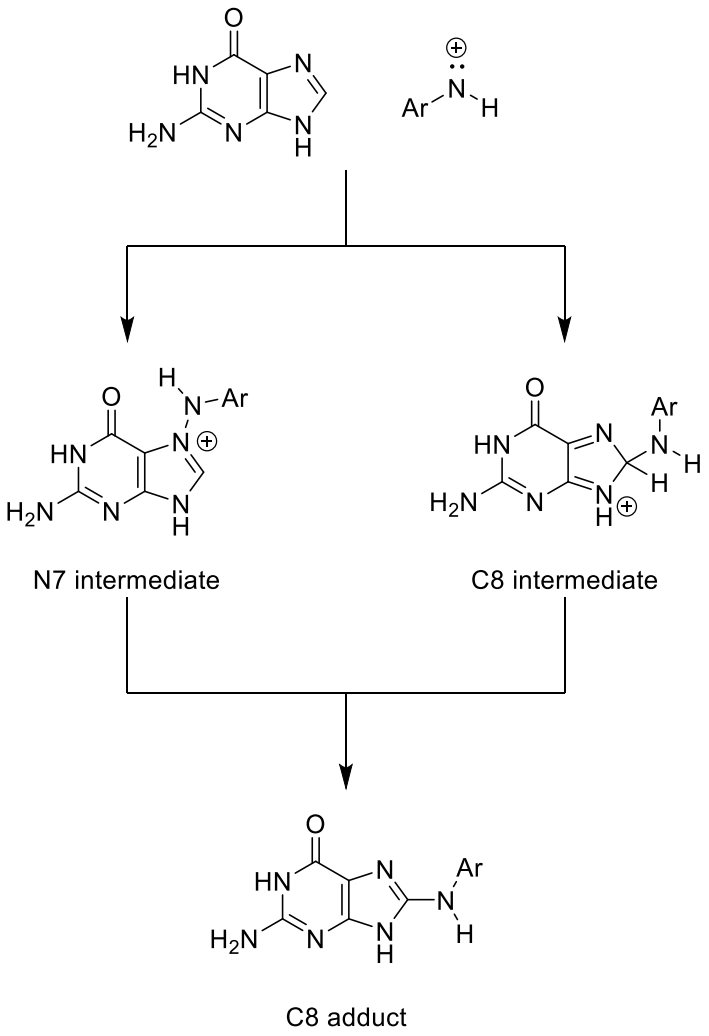

Humphreys and coworkers proposed initial addition to the N7 position due to the greater nucleophilicity of the N7 atom. Justification for this mechanism came from generating the 2-fluorenyl nitrenium ion in the presence of an 8-methyl guanine derivative. An unstable intermediate and reduction product were observed and characterized as N7 adducts.[143] Novak and coworkers supported this mechanism based upon kinetic analysis with different guanosine derivatives. It was observed that the rate constant for formation of the C8 adduct was dependent on the pK_a of the N7 position—

as the basicity of the N7 position decreased, the rate at which the nitrenium ion reacted also decreased, supporting initial addition to N7 followed by a 1,2-migration and deprotonation to yield the C8 adduct.[144]

Contrary to Humphreys and Novak, McClelland and coworkers claimed that arylnitrenium ions add directly to the C8 position. Using LFP, the 2-fluorenyl nitrenium ion was generated in the presence of 2'-deoxyguanosine (dG). The addition of dG increases the rate at which the signal corresponding to the nitrenium ion decays. Also observed was the growth of an absorption band at ca. 380 nm. The band grew in at the same rate as the disappearance of the nitrenium ion and was assigned as the C8 intermediate. Rate constants were measured for the reaction of the nitrenium ion with 8-deutero-dG and a kinetic isotope effect was observed indicating that the C8—H bond breaks in the rate determining step. In addition, an inverse secondary kinetic isotope effect was observed for the reaction of 4'-methoxybiphenylyl nitrenium ion with dG and 8-deutero-dG indicative of a change in hybridization from sp^2 to sp^3. These considerations suggest an initial addition to the C8 position followed by deprotonation to yield the C8 adduct.[145]

This chapter will study the behavior of diarylnitrenium ions towards guanosine to determine if their reactivity is similar to that of the monoarylnitrenium ions.

5.3 Generation of Diarylnitrenium Ions in the Presence of Guanosine

The diarylnitrenium ion that will be studied in this chapter is the *N*,*N*-di(4-bromophenyl)nitrenium ion **5.2**. Earlier studies by Falvey and coworkers demonstrated that this nitrenium ion can be generated by photolysis of *N*-(4,4'-dibromodiphenylamino)-2,4,6-trimethylpyridinium tetrafluoroborate **5.1**.[146] Upon

irradiation, this compound undergoes heterolytic cleavage to generate the nitrenium ion **5.2** as well as 2,4,6-collidine, as outlined in Scheme 5.3. This nitrenium ion was selected because the halogen substituents para to the nitrenium center significantly increases its lifetime relative to the unsubstituted derivative.[147]

Scheme 5.3. Photolysis of *N*-(4,4'-dibromodiphenylamino)-2,4,6-trimethylpyridinium tetrafluoroborate **5.1** to generate nitrenium ion **5.2**

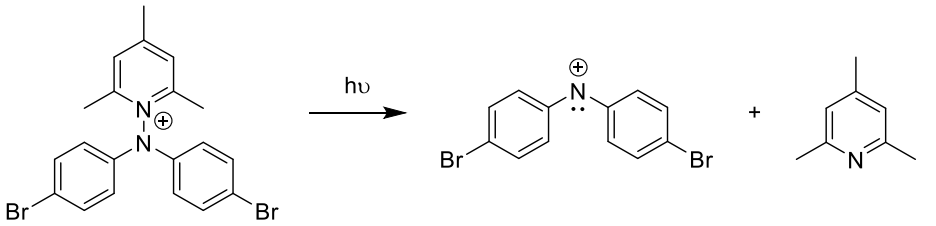

Figure 5.4 displays a transient absorption spectrum from the pulsed photolysis of pyridinium ion **5.1** in water. Immediately following the pulse, two bands are observed with maxima at 450 nm and 690 nm. These bands are consistent with the previously reported spectrum for the nitrenium ion **5.2**,[146] and are assigned as such. Both bands decay in a first-order fashion with a lifetime of 13.5 μs which indicates a relatively low reactivity towards water. This low reactivity towards water indicates the possibility for this nitrenium ion to survive long enough under biological conditions to react with DNA.

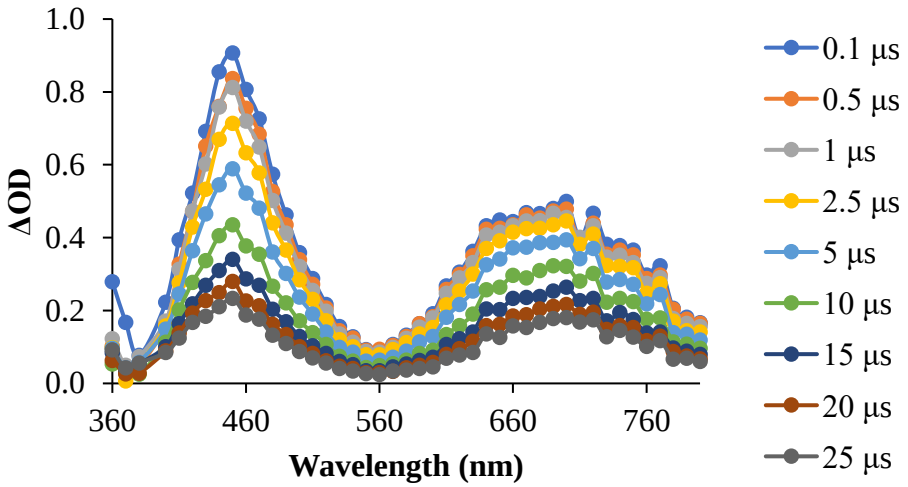

Figure 5.4. Transient absorption spectrum obtained from the pulsed 355 nm photolysis of **5.1** in 9:1 water: acetonitrile

Previous work examined the reaction of nitrenium ion **5.2** with 2'-deoxyguanosine monophosphate (dGMP) using LFP. It was shown that **5.2** reacts with dGMP with a second-order rate constant of 7.65×10^{8} $M^{-1}s^{-1}$.[146] However, no additional intermediates were detected nor were any products of the reaction characterized. To provide further insight into the biological reactivity of nitrenium ion **5.2**, these reactions were revisited using guanosine.

To determine the rate at which nitrenium ion **5.2** reacts with guanosine, kinetic decay traces monitored at 450 nm with increasing concentrations of guanosine were collected, which are displayed in Figure 5.5. As the concentration of guanosine increases, the rate at which **5.2** decays also increases. These data were used to perform a pseudo first-order analysis which resulted in a second-order rate constant of 2.48×10^{8} $M^{-1}s^{-1}$ for the reaction of **5.2** with guanosine. This result is consistent with the previous report for the reaction rate with dGMP.

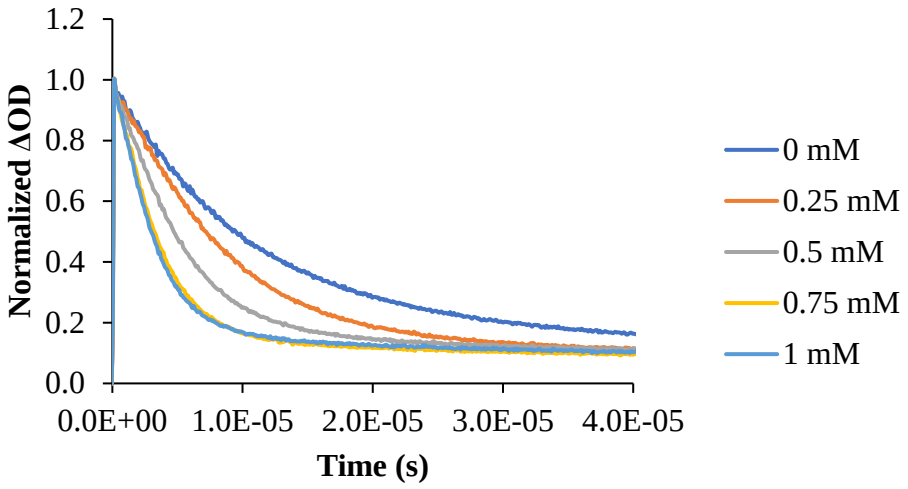

Figure 5.5. Kinetic traces collected at 450 nm corresponding to nitrenium ion **5.2** with increasing concentration of guanosine in 95:5 water: acetonitrile

To provide insight into the reaction between the nitrenium ion **5.2** and guanosine, a transient absorption spectrum was obtained in order to identify any intermediate species. Figure 5.6 displays the transient absorption spectrum obtained from the pulsed photolysis of pyridinium ion **5.1** with the addition of guanosine. When compared to the spectrum in the absence of guanosine, the lifetime of nitrenium ion **5.2** is significantly reduced. In addition, a band is observed growing in with a maximum absorption at 330 nm and a tail extending beyond 400 nm. This band forms at the same rate as the decay of the band corresponding to **5.2** which suggests that this species forms as a direct result of **5.2** reacting with guanosine. This intermediate shows no noticeable decay over 50 μs and no other intermediates are detected suggesting that this intermediate leads directly to the product of the reaction. This is similar to the results obtained by McClelland and coworkers, suggesting formation of the C8 intermediate.[145]

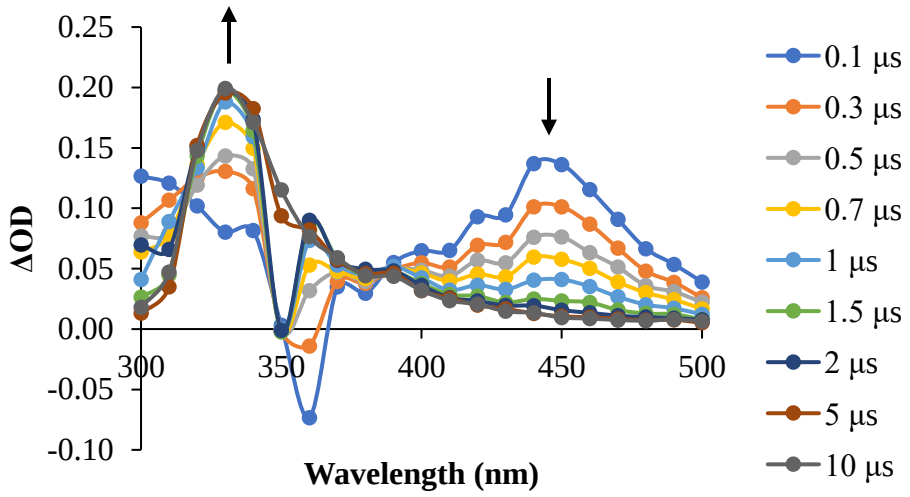

Figure 5.6. Transient absorption spectrum obtained from the pulsed 355 nm photolysis of **5.1** in 95:5 pH 7.3 water: acetonitrile with 2.22 mM guanosine

5.4 Product Analysis

Photoproduct analysis of the reaction between the nitrenium ion **5.2** and guanosine was performed in order to determine the nature of the adduct formed. Pyridinium ion **5.1** was photolyzed in the presence of guanosine and the isolated product was analyzed using mass spectrometry and ^{1}H NMR. Mass spectrometry confirmed adduct formation due to observation of a molecular ion peak with m/z=608.9135. Figure 5.7 displays the ^{1}H NMR spectra of the isolated product as well as pure guanosine and pure pyridinium ion **5.1**. The retention of symmetry of the aromatic peaks corresponding to the diaryl portion of the nitrenium ion is indicative of bond formation through the nitrogen, rather than at the ortho position. Additionally, the C8 proton of guanosine (δ = 7.93 ppm) is absent in the adduct indicating this is the site of bond formation in the adduct.

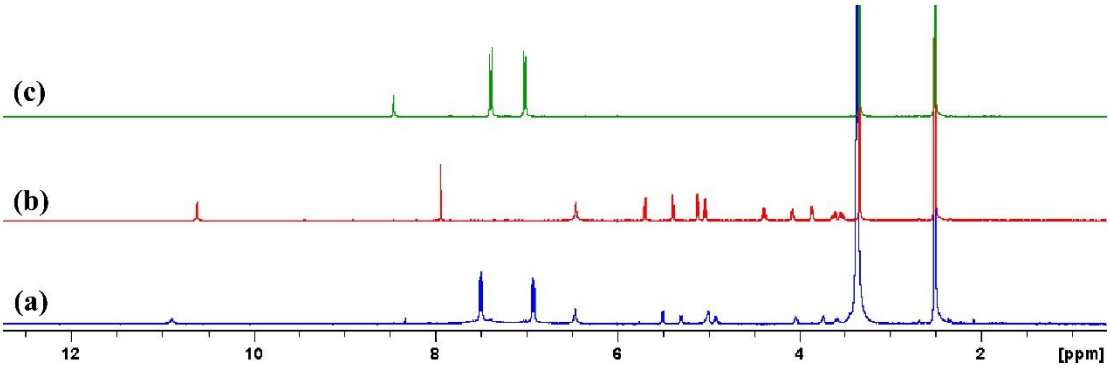

Figure 5.7. ^{1}H NMR analysis of the reaction between nitrenium ion **5.2** and guanosine. (a) Isolated product; (b) pure guanosine; (c) pure pyridinium ion **5.1**. All spectra in DMSO-d6

Based upon the LFP and product analysis, the reaction between nitrenium ion **5.2** and guanosine is proposed and shown in Scheme 5.4. Upon generation of the nitrenium ion **5.2**, the C8 carbon adds to the nitrogen of the nitrenium ion to generate the C8 intermediate which then undergoes deprotonation to yield the C8 adduct.

Scheme 5.4. Proposed reaction between nitrenium ion **5.2** and guanosine to generate the C8 adduct

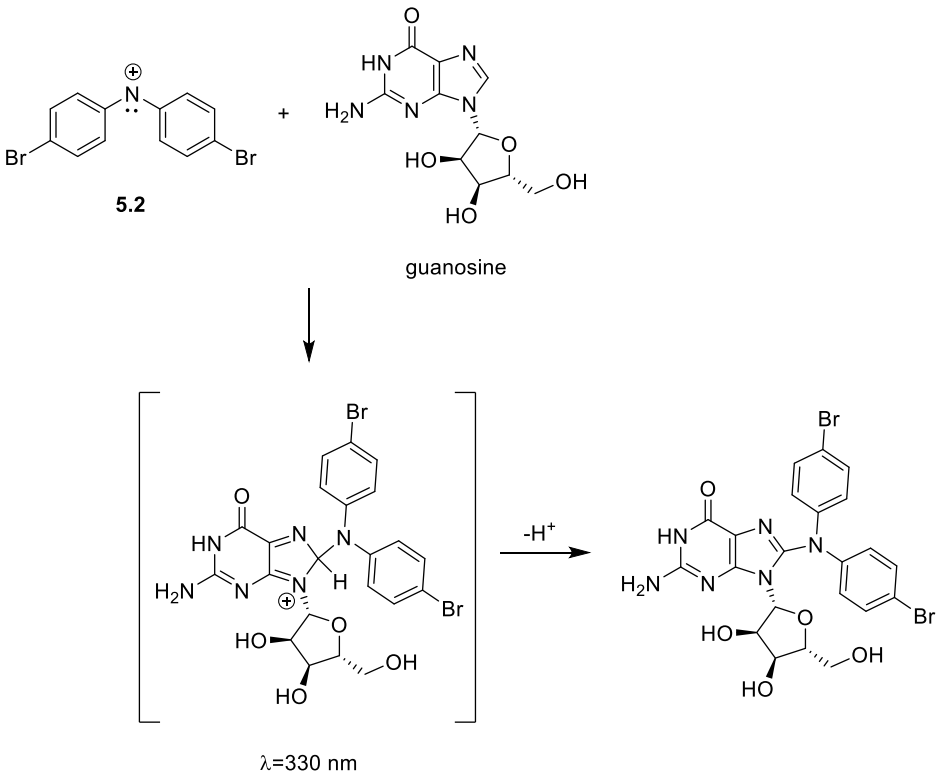

However, in 2020, Phillips and coworkers reported their results using the same system and conclude that the initial reaction between the nitrenium ion **5.2** and guanosine occurs at N7 followed by rearrangement to yield the C8 adduct. Through the use of nanosecond time-resolved resonance Raman spectroscopy and computational analysis, it was concluded that the calculated Raman spectrum for the N7 intermediate provided a better match with the experimental Raman spectrum.[148]

5.5 Conclusions & Future Directions

The experiments in this chapter examined the reaction between a diarylnitrenium ion and guanosine and it was found that, like monoarylnitrenium ions, the reaction occurs near the diffusion limit to yield a C8 adduct. However, there is still some uncertainty in the mechanism. To provide better insight into whether the N7 intermediate or the C8 intermediate is formed, a more in depth kinetic analysis must be performed. Kinetic isotope effect experiments similar to those performed by McClelland and coworkers could aid in the elucidation of the mechanism.

Chapter 6: Behavior of Diarylnitrenium Ions in Acidic Aqueous Solution

The majority of the work in this chapter has been published:[149]

Zeppuhar, A. N.; Falvey, D. E., Generation of *N*,*N*-Di(4-bromophenyl)nitrenium Ion under Acidic Conditions: Search for a Nitrenium Dication. *The Journal of Organic Chemistry* **2020,** *85* (14), 8844-8850

6.1 Nitrenium Dications

Although nitrenium ions are highly electrophilic and reactive, the aryl and diarylnitrenium ions have extensive charge delocalization from the nitrenium ion center into the aromatic ring, as illustrated in Scheme 6.1, which stabilizes them to an extent.

Scheme 6.1. Delocalization of positive charge in arylnitrenium ions

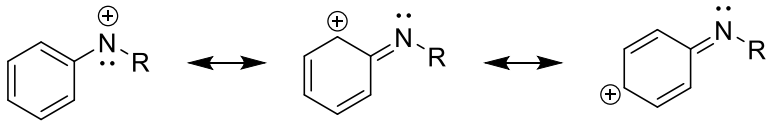

For this reason, it may be possible to form a nitrenium dication through protonation of the nitrogen lone pair. McClelland and coworkers found evidence of the formation of such a species through LFP studies of the 4-biphenylyl and 2-fluorenyl nitrenium ions acidic media.[150] Although the dication was not directly detected, its formation was inferred on the basis of the pH dependence on the decay kinetics of the nitrenium ion.

In a previous report by Falvey and coworkers, it was found that when *N*-(4,4'-dibromodiphenylamino)-2,4,6-trimethylpyridinium tetrafluoroborate **6.1** is photolyzed under acidic conditions the *N*,*N*-di(4-bromophenyl)nitrenium ion **6.2** is generated, as

expected. However, following its decay, a long-lived species was also observed which was identified as the cation radical **6.3** (Scheme 6.2).[146]

Scheme 6.2. Photolysis of *N*-(4,4'-dibromodiphenylamino)-2,4,6-trimethylpyridinium tetrafluoroborate **6.1** under acidic conditions to generate nitrenium ion **6.2** and cation radical **6.3**

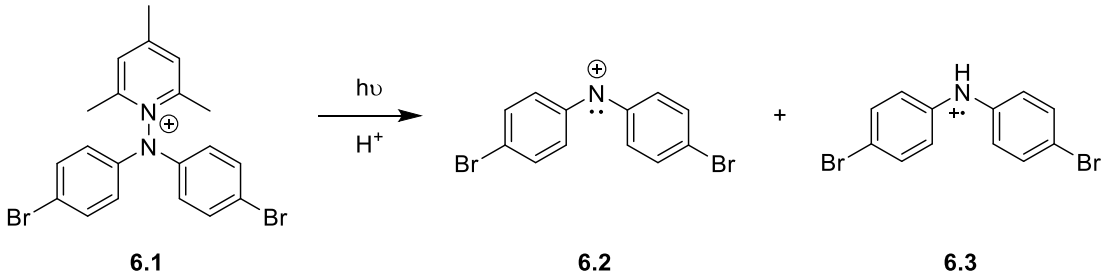

6.1 **6.2** **6.3**

Less clear was how the cation radical could be formed under these conditions. First, nitrenium ion **6.2** is calculated to be a ground state singlet. Cation radicals typically arise from hydrogen atom transfer to triplet state nitrenium ions. Second, formation of this species occurs at low pH which raises the possibility that it could be the dication **6.4** (Figure 6.1).

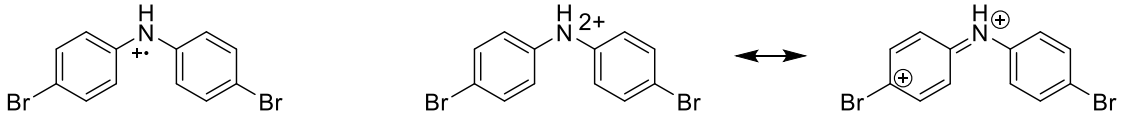

6.3 **6.4**

Figure 6.1. Possible identities of the long-lived species formed during photolysis of *N*-(4,4'-dibromodiphenylamino)-2,4,6-trimethylpyridinium tetrafluoroborate **6.1** under acidic conditions

In 2019, Phillips and coworkers studied the same system and reported the observation of dication **6.4**. Through the use of nanosecond time-resolved resonance Raman spectroscopy and computational analysis, it was concluded that the experimental spectrum was more consistent with the calculated spectrum for the dication **6.4** than for the cation radical **6.3**.[151]

However, one aspect left unaddressed is the unusually long lifetime of this species. Intuitively, it would be expected that a dication would be more reactive than the corresponding monocation (i.e., the nitrenium ion) due to the increased positive charge density. Indeed, McClelland's results are consistent with this expectation. Based upon their kinetic model, it is reported that the 4-biphenylyl nitrenium ion decays in aqueous solution with a rate constant of 1.1×10^{6} s^{-1} and the corresponding dication decays with a rate constant of 6.0×10^{7} s^{-1}.[150]

The ambiguities surrounding the formation and reactivity of the long-lived species encouraged a more detailed examination of this system. This chapter will revisit the behavior of *N*-(4,4'-dibromodiphenylamino)-2,4,6-trimethylpyridinium tetrafluoroborate **6.1** under acidic conditions using LFP and computational analysis to determine the identity of the long-lived species.

6.2 Generation of Diarylnitrenium Ions at Varying pH

The *N*,*N*-di(4-bromophenyl)nitrenium ion **6.2** was generated in the same manner as the previous chapter and is reiterated in Scheme 6.3.

Scheme 6.3. Photolysis of *N*-(4,4'-dibromodiphenylamino)-2,4,6-trimethylpyridinium tetrafluoroborate **6.1** to generate nitrenium ion **6.2**

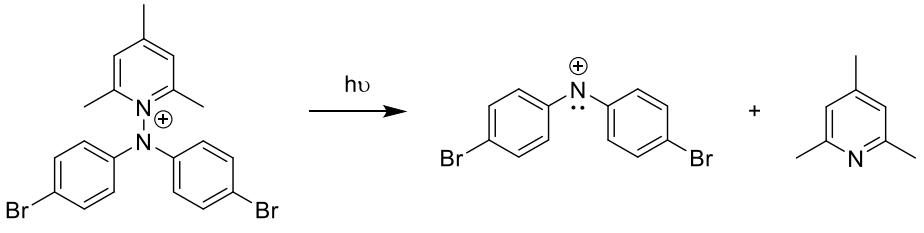

6.1 **6.2** **2,4,6-collidine**

Recalling from the previous chapter, when a transient absorption spectrum obtained from pulsed photolysis of **6.1** under neutral aqueous conditions, two bands at 450 nm

and 690 nm are observed and are assigned to nitrenium ion **6.2**. Figure 6.2 displays the spectrum on a longer timescale and following the decay of the nitrenium ion signals, little, if any, long-lived signals remain.

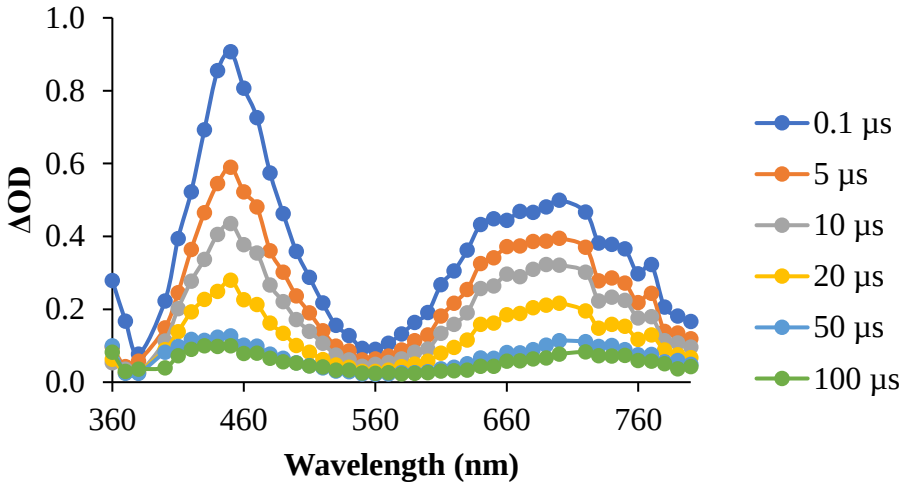

Figure 6.2. Transient absorption spectrum obtained from the pulsed 355 nm photolysis of **6.1** in 9:1 water: acetonitrile

When the experiment is performed under acidic aqueous conditions (pH 1.76), the same nitrenium ion signals are observed however, following their decay, long-lived signals at 350 nm and 720 nm are observed, as shown in Figure 6.3.

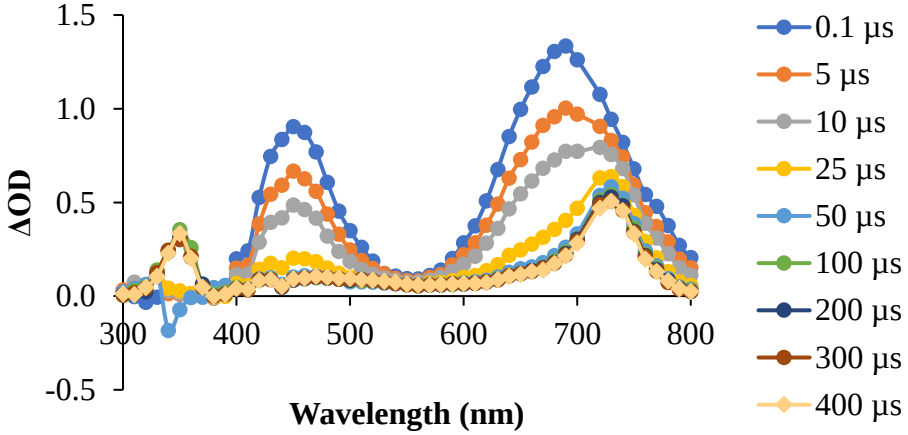

Figure 6.3. Transient absorption spectrum obtained from the 355 nm pulsed photolysis of **6.1** in 9:1 pH 1.76 water: acetonitrile

The latter signal overlaps with the long wavelength band of nitrenium ion **6.2**, however it is sharper and has a longer lifetime. In fact, the signal persists for over 500 μs. This signal is consistent with observations from previous reports involving LFP of **6.1** under nonaqueous, acidic conditions and has been attributed to cation radical **6.3**.[146]

To verify that cation radical **6.3** is a plausible potential assignment of this signal, the cation radical was generated via an alternative route. Lusztyk and coworkers demonstrated that arylamine cation radicals can be generated through photolysis of the corresponding nitrosamine under acidic conditions.[152] As outlined in Scheme 6.4, this methodology was applied to generate cation radical **6.3** under acidic aqueous conditions and the resulting transient absorption spectrum is displayed in Figure 6.4.

Scheme 6.4. Generation of cation radical **6.3** via photolysis of nitrosamine **6.5** under acidic conditions

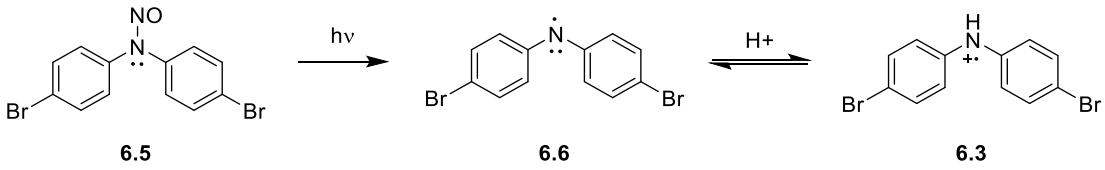

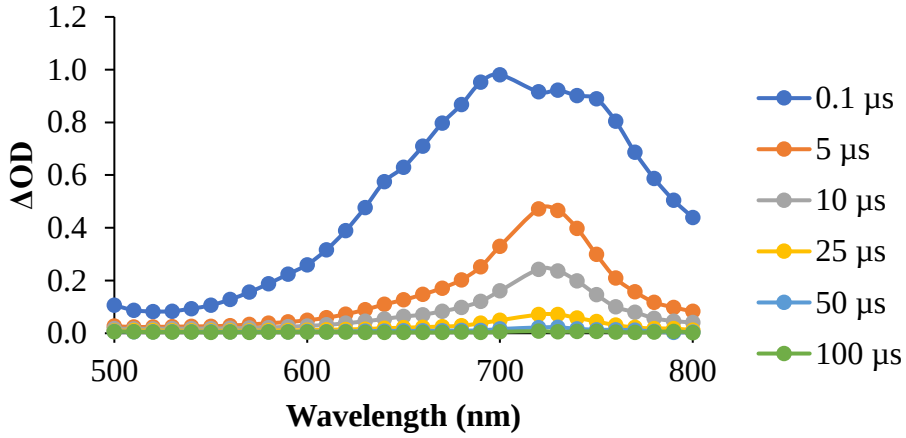

Figure 6.4. Transient absorption spectrum obtained from the 355 nm pulsed photolysis of **6.5** in 1:1 pH 1.90 water: acetonitrile

Immediately following the pulse, a broad signal centered around 700 nm is observed which decays into a sharper signal at 720 nm. The latter signal is consistent in both position and shape with that observed in Figure 6.3 indicating that the cation radical is plausible assignment of that signal.

If this species is indeed the cation radical **6.3**, its mechanism of formation is unclear. Generation of the cation radical **6.3** from the nitrenium ion **6.2** is the result of a net hydrogen atom transfer (Scheme 6.5, Eq. 1). The BDE for hydrogen atom abstraction from water is 119.3 kcal/mol[129] and thus it does not generally serve as a hydrogen atom donor. Furthermore, the fact that observation of this species occurs under acidic conditions still leaves open the possibility that it could be the dication **6.4** which would arise from protonation of the nitrenium ion **6.2** (Scheme 6.5, Eq. 2).

Scheme 6.5. Possible identities of the 720 nm species and routes to their generation

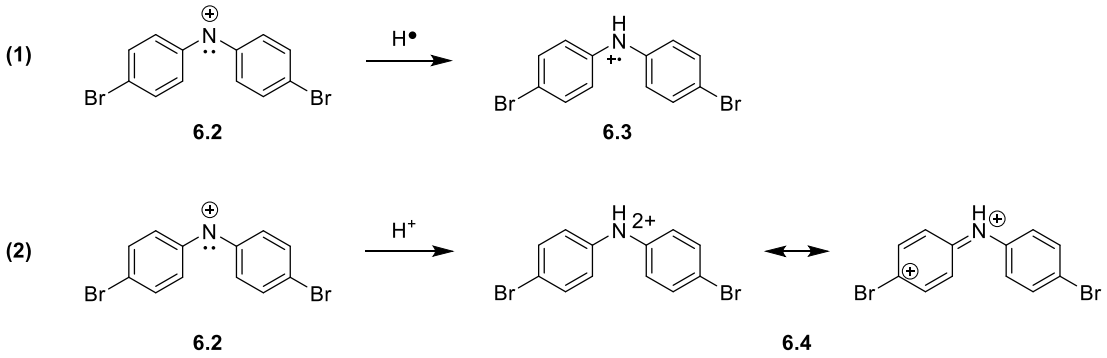

If formation of this species is the result of protonation of nitrenium ion **6.2**, then it would be expected that the rate that at which it forms would be increased as the concentration of hydronium increases, i.e., the decay of nitrenium ion **6.2** would increase with decreasing pH. To test for this, LFP was used to measure the decay rate of **6.2** in aqueous solution at varying pH values. Additionally, the yield of the 720 nm species (evaluated by comparing the initial signal to the persistent signal at 720 nm,

ΔA) as a function of pH was compared to the decay rates. These results are displayed in Figure 6.5.

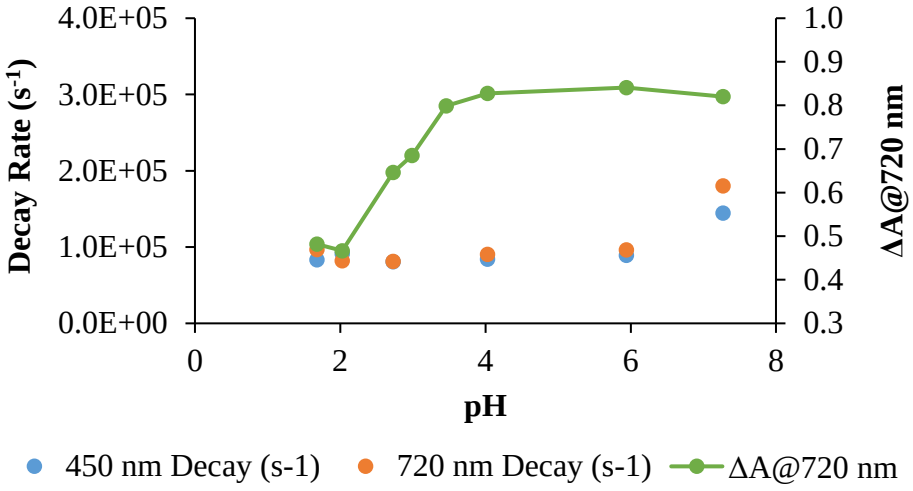

Figure 6.5. First-order decay rates of **6.2** at 450 nm (●) and 720 nm (●) in buffered water at varying pH. Change in initial vs. final absorbance at 720 nm (●)

Over the pH range of 1.7-5.9, there is less than 20% variation in the decay rate of **6.2** however, the yield of the long-lived species increases substantially as the pH decreases from 4 to 2. This experiment provides evidence that, regardless of the identity of the 720 nm species, it is not formed from direct protonation of **6.2**.

Because formation of the long-lived species does not appear to result directly from the nitrenium ion **6.2**, formation may be at the expense of **6.2**, i.e., from the same excited state intermediate. To test for this, LFP was used to measure the initial absorption at 450 nm, where only **6.2** absorbs, as a function of pH and, as seen in Figure 6.6, there is no apparent change. This indicates that the long-lived intermediate does not form from the same intermediate the gives rise to **6.2**.

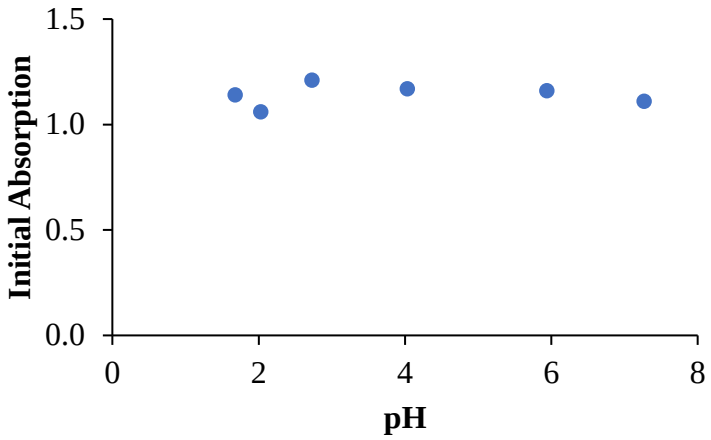

Figure 6.6. Initial absorption at 450 nm as a function of pH

6.3 DFT Calculations

To aid in the assignment of the long-lived species, DFT calculations were performed. Geometries of the singlet and triplet nitrenium ions **6.2**, the cation radical **6.3**, and the singlet and triplet dications **6.4** were optimized at the (U)M06-2X/6-311G++(d,p)[153, 154] level and the absorption spectra were calculated using TD-DFT. The calculated energetic predictions are summarized in Table 6.1.

Table 6.1. Calculated UV-Vis absorption bands and singlet-triplet energy splittings for the various intermediates considered in this study

Structure	Calculated λ_{max} (nm)	Oscillator Strength	ΔE_{st} (kcal/mol)
6.2 (Singlet)	400, 662	0.698, 0.283	-11.3
6.2 (Triplet)	302, 480	0.417, 0.387	
6.3	303, 763	0.394, 0.443	
6.4 (Singlet)	571	1.162	-6.8
6.4 (Triplet)	321, 674	0.311, 0.493	

The calculated absorption bands for the singlet nitrenium ion **6.2** show good agreement with the experimental. The calculations predict two strong bands in the short wavelength and long wavelength visible region, consistent with what is observed experimentally (recall Figure 6.2). The calculated spectra for two of the intermediates show reasonable agreement with the long-lived species. Both the cation radical **6.3** and the triplet dication **6.4** are expected to have absorption bands in the UV region as well as the long wavelength visible region. However, the triplet dication **6.4** is predicted to lie 6.8 kcal/mol above the singlet. It is unlikely that an excited triplet dication would have a lifetime of >500 μs.

6.4 Reactivity Toward Electron Donors

The experiments described thus far provide compelling evidence that this long-lived species is most likely the cation radical **6.3** rather than the dication **6.4**. To confirm that the reactivity of this species is consistent with that of a cation radical, an electron donor was added in order to quench the signal. The parent amine has an oxidation potential of +0.585 V[155] therefore, in order for electron transfer to be exergonic, the electron donor must possess a lower oxidation potential. *N*,*N*-dimethylaniline (DMA), which has an oxidation potential of 0.53 V,[156] was selected and a transient absorption spectrum was obtained, as displayed in Figure 6.7. Tetrabutylammonium chloride was also added in a sufficient concentration to suppress any direct reaction between nitrenium ion **6.2** and DMA.

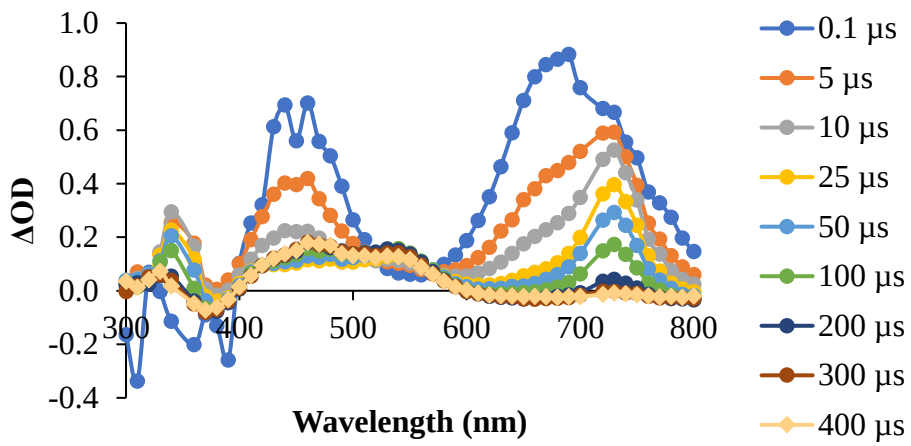

Figure 6.7. Transient absorption spectrum obtained from the 355 nm pulsed photolysis of **6.1** in 9:1 pH 1.9 water: acetonitrile in the presence of 0.947 mM DMA and 2.03 mM tetrabutylammonium chloride

Addition of DMA accelerates the decay the 720 nm species and a new band at 470 nm is formed at approximately the same rate. The 470 nm band is consistent with the previously reported spectrum of the DMA cation radical.[157] To determine the rate at which DMA quenches this signal, kinetic traces at 720 nm were collected with various concentrations of DMA, as displayed in Figure 6.8. Using the decay rate of the long-lived species, a pseudo first-order analysis was performed which provided a second-order rate constant of 5.00×10^{6} $M^{-1}s^{-1}$. This value is significantly lower than the diffusion limit however at the acidity necessary for generation of the long-lived intermediate, the majority of DMA is in its non-reactive, conjugate acid form (pK_a=5.1).[158]

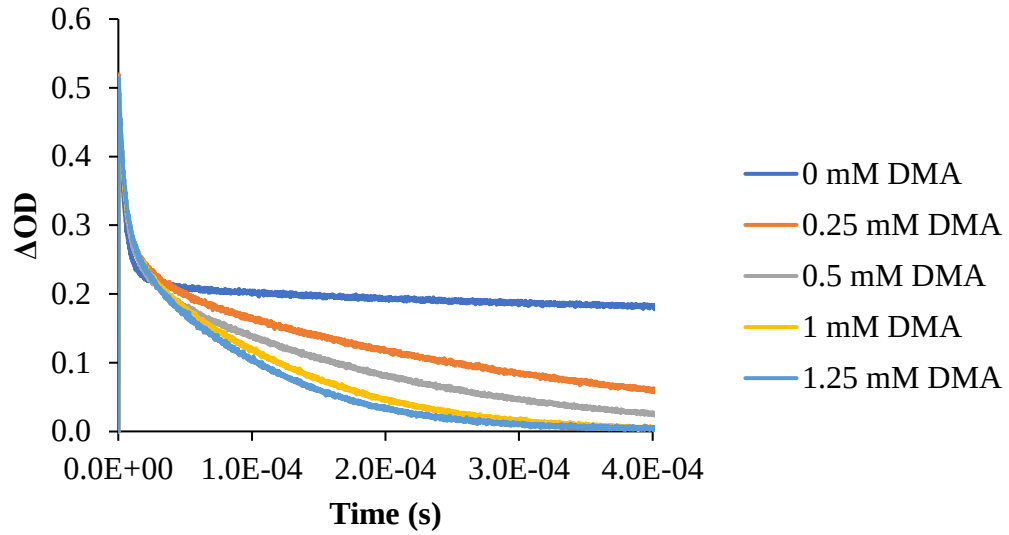

Figure 6.8. Kinetic traces resulting from 355 nm pulsed photolysis of **6.1** collected at 720 nm in 9:1 pH 2 water: acetonitrile with varying concentrations of DMA and 5.35 mM tetrabutylammonium chloride

Also examined was the reactivity of the long-lived species towards electron donors with higher oxidation potentials including 1,3,5-trimethoxybenzene (E_{ox}=1.49 V[159]) and 1,4-dimethoxybenzene (E_{ox}=1.34 V[159]). As seen in Figures 6.9 and 6.10, the long-lived species is unreactive towards both of these electron donors as evidenced by no observable change in lifetime as the concentration of electron donor is varied from 0-1 mM. This reactivity is consistent with what would be expected for the cation radical **6.3**.

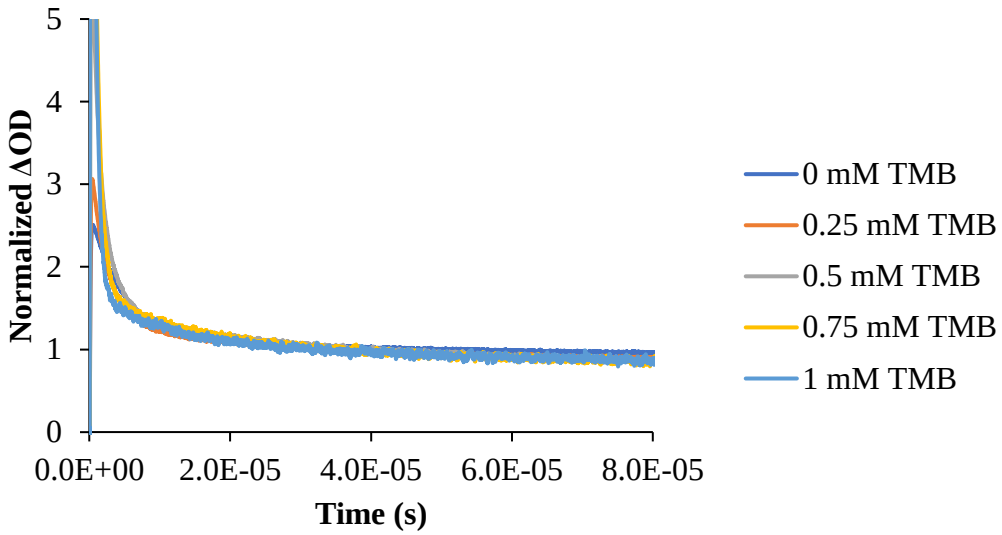

Figure 6.9. Kinetic traces resulting from 355 nm pulsed photolysis of **6.1** collected at 720 nm in 9:1 pH 2 water: acetonitrile with varying concentrations of 1,3,5-trimethoxybenzene (TMB) and 5.25 mM tetrabutylammonium chloride

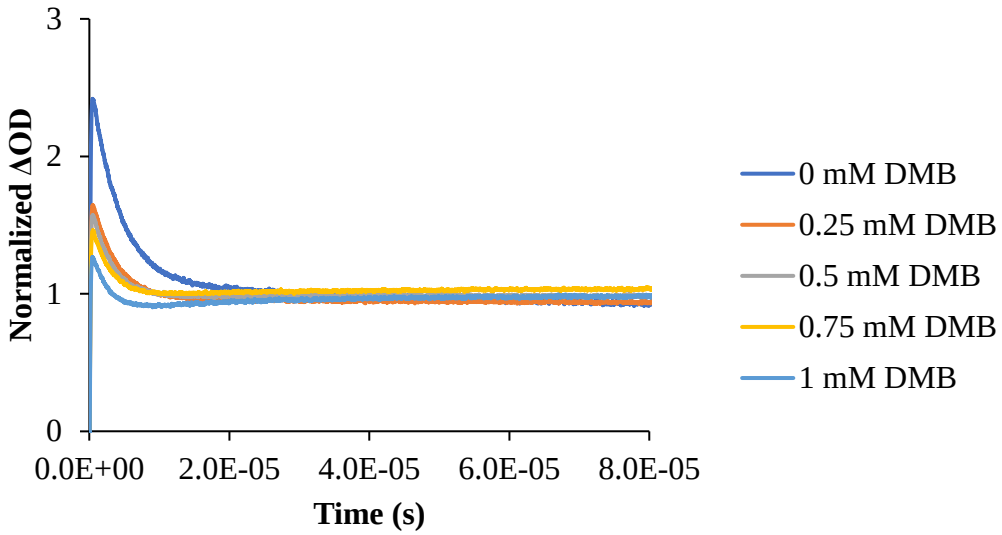

Figure 6.10. Kinetic traces resulting from 355 nm pulsed photolysis of **6.1** collected at 720 nm in 9:1 pH 2 water: acetonitrile with varying concentrations of 1,4-dimethoxybenzene (DMB) and 5.25 mM tetrabutylammonium chloride

6.5 Proposed Mechanism

The experiments described in this chapter provide strong evidence that this long-lived intermediate is indeed the cation radical **6.3**, as previously assigned.

However, its mechanism for formation remains to be addressed. Several experimental observations aid in the proposal of the pathway. Formation of this long-lived species only occurs at pH values less than 3, yet over the pH range of 2-6 there is no change in the initial yield nor the decay rate of the nitrenium ion **6.2**. This suggests that formation of **6.3** does not occur directly from **6.2** nor does it form at the expense of **6.2**. These observations indicate that formation of **6.3** is not from the same precursor that yields **6.2** which leads to the suggestion that **6.3** is formed from the excited triplet state of **6.1**, as proposed in Scheme 6.6.

Scheme 6.6. Proposed pathway for generation of **6.3** under acidic conditions

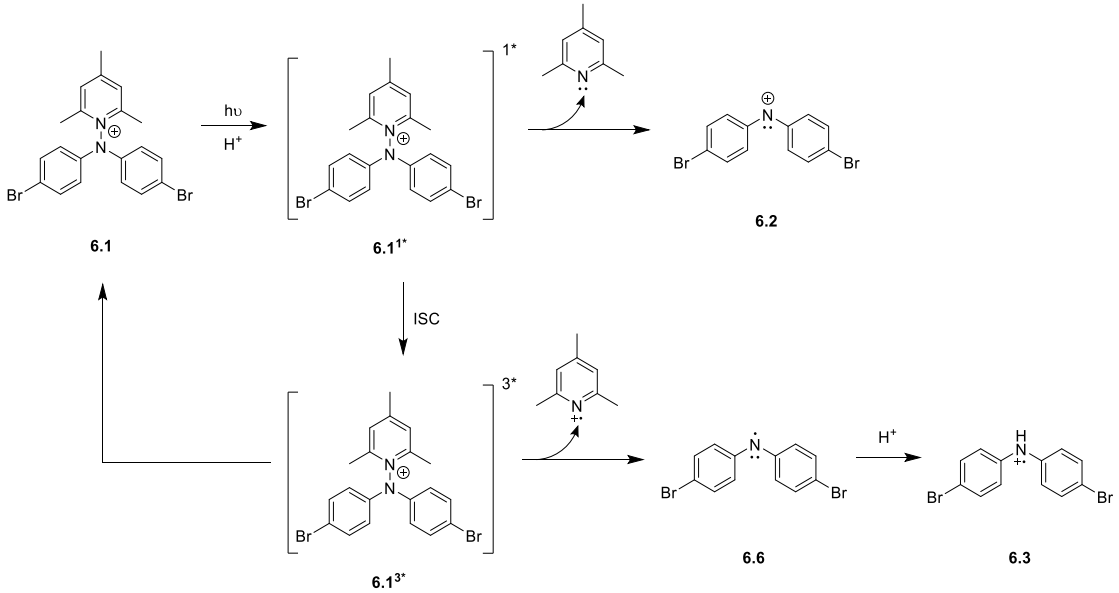

Initial excitation of **6.1** generates its excited singlet state. From here, heterolysis can occur to form the nitrenium ion **6.2** or it can undergo intersystem crossing to generate its first excited triplet state. Since the triplet state of **6.1** is not detected by LFP and addition of oxygen does not have a noticeable effect, it is predicted that the triplet state of **6.1** is very short-lived. The triplet state either relaxes back to ground state or, at low pH, undergoes acid-promoted formation of the cation radical **6.3**. At this time,

the specific steps involved in formation of **6.3** from the triplet state of **6.1** are not known. Homolysis of the N—N bond could occur from a protonated triplet state of **6.1** and form the cation radical **6.3** directly or homolysis could occur from the neutral triplet state to generate the aminyl radical **6.6** which would then be protonated to generate **6.3**. Several subtle shifts can be detected in the UV-Vis and ^{1}H NMR spectra of **6.1** at low pH as compared to neutral pH suggesting a pre-protonation of **6.1**.

6.6 Conclusions

The work described in this chapter revisits an earlier report where when *N*-(4,4'-dibromodiphenylamino)-2,4,6-trimethylpyridinium tetrafluoroborate is photolyzed at low pH, formation of a long-lived species is observed. Through LFP and computational analysis, the original assignment of the cation radical is reaffirmed. Quenching experiments demonstrate that this species is unreactive towards nucleophiles, but it is reactive toward strong electron donors, consistent with a cation radical. Mechanistic analysis with LFP demonstrate that pH does not affect formation or kinetic behavior of the nitrenium ion, suggesting that the cation radical forms via a pathway parallel to nitrenium ion generation. This pathway is likely through the excited triplet state of *N*-(4,4'-dibromodiphenylamino)-2,4,6-trimethylpyridinium tetrafluoroborate which, under acidic conditions, undergoes homolytic N—N cleavage and protonation to generate the cation radical. Future experiments could include ultrafast studies in order to further understand the early events in this process.

It should be noted that the experiments in this chapter were performed in aqueous solutions with 355 nm pulsed photolysis. There still remains a possibility of generating the dication in different solvents or via higher excited states.

Chapter 7: Supporting Information

7.1 General Methods

All chemicals and solvents were purchased from chemical suppliers and, unless otherwise stated, were used without further purification. ^{1}H NMR spectra were collected on a Bruker 400 MHz instrument. ^{13}C NMR spectra were collected using either a Bruker 400 MHz instrument or a Bruker 600 MHz instrument. Chemical shifts are reported in parts per million (ppm) and are referenced to the solvent signal. UV-Vis spectra were collected on a Shimadzu UV-1800 spectrometer using UVProbe 2.43 software. Samples were scanned using a fast scanning speed and a sampling interval of 1.0 nm. Each sample was blanked with the solvent of choice used in solvating the compound. Mass spectrometry experiments were performed on a JEOL AccuTOF-CS-ESI-TOF. Kinetic growth and decay curves were fitted using MATLAB software.

Laser flash photolysis experiments were conducted using a Nd:YAG laser supplied by Continuum with pulses 4-6 ns in duration as the excitation source. The probe beam that was used was a 350 W Xe arc lamp that passed through a monochromator to a PMT detector. Samples were prepared such that the absorption at the excitation wavelength was between 0.75 and 1.5. When obtaining a full spectrum, a fresh supply of the reaction mixture into the cuvette was attained by setting up a nitrogen purged flow cell that connects the cuvette to a stock solution via a double-headed needle. The photolyzate is then drained from the cuvette into a waste vessel. This setup prevents accumulation of photoproducts and avoids the depletion of the substrate during the experiment. For two-color experiments, the beams were aligned such that they were coincident.

7.2 Chapter 2 Experimental

7.2.1 Synthesis

1-hydroxy-2-methoxy-9,10-anthraquinone (2.3):[160]

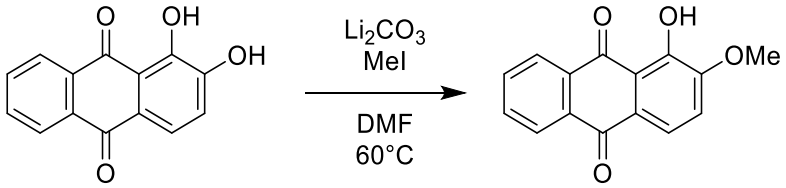

In a 50 mL round bottom flask equipped with a stir bar, 1,2-dihydroxyanthraquinone (2.4068 g, 10.02 mmol) and lithium carbonate (1.8499 g, 25.04 mmol) were dissolved in 25 mL of dry DMF. Methyl iodide (1.56 mL, 25.06 mmol) was added and the reaction was stirred at 60°C for 24 hours. Upon completion of the reaction, the reaction mixture was poured into 250 mL of 10% aqueous hydrochloric acid. The resulting solution was filtered and purified using flash chromatography with a mobile phase of 3:7 hexanes: chloroform to yield 2.2724 g (89%) of 1-hydroxy-2-methoxy-9,10-anthraquinone. ^{1}H NMR consistent with literature.[160]

1-tosyloxy-2-methoxy-9,10-anthraquinone (2.1a):

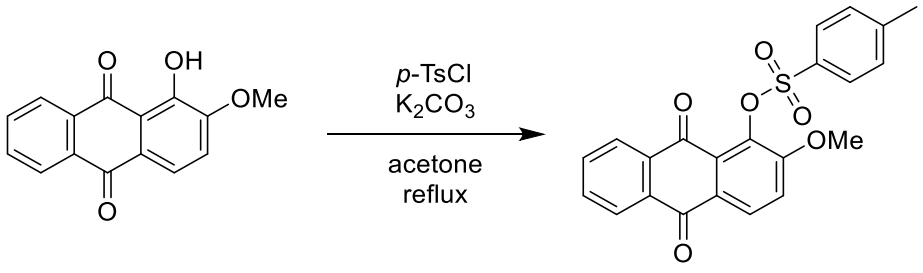

Following a procedure for tosylating hydroxyanthraquinone derivatives,[161] in a 50 mL round bottom flask equipped with a stir bar, 1-hydroxy-2-methoxyanthraquinone (0.2014 g, 0.792 mmol) was dissolved in 25 mL of

acetone. *p*-Toluenesulfonyl chloride (0.4104 g, 2.15 mmol) and potassium carbonate (2.1618 g, 15.6 mmol) were added and the reaction mixture was stirred at reflux for 4 hours. Upon completion of the reaction, the solution was left to cool to room temperature and the solvent was removed under reduced pressure. The crude mixture was redissolved in ethyl acetate and decanted from the potassium carbonate. The ethyl acetate was removed under reduced pressure and the resulting crude solid was purified using flash chromatography with a mobile phase of 1:4 ethyl acetate: hexanes to yield 0.2559 g (79%) of pure 1-tosyloxy-2-methoxy-9,10-anthraquinone. ^{1}H NMR (400 MHz, CD_3CN) δ = 8.27-8.25 (d, 1H), 8.20-8.18 (m, 1H), 8.02-8.00 (m, 1H), 7.85-7.82 (m, 2H), 7.68-7.66 (d, 2H), 7.41-7.39 (d, 1H), 7.37-7.34 (d, 1H), 3.52 (s, 3H), 2.40 (s, 3H). ^{13}C NMR (600 MHz, $CDCl_3$) δ = 181.12, 180.81, 157.27, 144.28, 136.29, 134.28, 134.16, 133.48, 133.32, 132.12, 128.86, 127.98, 127.73, 126.92, 126.73, 126.21, 116.11, 55.60, 21.16 (1 peak not accounted for and could be overlapping with previous peaks). HRMS (ESI+) Calcd for $C_{22}H_{16}O_6S$ $[M+H]^+$: 409.0740, Found: 409.0755

1-(trifluoromethylsulfonoxy)-2-methoxy-9,10-anthraquinone (2.1b):

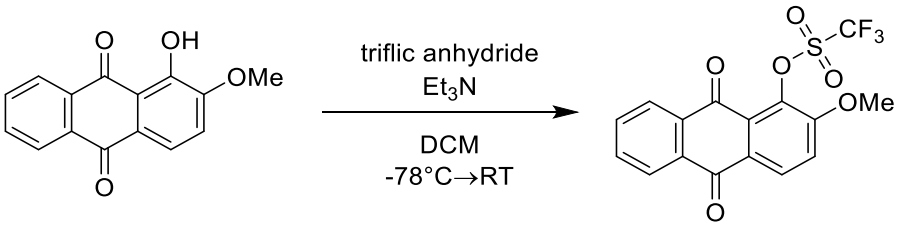

Following a procedure for preparation of a similar compound,[162] in a 50 mL round bottom flask equipped with a stir bar, 1-hydroxy-2-methoxyanthraquinone (0.2469 g, 0.971 mmol) was dissolved in 10 mL of

dichloromethane and the solution was cooled to -78°C. Triethylamine (0.6 mL, 4.30 mmol) was added and the reaction mixture was stirred for 5 minutes. Triflic anhydride (0.7 mL, 4.16 mmol) was then added dropwise and the reaction mixture was allowed to warm to room temperature. Upon completion of the reaction, the mixture was washed twice with saturated sodium bicarbonate. The organic layer was dried over magnesium sulfate and the solvent was removed under reduced pressure. The resulting solid was recrystallized from ethanol to yield 0.1298 g (35%) of 1-(trifluoromethylsulfonoxy)-2-methoxy-9,10-anthraquinone. ^{1}H NMR (400 MHz, $CDCl_3$) δ = 8.45-8.42 (d, 1H), 8.36-8.33 (m, 1H), 8.31-8.28 (m, 1H), 7.84-7.81 (m, 2H), 7.45-7.43 (d, 2H), 4.06 (s, 3H). ^{13}C NMR (600 MHz, $CDCl_3$) δ = 180.91, 180.53, 155.82, 135.80, 133.92, 133.86, 133.58, 132.03, 128.79, 127.14, 126.63, 126.46, 126.36, 116.67, 56.19 (1 peak not accounted for and could be overlapping with previous peaks). HRMS (ESI+) Calcd for $C_{16}H_9O_6F_3S$ $[M+H]^+$: 387.0145, Found: 387.0141

1-tosyloxy-9,10-anthraquinone (2.8):[163]

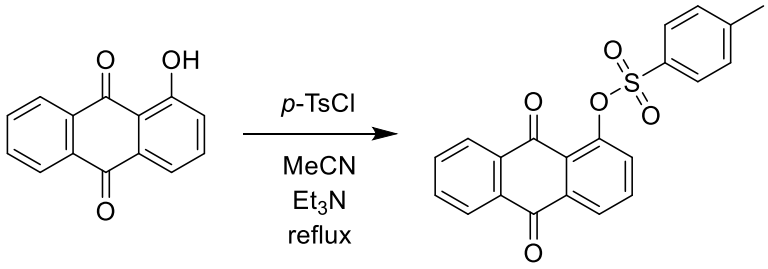

In a 250 mL round bottom flask equipped with a stir bar, 1-hydroxyanthraquinone (0.9864 g, 4.40 mmol) was dissolved in 80 mL of acetonitrile. Triethylamine (4 mL) and *p*-toluenesulfonyl chloride (1.6871 g,

8.85 mmol) was added and the reaction mixture was stirred at reflux for 5 hours. Upon completion of the reaction, the solvent was removed under reduced pressure. The resulting solid was dissolved in dichloromethane and washed with water three times. The organic layer was dried over magnesium sulfate and the solvent was removed under reduced pressure. The resulting solid was dissolved in 6 mL of hot chloroform and then 14 mL of hot petroleum ether was added. The solution was allowed to cool to room temperature and then placed in an ice bath for 15 minutes. The slurry was filtered to yield 0.8473 g (51%) of pure 1-tosyloxy-9,10-anthraquinone. ^{1}H NMR consistent with literature.[163]

1-hydroxy-2-(2-(2-(2-hydroxyethoxy)ethoxy)ethoxy)anthracene-9,10-dione:

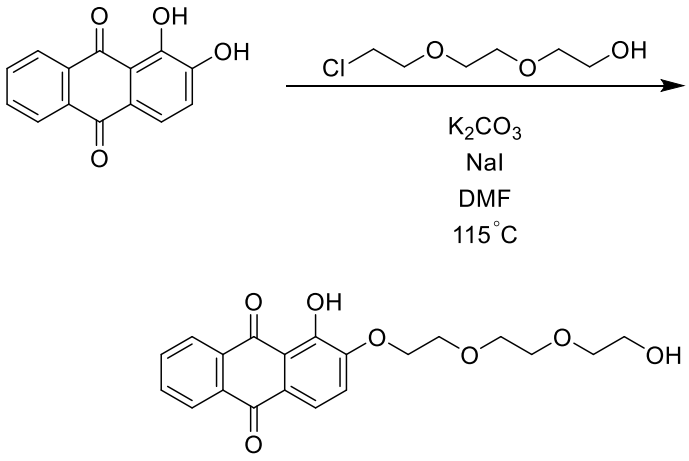

In a 25 mL round bottom flask equipped with a stir bar, 1,2-dihydroxyanthraquinone (0.7110 g, 2.96 mmol) was dissolved in 7 mL of DMF. Potassium carbonate (0.8291 g, 6.00 mmol) was added and the solution was stirred at 115°C for 30 minutes. 2-(2-(2-chloroethoxy)ethoxy)ethanol (0.54 mL, 3.71 mmol) and sodium iodide (0.0671 g, 0.45 mmol) were added and the reaction was stirred for 24 hours. Upon completion of the reaction, the reaction

mixture was poured into 75 mL of 10% aqueous hydrochloric acid. The resulting mixture was extracted with dichloromethane and the organic layer was dried over magnesium sulfate. The solvent was removed under reduced pressure and the resulting solid was purified using flash chromatography with a mobile phase of 95:5 chloroform: methanol to yield 0.4029 g (37%) of 1-hydroxy-2-(2-(2-(2-hydroxyethoxy)ethoxy)ethoxy)anthracene-9,10-dione. ^{1}H NMR (400 MHz, DMSO-d6) δ = 12.76 (s, 1H), 8.27-8.25 (m, 1H), 8.21-8.19 (m, 1H), 7.96-7.93 (m, 2H), 7.76-7.74 (d, 2H), 7.50-7.48 (d, 2H), 4.59-4.56 (t, 1H), 4.31-4.28 (m, 2H), 3.84-3.82 (m, 2H), 3.64-3.62 (m, 2H), 3.57-3.52 (m, 2H), 3.50-3.47 (m, 2H), 3.44-3.41 (m, 2H).

2-(2-(2-(2-hydroxyethoxy)ethoxy)ethoxy)-9,10-dioxo-9,10-dihydroanthracen-1-yl 4-methylbenzenesulfonate (2.10):

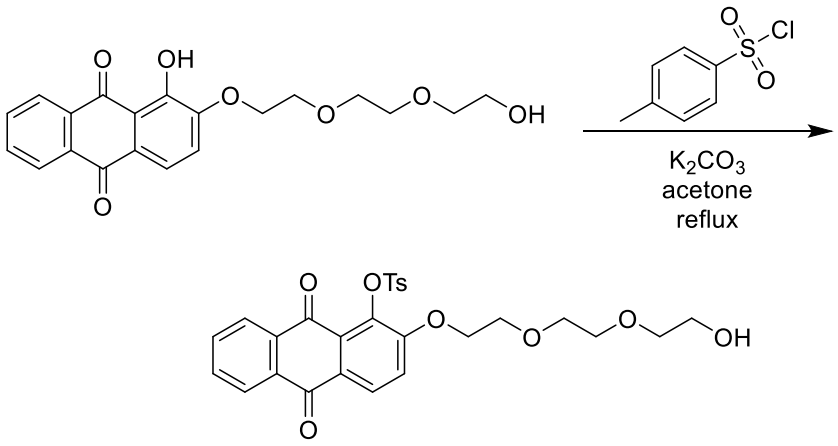

In a 50 mL round bottom flask equipped with a stir bar, 1-hydroxy-2-(2-(2-(2-hydroxyethoxy)ethoxy)ethoxy)anthracene-9,10-dione (0.2559 g, 0.687 mmol) was dissolved in 25 mL of acetone. *p*-Toluenesulfonyl chloride (0.4122 g, 2.16 mmol) and potassium carbonate (1.9207 g, 13.9 mmol) were added and the reaction mixture was stirred at reflux for 3 hours. Upon completion of the

reaction, the solution was left to cool to room temperature and the solvent was removed under reduced pressure. The crude mixture was redissolved in ethyl acetate and decanted from the potassium carbonate. The ethyl acetate was removed under reduced pressure and the resulting crude solid was purified using flash chromatography with chloroform as the mobile phase to yield 2-(2-(2-(2-hydroxyethoxy)ethoxy)ethoxy)-9,10-dioxo-9,10-dihydroanthracen-1-yl 4-methylbenzenesulfonate.

2-(2-(dimethylamino)ethoxy)-1-hydroxyanthracene-9,10-dione:

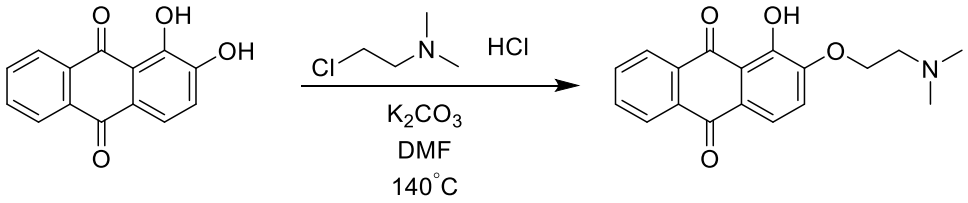

In a 25 mL round bottom flask equipped with a stir bar, 1,2-dihydroxyanthraquinone (0.5188 g, 2.16 mmol) and potassium carbonate (2.0304 g, 14.7 mmol) were dissolved in 10 mL of DMF and the mixture was heated to 140°C. 2-chloro-*N*,*N*-dimethylethylamine hydrochloride (0.9343 g, 6.49 mmol) was slowly added and the reaction was stirred for 26 hours. Upon completion of the reaction, the reaction mixture was poured into water and extracted with ethyl acetate. The organic layer was dried over magnesium sulfate and the solvent was removed under reduced pressure. The crude product was purified using flash chromatography with a mobile phase of 100% chloroform to 95:5 chloroform: methanol to yield 0.0549 g (8%) of pure 2-(2-(dimethylamino)ethoxy)-1-hydroxyanthracene-9,10-dione. ^{1}H NMR (400 MHz, DMSO-d6) δ = 8.27-8.24 (m, 1H), 8.21-8.19 (m, 1H), 7.96-7.93 (m, 2H),

7.76-7.74 (d, 1H), 7.51-7.49 (d, 1H), 4.27-4.24 (t, 2H), 2.76-2.74 (t, 2H), 2.28 (s, 6H).

2-(2-(dimethylamino)ethoxy)-9,10-dioxo-9,10-dihydroanthracen-1-yl 4-methylbenzenesulfonate (conjugate base of 2.11):

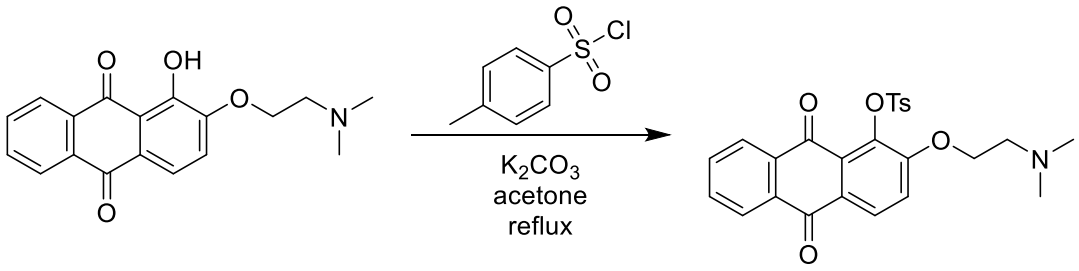

In a 25 mL round bottom flask equipped with a stir bar, 2-(2-(dimethylamino)ethoxy)-1-hydroxyanthracene-9,10-dione (0.0549 g, 0.176 mmol) was dissolved in 10 mL of acetone. *p*-Toluenesulfonyl chloride (0.1035 g, 0.543 mmol) and potassium carbonate (0.5061 g, 3.66 mmol) were added and the reaction mixture was stirred at reflux for 4 hours. Upon completion of the reaction, the solution was left to cool to room temperature and the solvent was removed under reduced pressure. The crude mixture was redissolved in ethyl acetate and decanted from the potassium carbonate. The ethyl acetate was removed under reduced pressure. Crude ^{1}H NMR (400 MHz, DMSO-d6) δ = 8.26-8.24 (d, 1H), 8.15-8.13 (m, 1H), 7.91-7.89 (m, 2H), 7.82-7.80 (m, 1H), 7.74-7.72 (d, 1H), 7.69-7.67 (d, 2H), 7.41-7.39 (d, 2H), 4.40-4.37 (t, 2H), 3.28-3.27 (t, 2H), 2.37 (s, 3H), 1.99 (s, 6H). The crude solid was purified using flash chromatography with chloroform as the mobile phase however, the ^{1}H NMR of the isolated product displayed signals that were shifted relative to the crude. There is a possibility that unwanted chemistry occurred during the purification

process. The addition of acid to the purified compound did not result in significant water solubility.

1-hydroxy-2-(2-hydroxyethoxy)anthracene-9,10-dione:

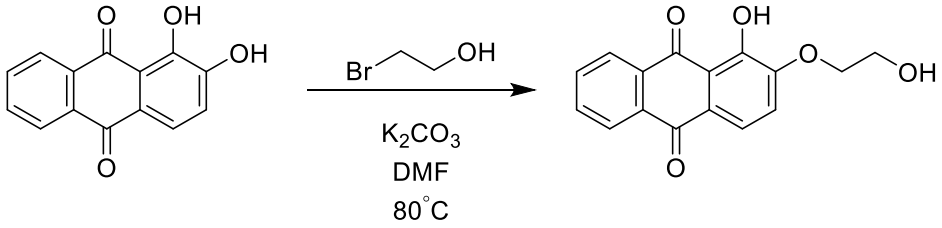

In a 50 mL round bottom flask equipped with a stir bar, 1,2-dihydroxyanthraquinone (0.9980 g, 4.15 mmol) and potassium carbonate (1.1831 g, 8.56 mmol) were dissolved in 15 mL of DMF and the solution was stirred at 80°C for 30 minutes. 2-bromoethanol (1.0 mL, 14.1 mmol) was added and the reaction was stirred for 20 hours. Upon completion of the reaction, the reaction mixture was poured into 100 mL of 10% aqueous hydrochloric acid. The resulting solution was vacuum filtered and the crude solid was purified using flash chromatography with a mobile phase of 3:1 chloroform: ethyl acetate to yield pure 1-hydroxy-2-(2-hydroxyethoxy)anthracene-9,10-dione. ^{1}H NMR (400 MHz, DMSO-d6) δ = 12.74 (s, 1H), 8.27-8.25 (m, 1H), 8.22-8.19 (m, 1H), 7.96-7.93 (m, 2H), 7.77-7.74 (d, 1H), 7.50-7.48 (d, 1H), 4.96 (t, 1H), 4.20-4.18 (t, 2H), 3.80-3.79 (q, 2H).

2-(2-hydroxyethoxy)-9,10-dioxo-9,10-dihydroanthracen-1-yl 4-methylbenzenesulfonate:

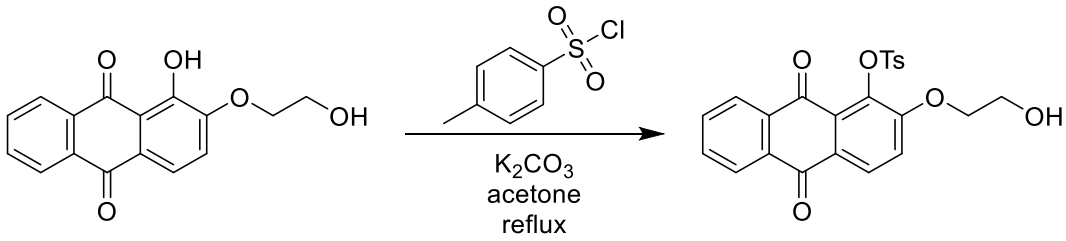

In a 25 mL round bottom flask equipped with a stir bar, 1-hydroxy-2-(2-hydroxyethoxy)anthracene-9,10-dione (0.0763 g, 0.268 mmol) was dissolved in 10 mL of acetone. *p*-Toluenesulfonyl chloride (0.1752 g, 0.919 mmol) and potassium carbonate (0.8152 g, 5.90 mmol) were added and the reaction mixture was stirred at reflux for 4 hours. Upon completion of the reaction, the solution was left to cool to room temperature and the solvent was removed under reduced pressure. The crude mixture was redissolved in ethyl acetate and decanted from the potassium carbonate. The ethyl acetate was removed under reduced pressure and the resulting crude solid was purified using flash chromatography with a mobile phase of 1:1 hexanes: ethyl acetate to yield pure 2-(2-hydroxyethoxy)-9,10-dioxo-9,10-dihydroanthracen-1-yl 4-methylbenzenesulfonate. ^{1}H NMR (400 MHz, DMSO-d6) δ = 8.20-8.18 (d, 1H), 8.16-8.14 (m, 1H), 7.95-7.89 (m, 3H), 7.67-7.64 (m, 3H), 7.40-7.38 (d, 2H), 4.78-4.76 (t, 1H), 3.88-3.86 (t, 2H), 3.41-3.37 (q, 2H), 2.37 (s, 3H).

2-((9,10-dioxo-1-(tosyloxy)-9,10-dihydroanthracen-2-yl)oxy)ethyl hydrogen sulfate (2.12):

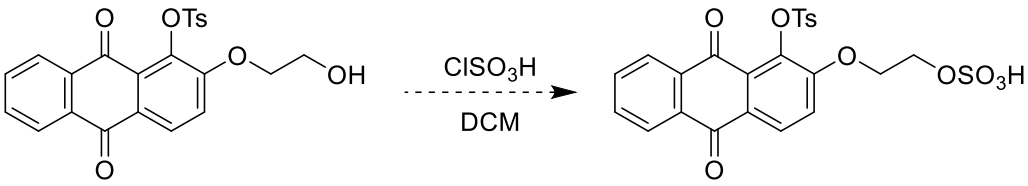

In a 10 mL round bottom flask equipped with a stir bar, 2-(2-hydroxyethoxy)-9,10-dioxo-9,10-dihydroanthracen-1-yl 4-methylbenzenesulfonate (0.0468 g, 0.107 mmol) was dissolved in 3 mL of dichloromethane and the solution was cooled to 0°C. Chlorosulfonic acid (16 μL, 0.241 mmol) was slowly added and the reaction was stirred for 1 hour. Upon completion of the reaction, the reaction mixture was neutralized with triethylamine and the solvent was removed under reduced pressure. NMR analysis of the crude product was indicative of hydrolysis of the tosyl group.

2-((1-hydroxy-9,10-dioxo-9,10-dihydroanthracen-2-yl)oxy)ethyl hydrogen sulfate:

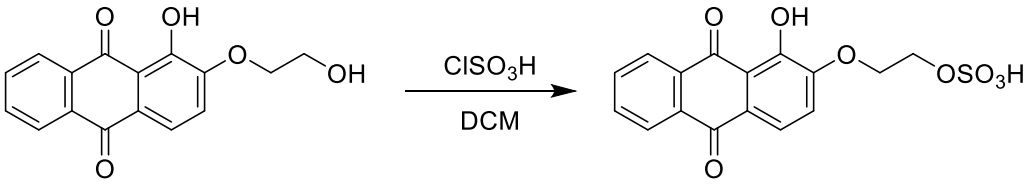

In a 25 mL round bottom flask equipped with a stir bar, 1-hydroxy-2-(2-hydroxyethoxy)anthracene-9,10-dione (0.2872 g, 1.01 mmol) was dissolved in 10 mL of dichloromethane and the solution was cooled to 0°C. Chlorosulfonic acid (140 μL, 2.11 mmol) was slowly added and the reaction was stirred for 1 hour. Upon completion of the reaction, the reaction mixture was poured into

water and neutralized with 10% aqueous sodium hydroxide. Extraction with dichloromethane removed unreacted starting material. Water was removed under reduced pressure to yield pure 2-((1-hydroxy-9,10-dioxo-9,10-dihydroanthracen-2-yl)oxy)ethyl hydrogen sulfate. ^{1}H NMR (400 MHz, DMSO-d6) δ = 8.28-8.25 (m, 1H), 8.21-8.19 (m, 1H), 7.95-7.93 (m, 2H), 7.76-7.74 (d, 1H), 7.51-7.49 (d, 1H), 4.35-4.33 (t, 2H), 4.11-4.09 (t, 2H).

2-((9,10-dioxo-1-(tosyloxy)-9,10-dihydroanthracen-2-yl)oxy)ethyl hydrogen sulfate (2.12):

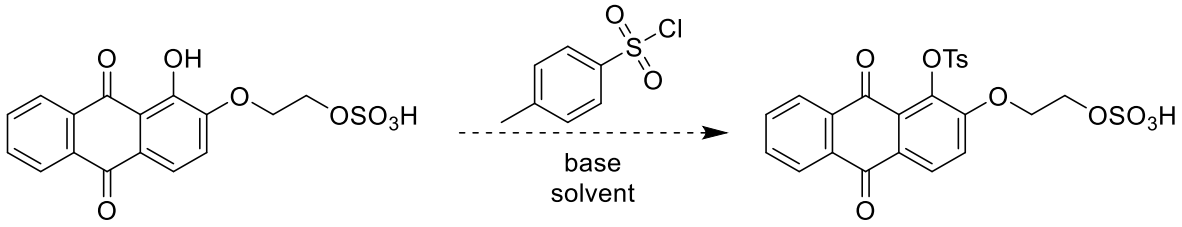

The following base/solvent conditions were attempted and resulted in no reaction:

- Base: potassium carbonate, solvent: acetone
- Base/solvent: pyridine
- Base/solvent: triethylamine
- Base: potassium carbonate, solvent: pyridine

2-(2-((9,10-dioxo-1-(tosyloxy)-9,10-dihydroanthracen-2-yl)oxy)ethoxy)ethane-1-sulfonate (2.13):

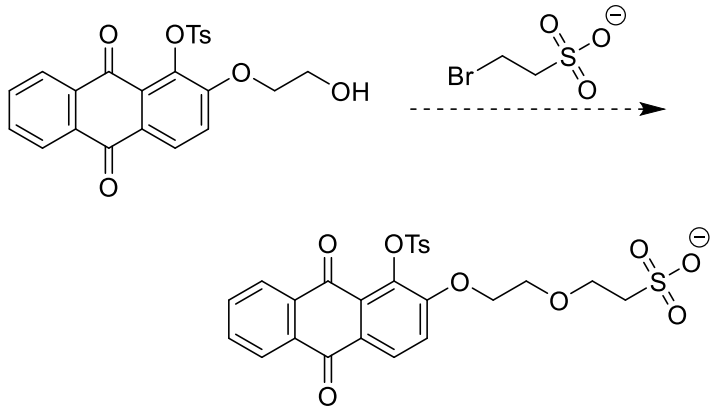

Method 1

In a 50 mL round bottom flask equipped with a stir bar, 2-(2-hydroxyethoxy)-9,10-dioxo-9,10-dihydroanthracen-1-yl 4-methylbenzenesulfonate (0.1717 g, 0.392 mmol) was dissolved in 6 mL of dichloromethane. Separately, sodium 2-bromoethanesulfonate (0.1729 g, 0.819 mmol) was dissolved in 1.5 mL of DMSO. The sodium 2-bromoethanesulfonate solution was added to the 2-(2-hydroxyethoxy)-9,10-dioxo-9,10-dihydroanthracen-1-yl 4-methylbenzenesulfonate solution and the reaction mixture was stirred at room temperature. After 3 hours of stirring, no reaction was detected, and the reaction mixture was the heated. After observing no reaction after 24 hours of total reaction time, *t*-butyl hydroxide (0.0453 g, 0.403 mmol) was added in an attempt to deprotonate the alcohol to improve its nucleophilicity. This caused the solution to turn red suggesting the tosyl group had been hydrolyzed and the base was deprotonating the phenol. It is hypothesized that hydrolysis occurred while the reaction mixture was at an elevated temperature.

Method 2

In a 25 mL, three-neck round bottom flask equipped with a stir bar and connected to nitrogen, sodium hydride (60% dispersion in mineral oil, 0.0183 g, 0.458 mmol) was added to 5 mL of anhydrous THF. To this was added sodium 2-bromoethanesulfonate (0.2463 g, 1.17 mmol) followed by 2-(2-hydroxyethoxy)-9,10-dioxo-9,10-dihydroanthracen-1-yl 4-methylbenzenesulfonate (0.0833 g, 0.190 mmol) and the reaction was stirred for 2 hours at room temperature. Excess sodium hydride was quenched by adding, dropwise, isopropyl alcohol followed by ethanol followed by methanol. The solvents were removed under reduced pressure. ^{1}H NMR analysis of the crude mixture was inconsistent with any reasonable expectation of the anticipated product. In addition, spiking *p*-TsOH into the NMR sample resulted in the growth of the aryl signals indicative of hydrolysis during the reaction.

2-(3-bromopropoxy)-1-hydroxyanthracene-9,10-dione:

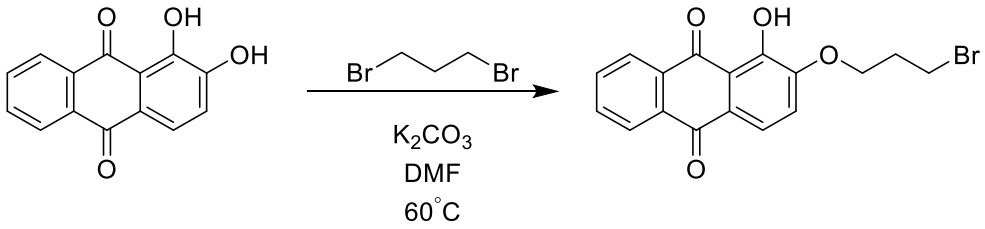

In a 50 mL round bottom flask equipped with a stir bar, 1,2-dihydroxyanthraquinone (1.0318 g, 4.30 mmol) and potassium carbonate (2.1574 g, 15.6 mmol) were dissolved in 15 mL of DMF. 1,3-dibromopropane (20 mL, 197 mmol) was added and the reaction was stirred at 60°C for 6 hours. Upon completion of the reaction, the reaction mixture was poured into 175 mL of 10% aqueous hydrochloric acid. The resulting solution was vacuum filtered

and the crude solid was purified using flash chromatography with chloroform as the mobile phase to yield 0.5396 g (35%) of pure 2-(3-bromopropoxy)-1-hydroxyanthracene-9,10-dione. ^{1}H NMR (400 MHz, DMSO-d6) δ = 12.73 (s, 1H), 8.27-8.25 (m, 1H), 8.21-8.19 (m, 1H), 7.96-7.94 (m, 2H), 7.77-7.75 (d, 1H), 7.53-7.51 (d, 1H), 4.29-4.26 (t, 2H), 3.72-3.69 (t, 2H), 2.37-2.32 (p, 2H).

2-(3-bromopropoxy)-9,10-dioxo-9,10-dihydroanthracen-1-yl 4-methylbenzenesulfonate:

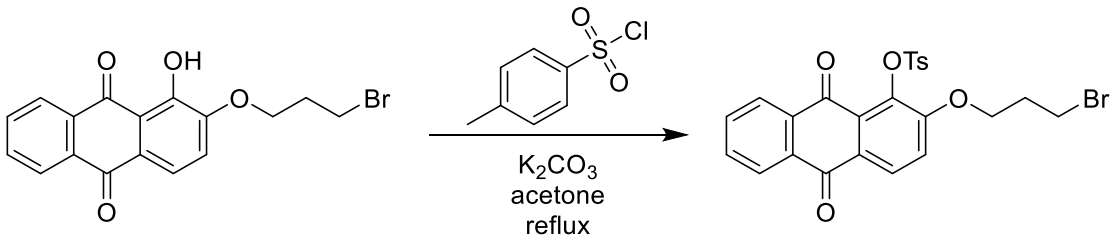

In a 50 mL round bottom flask equipped with a stir bar, 2-(3-bromopropoxy)-1-hydroxyanthracene-9,10-dione (0.2734 g, 0.757 mmol) was dissolved in 25 mL of acetone. *p*-Toluenesulfonyl chloride (0.4264 g, 2.24 mmol) and potassium carbonate (1.0557 g, 7.64 mmol) were added and the reaction mixture was stirred at reflux for 3 hours. Upon completion of the reaction, the solution was left to cool to room temperature and the solvent was removed under reduced pressure. The crude mixture was redissolved in dichloromethane and decanted from the potassium carbonate. The dichloromethane was removed under reduced pressure and the resulting crude solid was purified using flash chromatography with a mobile phase of 9:1 hexanes: ethyl acetate to yield 0.2540 g (65%) of pure 2-(3-bromopropoxy)-9,10-dioxo-9,10-dihydroanthracen-1-yl 4-methylbenzenesulfonate. ^{1}H NMR (400 MHz, DMSO-d6) δ = 8.22-8.20 (d, 1H), 8.15-8.14 (m, 1H), 7.92-7.90 (m, 3H), 7.69-

7.66 (m, 3H), 7.41-7.39 (d, 2H), 4.04-4.01 (t, 2H), 3.52-3.49 (t, 2H), 2.39 (s, 3H), 1.93-1.90 (p, 2H).

3-((3-((9,10-dioxo-1-(tosyloxy)-9,10-dihydroanthracen-2-yl)oxy)propyl)thio)propane-1-sulfonate (2.14):

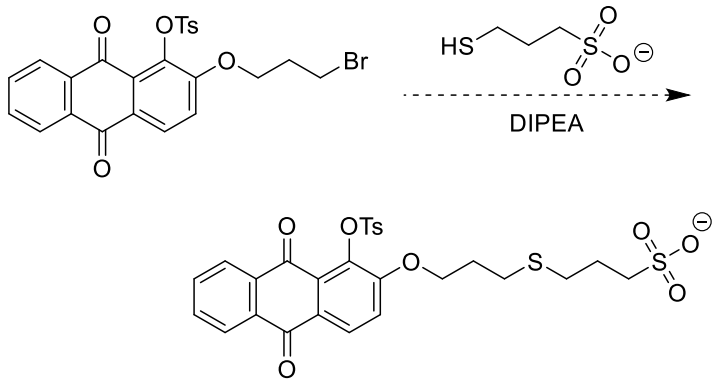

In a 25 mL round bottom flask equipped with a stir bar, 2-(3-bromopropoxy)-9,10-dioxo-9,10-dihydroanthracen-1-yl 4-methylbenzenesulfonate (0.0963 g, 0.187 mmol) was dissolved in 10 mL of dichloromethane. Separately, sodium 3-mercapto-1-propanesulfonate (0.0766 g, 0.430 mmol) was dissolved in 1.5 mL of DMSO and this was added to the 2-(3-bromopropoxy)-9,10-dioxo-9,10-dihydroanthracen-1-yl 4-methylbenzenesulfonate solution. *N*,*N*-diisopropylethylamine (100 μL, 1.04 mmol) was added and the solution was stirred at room temperature. After 2 hours, no noticeable reaction was observed and more sodium 3-mercapto-1-propanesulfonate and *N*,*N*-diisopropylethylamine were added. After 48 hours of total reaction time, the solvents were removed under reduced pressure. The resulting solid was redissolved in dichloromethane and filtered to remove excess sodium 3-mercapto-1-propanesulfonate and the dichloromethane was removed under

reduced pressure. ^{1}H NMR analysis revealed mostly starting material remaining.

6-hydroxytetracene-5,12-dione (2.16):[164, 165]

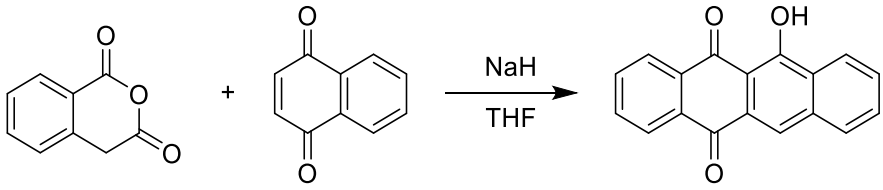

In a 100 mL round bottom flask equipped with a stir bar, homophthalic anhydride (0.5015 g, 3.09 mmol) and sodium hydride (60% dispersion in mineral oil, 0.1528 g, 3.82 mmol) were added to 40 mL of anhydrous THF and the solution was cooled to 0°C. To this was added a solution of 1,4-naphthoquinone (0.4876 g, 3.08 mmol) in 10 mL of anhydrous THF. The resulting solution was stirred for 20 minutes at 0°C then at room temperature overnight. Upon completion of the reaction, the solution was quenched with 40 mL of saturated ammonium chloride. Next, the solution was acidified with 10% aqueous hydrochloric acid. The reaction mixture was extracted with dichloromethane and the organic layer was washed with brine and dried over magnesium sulfate. The solvent was removed under reduced pressure and the resulting crude solid was recrystallized from chloroform to yield 0.0504 g (6%) of 6-hydroxytetracene-5,12-dione. ^{1}H NMR consistent with literature.[165]

6-tosyloxy-5,12-naphthacenequinone (2.15):

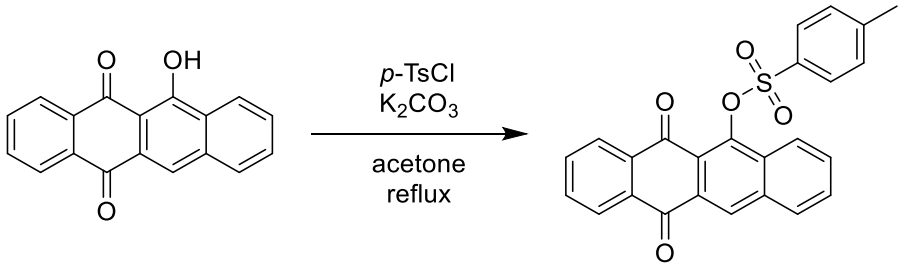

In a 25 mL round bottom flask equipped with a stir bar, 6-hydroxytetracene-5,12-dione (0.0504 g, 0.184 mmol) was dissolved in 10 mL of acetone. *p*-Toluenesulfonyl chloride (0.0989 g, 0.519 mmol) and potassium carbonate (0.5156 g, 3.73 mmol) were added and the reaction mixture was stirred at reflux for 1 hour. Upon completion of the reaction, the solution was left to cool to room temperature and the solvent was removed under reduced pressure. The crude mixture was redissolved in ethyl acetate and decanted from the potassium carbonate. The ethyl acetate was removed under reduced pressure and the resulting crude solid was purified using flash chromatography with a mobile phase of 1:4 ethyl acetate: hexanes to yield 0.0513 g (65%) of pure 6-tosyloxy-5,12-naphthacenequinone. ^{1}H NMR (400 MHz, DMSO-d6): δ = 8.93 (s, 1H), 8.40-8.38 (d, 1H), 8.23-8.21 (m, 1H), 7.99-7.97 (d, 1H), 7.94-7.93 (m, 3H), 7.84-7.80 (td, 1H), 7.74-7.70 (m, 3H), 7.37-7.35 (d, 2H), 2.33 (s, 3H).

1-hydroxy-2-tosyloxy-9,10-anthraquinone (2.17):[166]

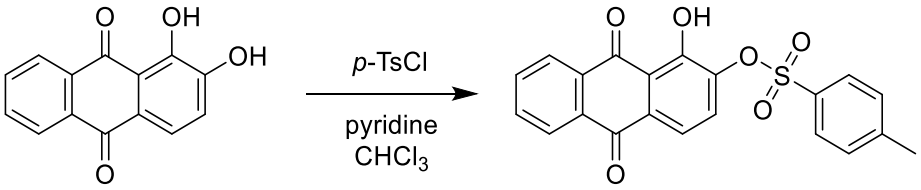

In a 25 mL round bottom flask equipped with a stir bar, 1,2-dihydroxyanthraquinone (1.1567 g, 4.82 mmol) and *p*-toluenesulfonyl chloride (1.8077 g, 9.48 mmol) were dissolved in 6 mL of chloroform. 2 mL of pyridine was added dropwise and the reaction mixture was stirred at room temperature for 1 hour. Upon completion of the reaction, the mixture was poured into ethanol and the precipitate was vacuum filtered to yield 1.6575 g (87%) of pure 1-hydroxy-2-tosyloxy-9,10-anthraquinone. ^{1}H NMR (400 MHz, DMSO-d6): δ = 12.47 (s, 1H), 8.24-8.19 (m, 2H), 7.98-7.95 (m, 2H), 7.86-7.84 (d, 2H), 7.75-7.72 (d, 1H), 7.62-7.60 (d, 1H), 7.52-7.50 (d, 2H), 2.44 (s, 3H).

7.2.2 UV-Vis Spectra

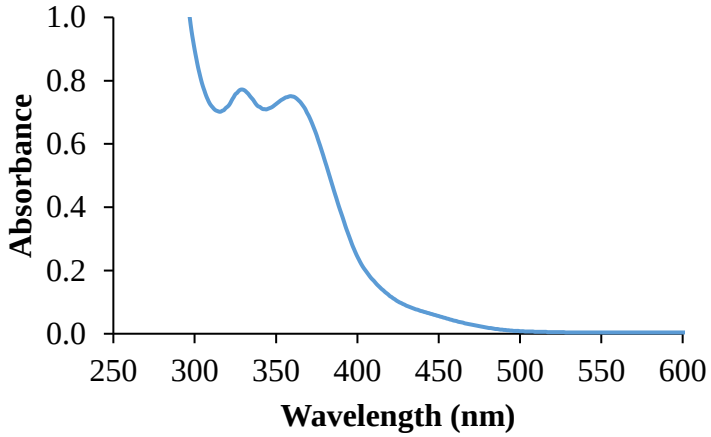

Figure 7.1. UV-Vis spectrum of 1-tosyloxy-2-methoxyanthraquinone **2.1a** in acetonitrile

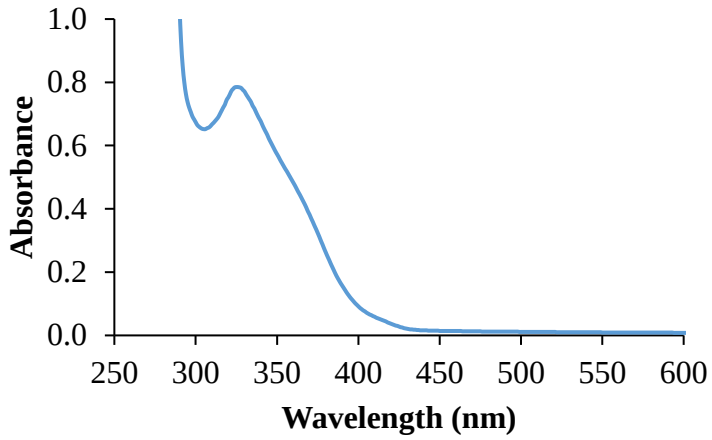

Figure 7.2. UV-Vis spectrum of 1-(trifluoromethylsulfonoxy)-2-methoxy-9,10-anthraquinone **2.1b** in acetonitrile

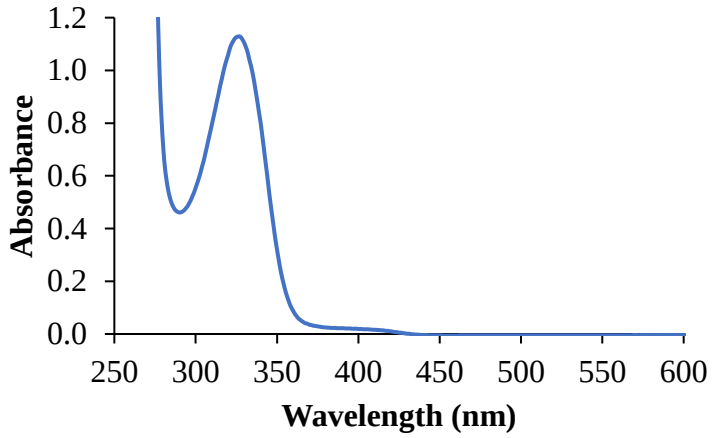

Figure 7.3. UV-Vis spectrum of 1-tosyloxyanthraquinone **2.8** in acetonitrile

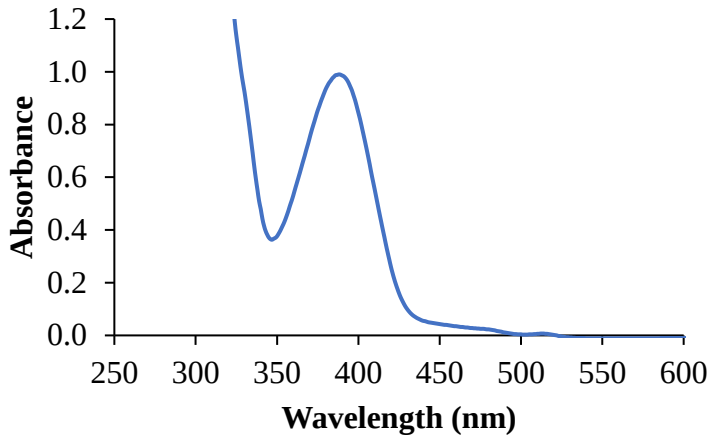

Figure 7.4. UV-Vis spectrum of 6-tosyloxy-5,12-naphthacenequinone **2.15** in acetonitrile

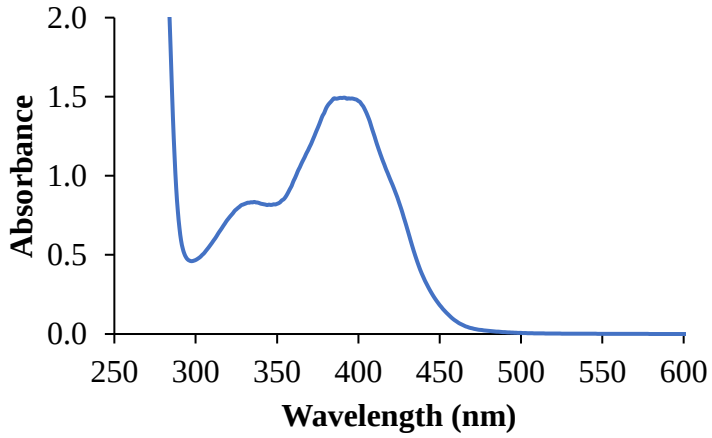

Figure 7.5. UV-Vis spectrum of 1-hydroxy-2-tosyloxyanthraquinone **2.17** in acetonitrile

7.2.3 NMR Analysis Procedure

A 10 mg/10 mL solution of PAGs **2.1a** and **2.1b** in CD_3CN were prepared and a 1 mL sample was photolyzed in a quartz cuvette, with stirring, for the allotted time. For samples in a nitrogen or oxygen saturated atmosphere, the sample was purged for 10 minutes in the solution and 5 minutes in the headspace prior to photolysis. After photolysis, the solution was transferred to an NMR tube and a spectrum was obtained. For **2.1a**, *p*-toluenesulfonic acid

yields were quantified by integrating relative to the solvent signal. For **2.1b**, triflic acid yields were quantified using trifluoroacetic acid as an internal standard.

7.2.4 Titration Procedure

A 10 mg/10 mL solution of PAG **2.1b** in acetonitrile was prepared and a 1 mL sample was photolyzed in a quartz cuvette, with stirring, for the allotted time. Upon completion of photolysis, the sample was added to 1 mL of water and then the acetonitrile was removed under reduced pressure. The remaining 1 mL of the now aqueous photolysis mixture was titrated with 3.20 mM aqueous sodium hydroxide. The titration was monitored by pH.

7.2.5 Quantification of Fluoride Yields

Yields of fluoride were determined using a photometric fluoride cell test supplied by Millipore Sigma. Using a stock solution of sodium fluoride in water, a calibration curve was generated (Figure 7.1).

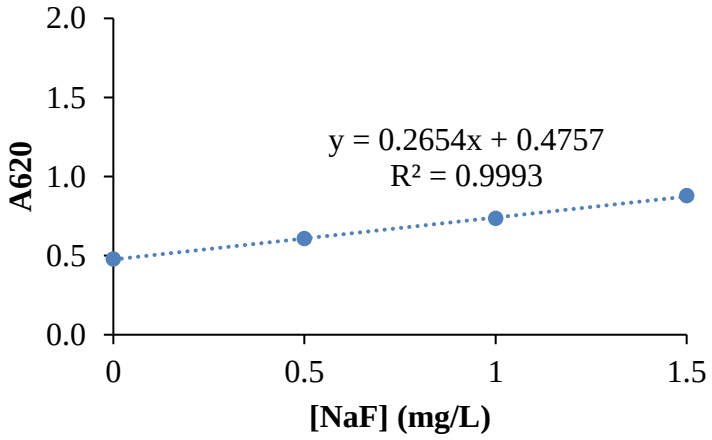

Figure 7.6. Calibration curve for quantification of fluoride ions using a fluoride cell test

A 10 mg/10 mL solution of PAG **2.1b** in acetonitrile was prepared and a 1 mL sample was photolyzed in a quartz cuvette, with stirring, for the allotted time. Upon completion of photolysis, 45 µL of photolyzate was diluted into 5 mL of HPLC water and this solution was added to the fluoride cell test. The resulting solution was analyzed spectrophotometrically and a yield of fluoride was determined.

7.2.6 Malachite Green Carbinol Base Procedure

For pulsed photolysis experiments, a 239 µM solution of **2.1a** in acetonitrile was prepared and a 1 mL sample was photolyzed in a quartz cuvette, with stirring, for the allotted time. After photolysis, 80 µL of photolyzate was added to 0.2 mL of 318 µM malachite green carbinol base in acetonitrile and this sample was diluted to 2 mL with acetonitrile. The sample sat for 15 minutes and then a UV-Vis spectrum was obtained.

For 447 nm CW laser experiments, 1.5 mL of a 79.7 µM solution of **2.1a** in acetonitrile was photolyzed in a quartz cuvette, with stirring, for the allotted time. After photolysis, 0.5 mL of 318 µM malachite green carbinol base in acetonitrile was added and the sample sat for 10 minutes and then a UV-Vis spectrum was obtained.

7.2.7 TEMPO Trapping

A 1 mL sample containing 1.56 mM **2.1b** and 3.11 mM TEMPO in CD_3CN was photolyzed in a quartz cuvette, with stirring, for 20 minutes. Upon completion of photolysis, the sample was transferred to an NMR tube and a ^{19}F

NMR spectrum was obtained. A new signal is observed at -56.1164 ppm which is consistent with formation of the TEMPO-CF_3 adduct.[60]

7.2.8 Photopolymerization

In a vial, 0.0031 g of **2.1a** was added to 1.5 mL of ethyl vinyl ether. 0.5 mL of chloroform was added for solubility. The solution was photolyzed with stirring for 2 hours. After the polymerization was complete, an aliquot of the photolysis mixture was dissolved in $CDCl_3$ and an NMR spectrum was obtained.

In a vial, 0.0030 g of **2.1b** was added to 1.5 mL of ethyl vinyl ether. A couple drops of dichloromethane was added for solubility. The solution was photolyzed with stirring for 10 minutes. After the polymerization was complete, an aliquot of the photolysis mixture was dissolved in $CDCl_3$ and an NMR spectrum was obtained.

7.2.9 Kinetic Data from LFP

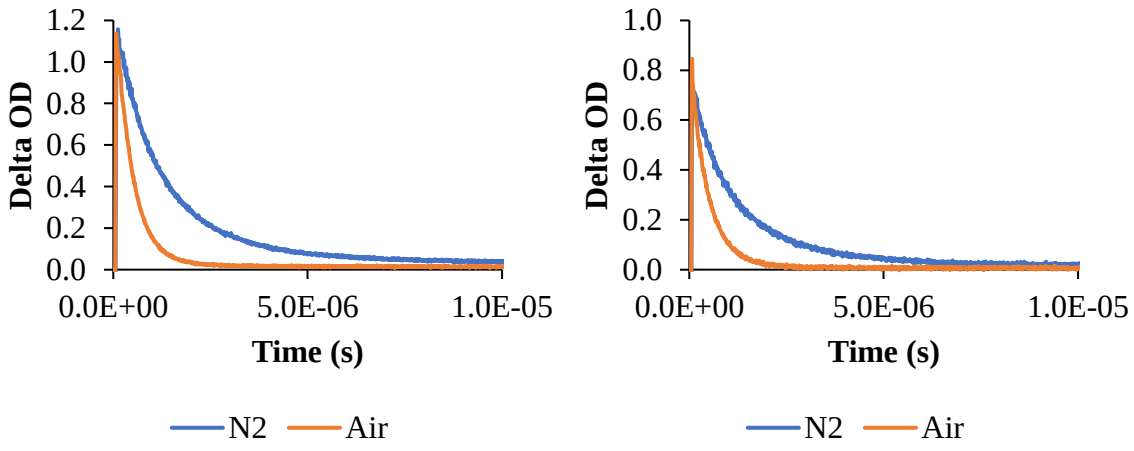

Figure 7.7. Kinetic traces resulting from pulsed 355 nm photolysis of 1-tosyloxy-2-methoxyanthraquinone **2.1a** in acetonitrile under N_2 and air. Left: 470 nm; Right: 600 nm

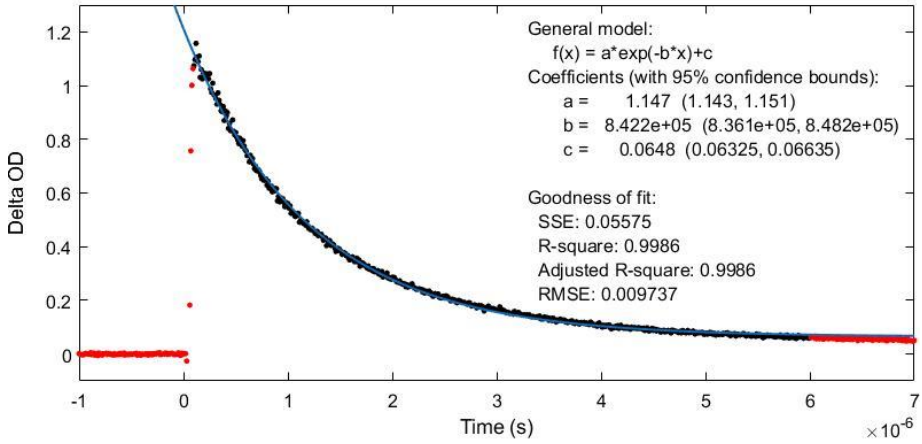

Figure 7.8. Curve fitting for the kinetic decay of 1-tosyloxy-2-methoxyanthraquinone **2.1a** in acetonitrile under N_2 at 470 nm

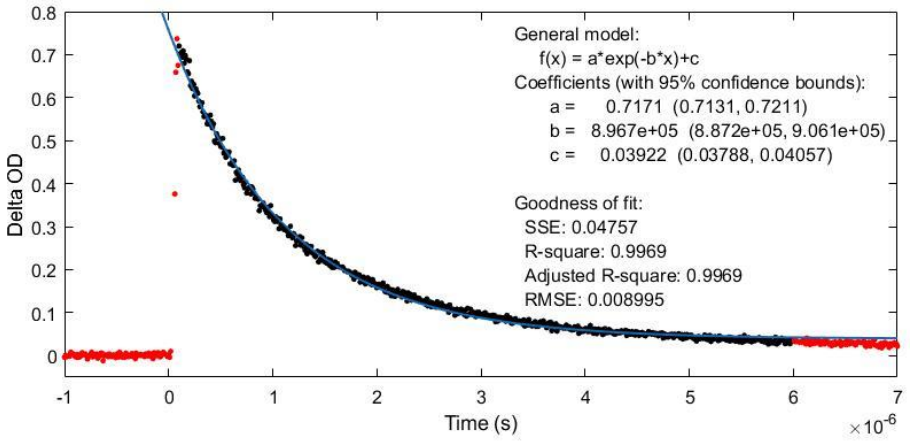

Figure 7.9. Curve fitting for the kinetic decay of 1-tosyloxy-2-methoxyanthraquinone **2.1a** in acetonitrile under N_2 at 600 nm

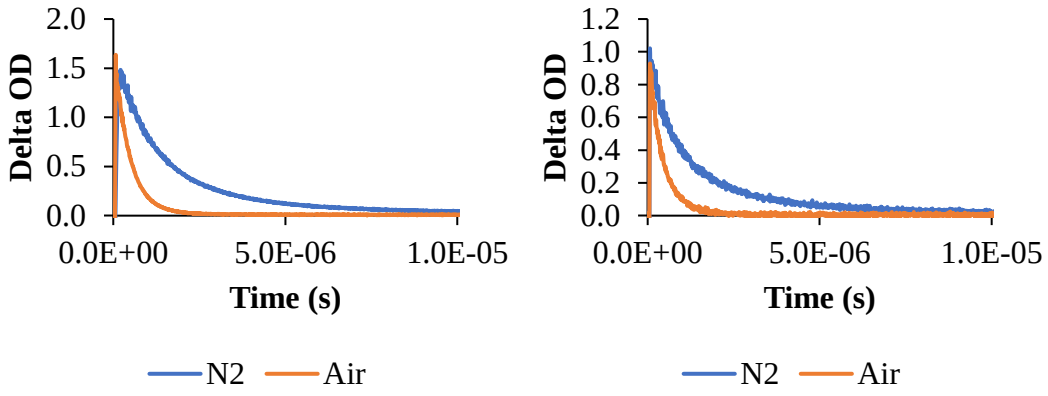

Figure 7.10. Kinetic traces resulting from pulsed 355 nm photolysis of 1-(trifluoromethylsulfonoxy)-2-methoxy-9,10-anthraquinone **2.1b** in acetonitrile under N_2 and air. Left: 470 nm; Right: 600 nm

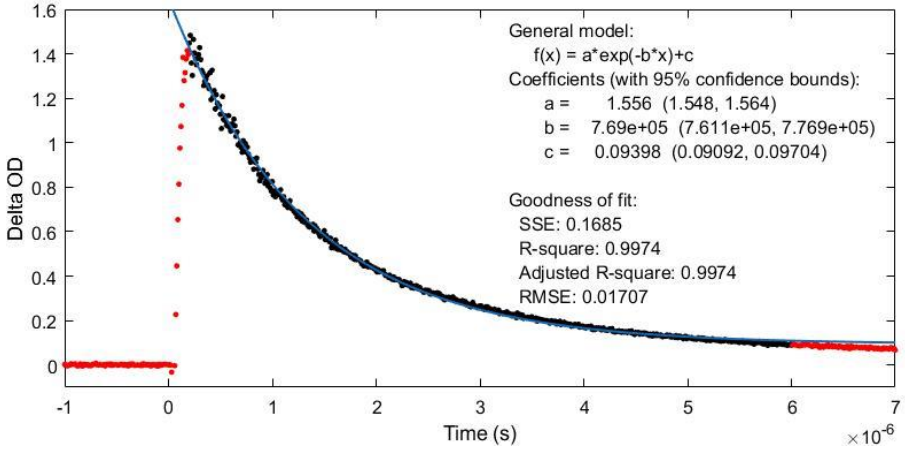

Figure 7.11. Curve fitting for the kinetic decay of 1-(trifluoromethylsulfonoxy)-2-methoxy-9,10-anthraquinone **2.1b** in acetonitrile under N_2 at 470 nm

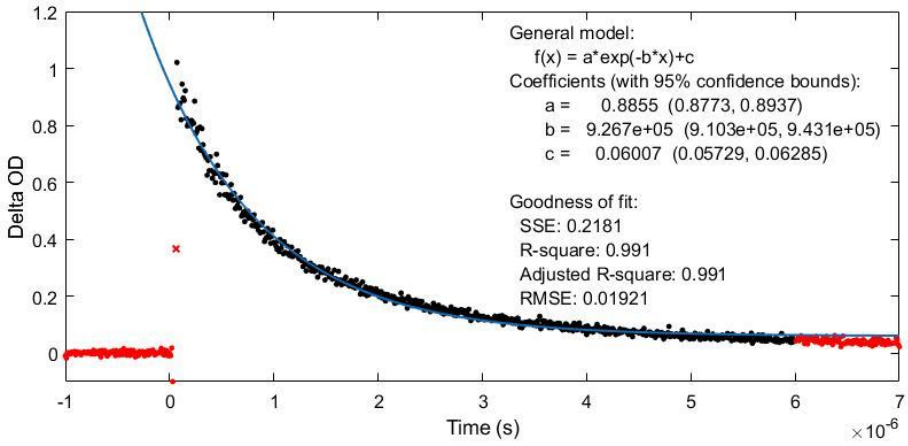

Figure 7.12. Curve fitting for the kinetic decay of 1-(trifluoromethylsulfonoxy)-2-methoxy-9,10-anthraquinone **2.1b** in acetonitrile under N_2 at 600 nm

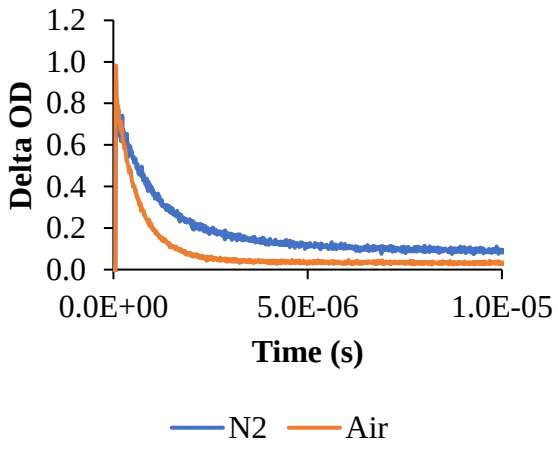

Figure 7.13. Kinetic traces resulting from pulsed 355 nm photolysis of 1-tosyloxyanthraquinone **2.8** in acetonitrile under N_2 and air collected at 380 nm

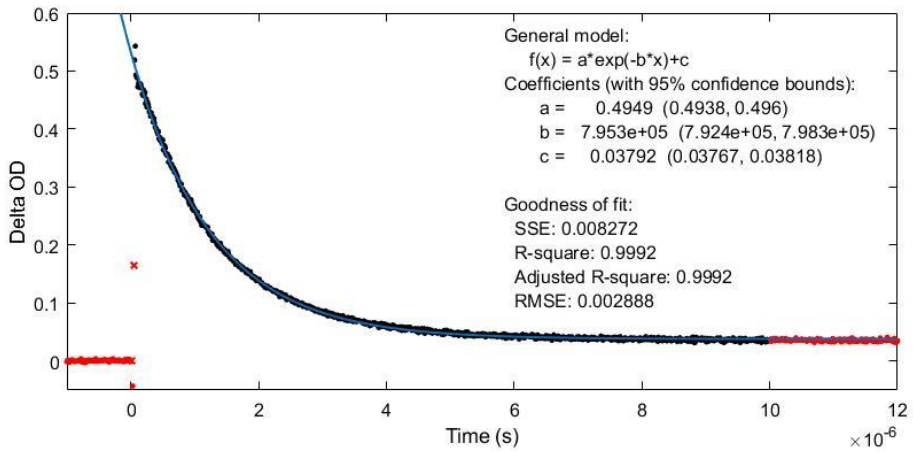

Figure 7.14. Curve fitting for the kinetic decay of 1-tosyloxyanthraquinone **2.8** in acetonitrile under N_2 at 380 nm

7.2.10 Benchmarking DFT Methods

Table 7.1. Benchmarking DFT methods for determining bond dissociation energies of S—O bonds

Compound	Experimental[a] (kcal/mol)	(u)B3LYP/ 6-311G(d) (kcal/mol)	(u)MN062x/ 6-311G(d) (kcal/mol)	(u)MN12SX/ 6-311G(3d) (kcal/mol)	(u)MN12SX/ 6-311G(3d)// (u)B3LYP/6-311G(d) (kcal/mol)
HO-S-SH	70.6 ± 4	59.1	63.6	71.9	71.5
HO-S(OH)	75.4 ± 3	62.6	64.9	75.3	74.7
HO-S(=O)(=O)-OH	93.4 ± 2 92.5 ± 2	73.0	84.4	94.4	93.8
HO-S-CH3	73.1 ± 3	60.9	66.8	72.7	72.1
HO-S(=O)(=O)-CH3	86.6 ± 3	70.9	80.5	90.3	88.6

[a]Experimental values obtained from Luo's Handbook of Bond Dissociation Energies in Organic Compounds[167]

Table 7.2. Benchmarking DFT methods for determining triplet energies of quinone derivatives

Compound	Literature (kcal/mol)	(u)B3LYP/ 6-311G(d) (kcal/mol)	(u)MN12SX/ 6-311G(3d)// (u)B3LYP/6-311G(d) (kcal/mol)	(u)M062X/6-311G(3d,2p)// (u)B3LYP/6-311G(d) (kcal/mol)
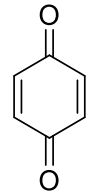	53.5[a] 52.9[b]	43.9	46.6	53.9
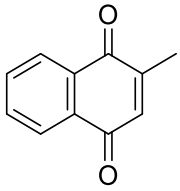	58.2[b]	50.6	52.9	54.4
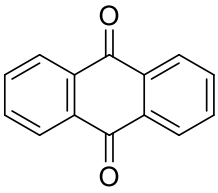	62.4[a] 63.0[b]	57.1	59.0	60.9

[a]Murov, S. L.; Carmichael, I.; Hug, G. L. Handbook of Photochemistry; 2nd ed.; Marcel Dekker: New York, 1993[168]

[b]Serpa, C.; Arnaut, L. G. *J. Phys. Chem. A.* **2000**, *104*, 11075−11086[95]

7.2.11 Cartesian Coordinates & Energies

2.1a Singlet
B3LYP/6-311G(d)

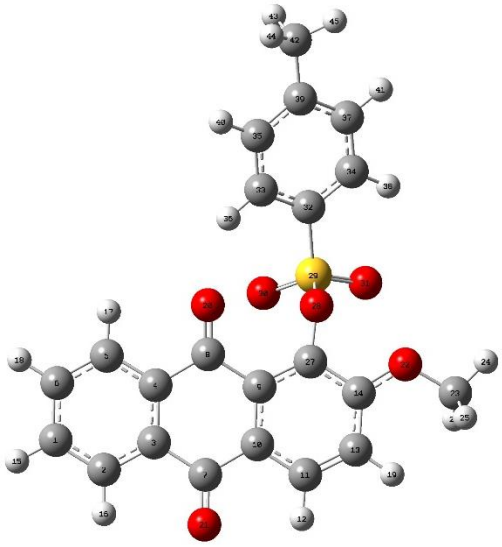

Standard orientation:

Center Number	Atomic Number	Atomic Type	Coordinates (Angstroms) X	Y	Z
1	6	0	-4.949915	-3.269100	0.272371
2	6	0	-5.049856	-1.889186	0.152916
3	6	0	-3.900505	-1.117130	-0.038284
4	6	0	-2.644745	-1.736556	-0.119387
5	6	0	-2.555023	-3.127744	-0.008001
6	6	0	-3.699610	-3.888638	0.192638
7	6	0	-4.027542	0.358716	-0.164326
8	6	0	-1.389849	-0.955938	-0.349731
9	6	0	-1.492933	0.540939	-0.310161
10	6	0	-2.772258	1.147659	-0.285582
11	6	0	-2.888885	2.533930	-0.351166
12	1	0	-3.883663	2.962146	-0.329929
13	6	0	-1.770241	3.346776	-0.443573
14	6	0	-0.495068	2.775308	-0.450572
15	1	0	-5.843020	-3.865826	0.426169
16	1	0	-6.006833	-1.383682	0.204543
17	1	0	-1.578577	-3.590699	-0.080616
18	1	0	-3.621390	-4.966840	0.286651
19	1	0	-1.891815	4.420597	-0.503001
20	8	0	-0.350365	-1.541328	-0.590736

21	8	0	-5.120724	0.902985	-0.151001
22	8	0	0.654050	3.464413	-0.544812
23	6	0	0.613266	4.886263	-0.518218
24	1	0	1.652226	5.205211	-0.548554
25	1	0	0.082619	5.286290	-1.387963
26	1	0	0.147286	5.250924	0.401790
27	6	0	-0.364253	1.368897	-0.362598
28	8	0	0.922621	0.871138	-0.399154
29	16	0	1.730914	0.611024	1.065493
30	8	0	0.867543	-0.203616	1.903575
31	8	0	2.230440	1.881851	1.561807
32	6	0	3.080566	-0.340992	0.397778
33	6	0	2.843375	-1.623207	-0.093928
34	6	0	4.357803	0.210926	0.416363
35	6	0	3.920403	-2.358395	-0.572043
36	1	0	1.836669	-2.019606	-0.120466
37	6	0	5.421021	-0.547416	-0.063920
38	1	0	4.510546	1.212179	0.799471
39	6	0	5.221886	-1.839078	-0.561559
40	1	0	3.745223	-3.355449	-0.964687
41	1	0	6.420701	-0.124108	-0.051775
42	6	0	6.382448	-2.666510	-1.053549
43	1	0	6.757847	-3.321633	-0.259926
44	1	0	6.093191	-3.306482	-1.890366
45	1	0	7.215342	-2.040103	-1.379473

Zero-point correction= 0.333815 (Hartree/Particle)
Thermal correction to Energy= 0.358834
Thermal correction to Enthalpy= 0.359778
Thermal correction to Gibbs Free Energy= 0.276125
Sum of electronic and zero-point Energies= -1697.432901
Sum of electronic and thermal Energies= -1697.407882
Sum of electronic and thermal Enthalpies= -1697.406938
Sum of electronic and thermal Free Energies= -1697.490592

2.1a Singlet
MN12-SX/6-311G(3d)//B3LYP/6-311G(d)

HF=-1696.8182592

2.1a Singlet
M06-2X/6-311G(3d,2p)//B3LYP/6-311G(d)

HF=-1697.3559339

2.1a Triplet
B3LYP/6-311G(d)

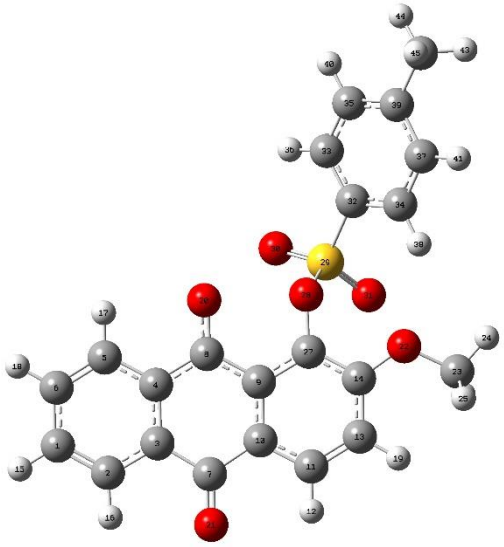

Standard orientation:

Center Number	Atomic Number	Atomic Type	Coordinates (Angstroms) X	Y	Z
1	6	0	-5.909873	-2.282172	-0.216450
2	6	0	-5.640591	-0.925299	-0.167194
3	6	0	-4.322578	-0.449517	-0.196141
4	6	0	-3.255975	-1.379901	-0.273379
5	6	0	-3.542757	-2.764360	-0.323604
6	6	0	-4.851298	-3.202778	-0.294708
7	6	0	-4.083111	1.007094	-0.145603
8	6	0	-1.894754	-0.902109	-0.306664
9	6	0	-1.608339	0.500639	-0.212375
10	6	0	-2.672852	1.435566	-0.161479
11	6	0	-2.366771	2.798507	-0.139847
12	1	0	-3.195041	3.496446	-0.099751
13	6	0	-1.060320	3.250393	-0.192423
14	6	0	0.007531	2.334524	-0.246718
15	1	0	-6.935468	-2.634927	-0.193100
16	1	0	-6.434704	-0.190038	-0.104967
17	1	0	-2.726383	-3.475919	-0.375631
18	1	0	-5.060507	-4.267108	-0.329474
19	1	0	-0.865007	4.314555	-0.197474
20	8	0	-0.934365	-1.769784	-0.450929
21	8	0	-5.007109	1.819021	-0.093212
22	8	0	1.310011	2.692191	-0.340464

23	6	0	1.661094	4.053245	-0.111980
24	1	0	2.748652	4.084615	-0.131242
25	1	0	1.269820	4.705172	-0.898603
26	1	0	1.306981	4.391743	0.865140
27	6	0	-0.273778	0.965411	-0.215255
28	8	0	0.748804	0.037365	-0.265606
29	16	0	1.627763	-0.315855	1.181166
30	8	0	1.097709	-1.542841	1.742360
31	8	0	1.668440	0.903964	1.967490
32	6	0	3.197753	-0.646704	0.406802
33	6	0	3.726312	-1.929868	0.488404
34	6	0	3.882847	0.388130	-0.229611
35	6	0	4.976445	-2.174760	-0.074644
36	1	0	3.169744	-2.715839	0.983427
37	6	0	5.123349	0.118724	-0.788712
38	1	0	3.437406	1.372368	-0.297209
39	6	0	5.691832	-1.162021	-0.718567
40	1	0	5.397944	-3.172810	-0.010288
41	1	0	5.663164	0.916404	-1.290317
42	6	0	7.038221	-1.431932	-1.340888
43	1	0	7.780539	-0.697020	-1.017420
44	1	0	7.412271	-2.423293	-1.079869
45	1	0	6.984146	-1.374877	-2.432798

Zero-point correction= 0.330703 (Hartree/Particle)
Thermal correction to Energy= 0.355993
Thermal correction to Enthalpy= 0.356938
Thermal correction to Gibbs Free Energy= 0.271927
Sum of electronic and zero-point Energies= -1697.347788
Sum of electronic and thermal Energies= -1697.322497
Sum of electronic and thermal Enthalpies= -1697.321553
Sum of electronic and thermal Free Energies= -1697.406563

2.1a Triplet

M06-2X/6-311G(3d,2p)//B3LYP/6-311G(d)

HF=-1697.2588969

2.1b Singlet
B3LYP/6-311G(d)

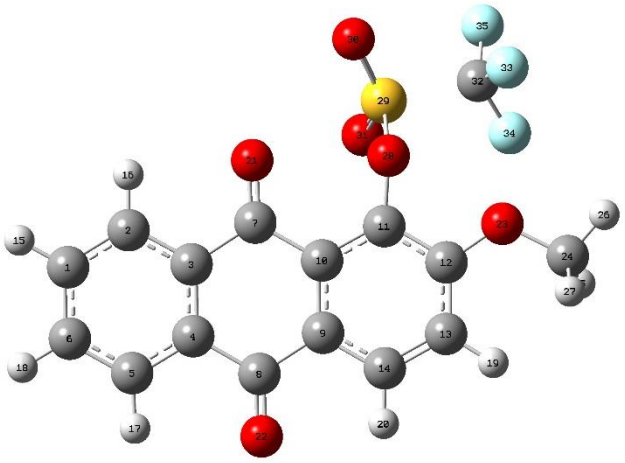

Standard orientation:

Center Number	Atomic Number	Atomic Type	Coordinates (Angstroms) X	Y	Z
1	6	0	-5.000064	-2.205236	-0.211395
2	6	0	-3.624707	-2.112381	-0.382630
3	6	0	-2.976559	-0.885859	-0.205363
4	6	0	-3.722702	0.248357	0.150407
5	6	0	-5.105602	0.146052	0.325570
6	6	0	-5.741858	-1.075115	0.143607
7	6	0	-1.495885	-0.833186	-0.384966
8	6	0	-3.061012	1.564815	0.344447
9	6	0	-1.591753	1.638631	0.107130
10	6	0	-0.827478	0.502487	-0.241930
11	6	0	0.543380	0.669312	-0.463179
12	6	0	1.152484	1.939280	-0.376372
13	6	0	0.375818	3.045053	-0.021130
14	6	0	-0.979652	2.885000	0.219827
15	1	0	-5.497892	-3.158910	-0.352035
16	1	0	-3.030118	-2.977205	-0.650926
17	1	0	-5.657678	1.036089	0.603056
18	1	0	-6.815732	-1.151170	0.278575
19	1	0	0.823654	4.026715	0.062186
20	1	0	-1.596595	3.732368	0.493274
21	8	0	-0.872326	-1.845852	-0.641566
22	8	0	-3.695752	2.554492	0.671505
23	8	0	2.467869	1.977630	-0.655079
24	6	0	3.172088	3.208971	-0.521114

25	1	0	3.114798	3.586964	0.503659
26	1	0	4.205575	2.977049	-0.766284
27	1	0	2.791240	3.960483	-1.218522
28	8	0	1.367476	-0.356330	-0.911798
29	16	0	1.936940	-1.530740	0.108266
30	8	0	2.092527	-2.721156	-0.683756
31	8	0	1.274021	-1.460772	1.390652
32	6	0	3.687935	-0.873522	0.390241
33	9	0	4.257623	-0.532662	-0.757903
34	9	0	3.660288	0.173743	1.211556
35	9	0	4.390378	-1.852258	0.959258

Zero-point correction= 0.230671 (Hartree/Particle)
Thermal correction to Energy= 0.252539
Thermal correction to Enthalpy= 0.253483
Thermal correction to Gibbs Free Energy= 0.178475
Sum of electronic and zero-point Energies= -1764.225853
Sum of electronic and thermal Energies= -1764.203985
Sum of electronic and thermal Enthalpies= -1764.203040
Sum of electronic and thermal Free Energies= -1764.278049

2.1b Singlet
MN12-SX/6-311G(3d)//B3LYP/6-311G(d)

HF= -1763.5567359

2.1b Singlet
M06-2X/6-311G(3d,2p)//B3LYP/6-311G(d)

HF=-1764.0611202

2.1b Triplet
B3LYP/6-311G(d)

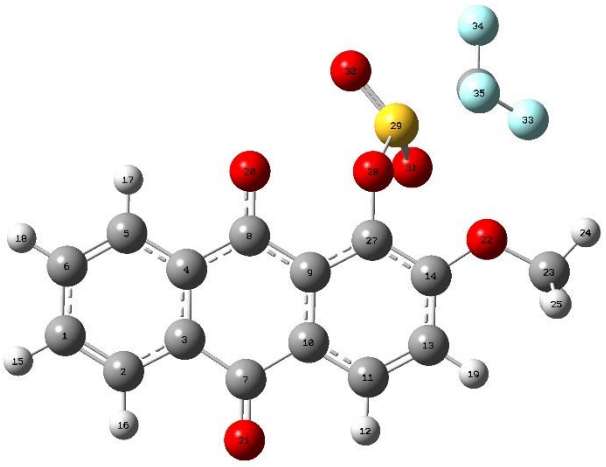

Standard orientation:

Center Number	Atomic Number	Atomic Type	Coordinates (Angstroms) X	Y	Z
1	6	0	-5.831159	-1.190801	0.054551
2	6	0	-5.228089	0.051414	0.154746
3	6	0	-3.838268	0.189028	0.041093
4	6	0	-3.048052	-0.965711	-0.180706
5	6	0	-3.673912	-2.229961	-0.282271
6	6	0	-5.045586	-2.334325	-0.165155
7	6	0	-3.237269	1.533756	0.151754
8	6	0	-1.616161	-0.835260	-0.304363
9	6	0	-0.980099	0.445611	-0.190417
10	6	0	-1.769178	1.605462	0.023457
11	6	0	-1.134421	2.846366	0.117228
12	1	0	-1.761333	3.714428	0.285064
13	6	0	0.238340	2.976061	-0.001406
14	6	0	1.033254	1.836816	-0.219158
15	1	0	-6.908229	-1.281580	0.145139
16	1	0	-5.806837	0.952366	0.322955
17	1	0	-3.069035	-3.113763	-0.451469
18	1	0	-5.516956	-3.308498	-0.243959
19	1	0	0.694303	3.954392	0.072758
20	8	0	-0.910883	-1.911324	-0.520079
21	8	0	-3.919135	2.539986	0.339420
22	8	0	2.376170	1.840974	-0.356585
23	6	0	3.088849	3.064657	-0.188867
24	1	0	4.137677	2.806791	-0.310840

25	1	0	2.801117	3.795233	-0.949720
26	1	0	2.927509	3.479079	0.809743
27	6	0	0.418360	0.588353	-0.300893
28	8	0	1.180017	-0.543129	-0.586523
29	16	0	2.173350	-1.225436	0.580810
30	8	0	1.989724	-2.651268	0.477565
31	8	0	2.061263	-0.487066	1.818693
32	6	0	3.890257	-0.873673	-0.189912
33	9	0	4.465623	0.141626	0.441561
34	9	0	4.623173	-1.967259	-0.011134
35	9	0	3.790064	-0.612545	-1.482719

Zero-point correction= 0.227406 (Hartree/Particle)
Thermal correction to Energy= 0.249642
Thermal correction to Enthalpy= 0.250586
Thermal correction to Gibbs Free Energy= 0.173871
Sum of electronic and zero-point Energies= -1764.140087
Sum of electronic and thermal Energies= -1764.117851
Sum of electronic and thermal Enthalpies= -1764.116907
Sum of electronic and thermal Free Energies= -1764.193622

2.1b Triplet
M06-2X/6-311G(3d,2p)//B3LYP/6-311G(d)

HF=-1763.9623354

Oxygen-centered Radical 2.4
B3LYP/6-311G(d)

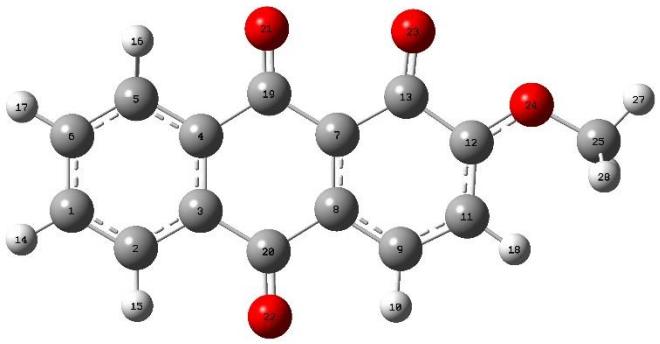

Standard orientation:

Center Number	Atomic Number	Atomic Type	Coordinates (Angstroms) X	Y	Z

1	6	0	-4.622055	0.413386	0.000062
2	6	0	-3.510595	1.245115	0.000116
3	6	0	-2.224548	0.694301	0.000065
4	6	0	-2.054772	-0.697921	-0.000061
5	6	0	-3.180074	-1.526760	-0.000109
6	6	0	-4.455144	-0.974594	-0.000049
7	6	0	0.486726	-0.424869	-0.000045
8	6	0	0.307959	0.956031	0.000067
9	6	0	1.412598	1.833875	0.000130
10	1	0	1.203256	2.896658	0.000217
11	6	0	2.723749	1.373489	0.000099
12	6	0	2.965547	0.006776	0.000012
13	6	0	1.850487	-0.982937	-0.000056
14	1	0	-5.619272	0.840880	0.000108
15	1	0	-3.611143	2.324058	0.000211
16	1	0	-3.028836	-2.599489	-0.000208
17	1	0	-5.324043	-1.624652	-0.000093
18	1	0	3.537190	2.088564	0.000152
19	6	0	-0.695699	-1.337083	-0.000186
20	6	0	-1.047228	1.593550	0.000167
21	8	0	-0.599126	-2.549194	-0.000169
22	8	0	-1.163888	2.808809	0.000109
23	8	0	2.119624	-2.183003	-0.000176
24	8	0	4.166598	-0.561096	-0.000020
25	6	0	5.333670	0.261416	0.000038
26	1	0	5.370025	0.887801	0.895471
27	1	0	6.173405	-0.428521	-0.000001
28	1	0	5.370035	0.887913	-0.895317

Zero-point correction= 0.203601 (Hartree/Particle)
Thermal correction to Energy= 0.218534
Thermal correction to Enthalpy= 0.219479
Thermal correction to Gibbs Free Energy= 0.159082
Sum of electronic and zero-point Energies= -877.870902
Sum of electronic and thermal Energies= -877.855969
Sum of electronic and thermal Enthalpies= -877.855025
Sum of electronic and thermal Free Energies= -877.915421

Oxygen-centered Radical 2.4
MN12-SX/6-311G(3d)//B3LYP/6-311G(d)

HF=-877.4395648

Sulfur-centered Radical 2.5a
B3LYP/6-311G(d)

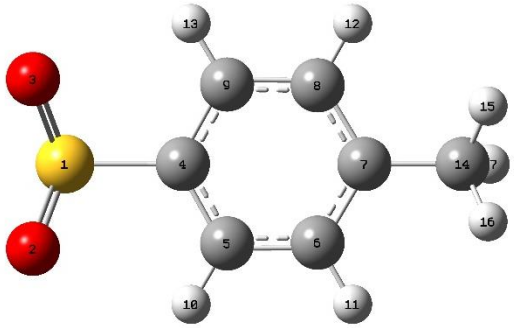

Standard orientation:

Center Number	Atomic Number	Atomic Type	Coordinates (Angstroms) X	Y	Z
1	16	0	-2.167813	-0.000012	-0.245990
2	8	0	-2.658403	-1.297348	0.282240
3	8	0	-2.658431	1.297329	0.282178
4	6	0	-0.359740	0.000006	-0.093187
5	6	0	0.317354	-1.215930	-0.070987
6	6	0	1.706074	-1.203341	0.001081
7	6	0	2.421600	0.000034	0.033091
8	6	0	1.706058	1.203381	0.001112
9	6	0	0.317321	1.215943	-0.070956
10	1	0	-0.234646	-2.148011	-0.080445
11	1	0	2.241861	-2.146925	0.038641
12	1	0	2.241820	2.146975	0.038694
13	1	0	-0.234694	2.148015	-0.080395
14	6	0	3.928705	-0.000014	0.076924
15	1	0	4.316569	0.884443	0.586694
16	1	0	4.316396	-0.882720	0.589875
17	1	0	4.348140	-0.001907	-0.935029

Zero-point correction= 0.125355 (Hartree/Particle)
Thermal correction to Energy= 0.134976
Thermal correction to Enthalpy= 0.135920
Thermal correction to Gibbs Free Energy= 0.087595
Sum of electronic and zero-point Energies= -819.511558
Sum of electronic and thermal Energies= -819.501937
Sum of electronic and thermal Enthalpies= -819.500993
Sum of electronic and thermal Free Energies= -819.549318

Sulfur-centered Radical 2.5a
MN12-SX/6-311G(3d)//B3LYP/6-311G(d)

HF=-819.2907336

Sulfur-centered Radical 2.5b
B3LYP/6-311G(d)

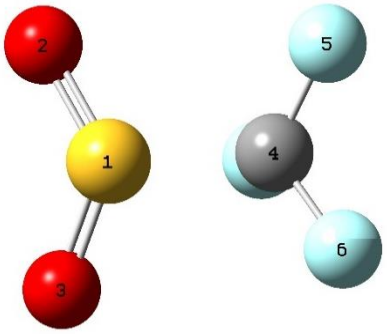

Standard orientation:

Center Number	Atomic Number	Atomic Type	Coordinates (Angstroms) X	Y	Z
1	16	0	1.035074	-0.000073	-0.331178
2	8	0	1.502429	1.293276	0.203170
3	8	0	1.501434	-1.293699	0.203145
4	6	0	-0.888347	0.000098	0.008638
5	9	0	-1.403286	1.086974	-0.545556
6	9	0	-1.403422	-1.086814	-0.545302
7	9	0	-1.111294	0.000280	1.312691

Zero-point correction= 0.021632 (Hartree/Particle)
Thermal correction to Energy= 0.028488
Thermal correction to Enthalpy= 0.029433
Thermal correction to Gibbs Free Energy= -0.011388
Sum of electronic and zero-point Energies= -886.303603
Sum of electronic and thermal Energies= -886.296747
Sum of electronic and thermal Enthalpies= -886.295803
Sum of electronic and thermal Free Energies= -886.336624

Sulfur-centered Radical 2.5b
MN12-SX/6-311G(3d)//B3LYP/6-311G(d)

HF=-886.023887

Transition State for Bond Dissociation of 2.1a
B3LYP/6-311G(d)

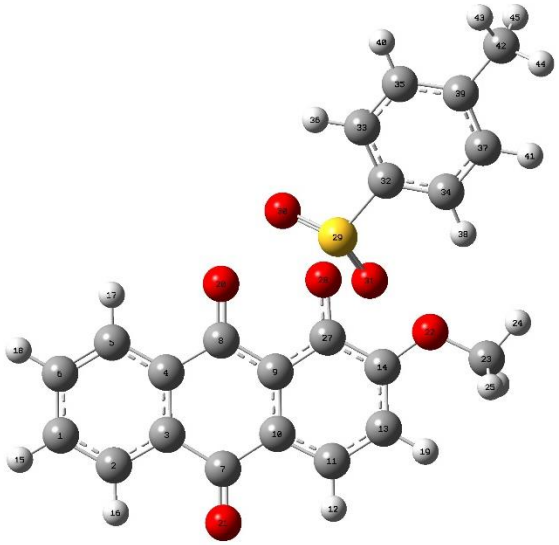

Standard orientation:

Center Number	Atomic Number	Atomic Type	Coordinates (Angstroms) X	Y	Z
1	6	0	-6.089619	-1.975517	-0.132565
2	6	0	-5.732901	-0.640897	-0.016829
3	6	0	-4.394075	-0.244046	-0.112970
4	6	0	-3.400080	-1.228801	-0.331577
5	6	0	-3.771907	-2.582823	-0.447612
6	6	0	-5.102670	-2.947775	-0.348365
7	6	0	-4.062638	1.199046	0.016826
8	6	0	-2.005614	-0.827837	-0.434917
9	6	0	-1.654882	0.541281	-0.282089
10	6	0	-2.632318	1.544667	-0.083269
11	6	0	-2.208170	2.865713	0.004840
12	1	0	-2.959013	3.632773	0.156239
13	6	0	-0.859913	3.206919	-0.105062
14	6	0	0.117029	2.224037	-0.293710
15	1	0	-7.131562	-2.267700	-0.055130
16	1	0	-6.474272	0.131879	0.151002
17	1	0	-3.004602	-3.331023	-0.609667
18	1	0	-5.380643	-3.993014	-0.436358
19	1	0	-0.576372	4.248953	-0.034965
20	8	0	-1.095609	-1.706704	-0.669278
21	8	0	-4.931001	2.049713	0.192434
22	8	0	1.441802	2.461189	-0.402221
23	6	0	1.901059	3.806154	-0.327812

24	1	0	2.980080	3.755034	-0.457552
25	1	0	1.470705	4.417148	-1.126746
26	1	0	1.669542	4.251314	0.644240
27	6	0	-0.273904	0.861832	-0.390396
28	8	0	0.598416	-0.105267	-0.587348
29	16	0	1.577476	-0.767777	1.116172
30	8	0	1.143725	-2.131244	1.412572
31	8	0	1.404283	0.332426	2.065485
32	6	0	3.244025	-0.799912	0.484133
33	6	0	3.717090	-1.971047	-0.104539
34	6	0	4.015255	0.358806	0.532262
35	6	0	5.004003	-1.979020	-0.628752
36	1	0	3.093644	-2.856019	-0.135912
37	6	0	5.300658	0.324178	0.006309
38	1	0	3.613697	1.258219	0.980782
39	6	0	5.815525	-0.838762	-0.580993
40	1	0	5.384007	-2.889142	-1.082433
41	1	0	5.916002	1.217644	0.051941
42	6	0	7.220944	-0.870650	-1.125078
43	1	0	7.312555	-1.565659	-1.962472
44	1	0	7.543294	0.115106	-1.467113
45	1	0	7.929008	-1.195253	-0.354781

Zero-point correction= 0.329119 (Hartree/Particle)
Thermal correction to Energy= 0.354342
Thermal correction to Enthalpy= 0.355286
Thermal correction to Gibbs Free Energy= 0.269330
Sum of electronic and zero-point Energies= -1697.342483
Sum of electronic and thermal Energies= -1697.317260
Sum of electronic and thermal Enthalpies= -1697.316316
Sum of electronic and thermal Free Energies= -1697.402272

Imaginary frequency=-365.04 cm^{-1}

Transition State for Bond Dissociation of 2.1a
MN12-SX/6-311G(3d)//B3LYP/6-311G(d)

HF= -1696.6996361

Transition State for Bond Dissociation of 2.1b
B3LYP/6-311G(d)

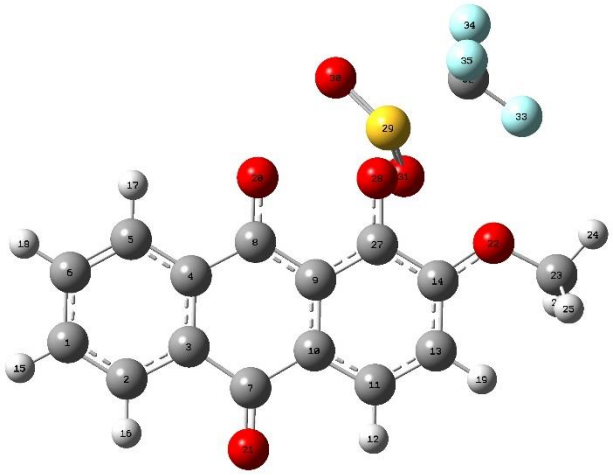

Standard orientation:

Center Number	Atomic Number	Atomic Type	Coordinates (Angstroms) X	Y	Z
1	6	0	-5.725904	-1.377072	0.135658
2	6	0	-5.180001	-0.111328	0.284299
3	6	0	-3.810772	0.106784	0.094428
4	6	0	-2.983734	-0.987439	-0.253912
5	6	0	-3.546246	-2.271120	-0.402610
6	6	0	-4.903126	-2.458594	-0.208754
7	6	0	-3.271681	1.480361	0.264069
8	6	0	-1.560557	-0.769752	-0.456764
9	6	0	-1.005030	0.528678	-0.282284
10	6	0	-1.819043	1.636120	0.056848
11	6	0	-1.216193	2.882951	0.194122
12	1	0	-1.849217	3.723077	0.456332
13	6	0	0.153057	3.061615	0.005132
14	6	0	0.969944	1.976203	-0.327057
15	1	0	-6.789047	-1.530652	0.286614
16	1	0	-5.791866	0.742882	0.550514
17	1	0	-2.907013	-3.105816	-0.666599
18	1	0	-5.329040	-3.449834	-0.323616
19	1	0	0.579049	4.049383	0.123465
20	8	0	-0.808479	-1.760735	-0.800709
21	8	0	-3.994288	2.428252	0.556523
22	8	0	2.300198	2.028109	-0.510887
23	6	0	2.986776	3.256279	-0.279298
24	1	0	4.038034	3.035375	-0.445845

25	1	0	2.659035	4.028476	-0.980856
26	1	0	2.841631	3.598064	0.748922
27	6	0	0.390614	0.692571	-0.494888
28	8	0	1.126781	-0.350716	-0.850678
29	16	0	2.152553	-1.211755	0.623487
30	8	0	1.903137	-2.644943	0.634500
31	8	0	2.026191	-0.368270	1.806533
32	6	0	3.934923	-1.004568	-0.071265
33	9	0	4.404422	0.197030	0.229734
34	9	0	4.701534	-1.933579	0.492226
35	9	0	3.916389	-1.175293	-1.383440

Zero-point correction= 0.225572 (Hartree/Particle)
Thermal correction to Energy= 0.247890
Thermal correction to Enthalpy= 0.248834
Thermal correction to Gibbs Free Energy= 0.170636
Sum of electronic and zero-point Energies= -1764.133922
Sum of electronic and thermal Energies= -1764.111604
Sum of electronic and thermal Enthalpies= -1764.110660
Sum of electronic and thermal Free Energies= -1764.188859

Imaginary frequency=-398.82 cm^{-1}

Transition State for Bond Dissociation of 2.1b
MN12-SX/6-311G(3d)//B3LYP/6-311G(d)

HF=-1763.4325556

7.2.12 Calculated UV-Vis Bands & Oscillator Strengths

Table 7.3. Calculated UV-Vis bands and oscillator strengths for **2.1a** (singlet)

State	Energy (kcal/mol)	Excitation Wavelength (nm)	Oscillator Strength
S0	0		
S1	68.6	417	0.0002
S2	74.3	385	0.0614
S3	76.3	375	0.0159
S4	88.1	324	0.0307
S5	90.6	315	0.0453
S6	92.6	309	0.0003
S7	95.7	299	0.0000
S8	99.6	287	0.0544

S9	100.9	283	0.1000
S10	103.6	276	0.1696
S11	106.6	268	0.0035
S12	108.3	264	0.0032

Table 7.4. Calculated UV-Vis bands and oscillator strengths for **2.1a** (triplet)

State	Energy (kcal/mol)	Excitation Wavelength (nm)	Oscillator Strength
T1	59.1		
T2	73.5	1991	0.0001
T3	77.4	1561	0.0001
T4	82.8	1204	0.0017
T5	85.6	1079	0.0000
T6	88.6	970	0.0002
T7	104.7	627	0.0025
T8	106.1	608	0.0161
T9	109.3	569	0.0004
T10	118.6	481	0.0053
T11	121.1	462	0.0211
T12	122.1	454	0.0494
T13	126.6	424	0.0044
T14	126.8	422	0.0194
T15	131.8	393	0.0209
T16	134.6	379	0.0017
T17	135.5	374	0.0421
T18	136.4	370	0.0002
T19	136.4	370	0.0059
T20	138.0	362	0.0365
T21	138.8	359	0.1207
T22	140.6	351	0.0006
T23	142.2	344	0.0090
T24	142.9	341	0.0065
T25	143.5	339	0.0000
T26	146.3	328	0.0001
T27	149.5	316	0.0071
T28	151.8	309	0.0104
T29	152.0	308	0.0178
T30	153.2	304	0.0009

Table 7.5. Calculated UV-Vis bands and oscillator strengths for **2.1b** (singlet)

State	Energy (kcal/mol)	Excitation Wavelength (nm)	Oscillator Strength
S0	0		
S1	68.8	416	0.0016
S2	75.9	377	0.0035
S3	77.7	368	0.0528
S4	88.7	322	0.0591
S5	90.0	318	0.0386
S6	100.1	286	0.0090
S7	102.0	280	0.1027
S8	106.4	269	0.2177
S9	108.1	264	0.0475
S10	114.0	251	0.0178
S11	116.3	246	0.2313
S12	120.0	238	0.0091

Table 7.6. Calculated UV-Vis bands and oscillator strengths for **2.1b** (triplet)

State	Energy (kcal/mol)	Excitation Wavelength (nm)	Oscillator Strength
T1	60.2		
T2	74.0	2073	0.0000
T3	76.5	1756	0.0000
T4	81.4	1348	0.0019
T5	84.6	1173	0.0000
T6	87.5	1046	0.0000
T7	108.3	594	0.0111
T8	114.9	523	0.0000
T9	122.9	456	0.0280
T10	125.9	435	0.0000
T11	127.5	424	0.0212
T12	131.4	401	0.0160
T13	132.2	397	0.0274
T14	135.9	378	0.0023
T15	137.1	372	0.0014
T16	139.1	362	0.1690
T17	139.2	362	0.0022
T18	140.9	354	0.0003
T19	143.0	345	0.0254
T20	144.8	338	0.0070

7.3 Chapter 3 Experimental

7.3.1 UV-Vis Spectra

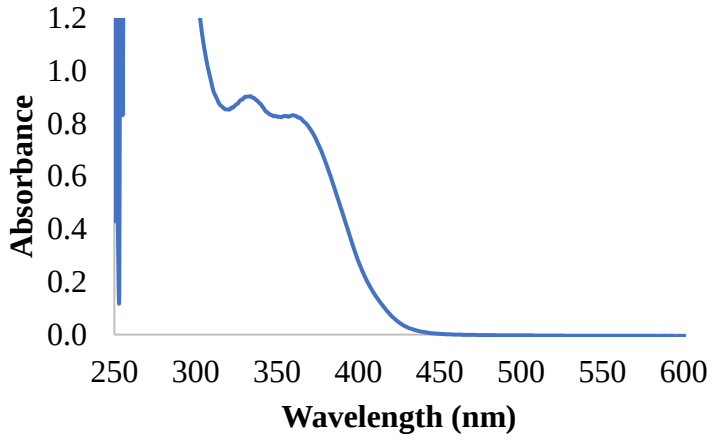

Figure 7.15. UV-Vis spectrum of 1-tosyloxy-2-methoxyanthraquinone **3.1** in DMSO

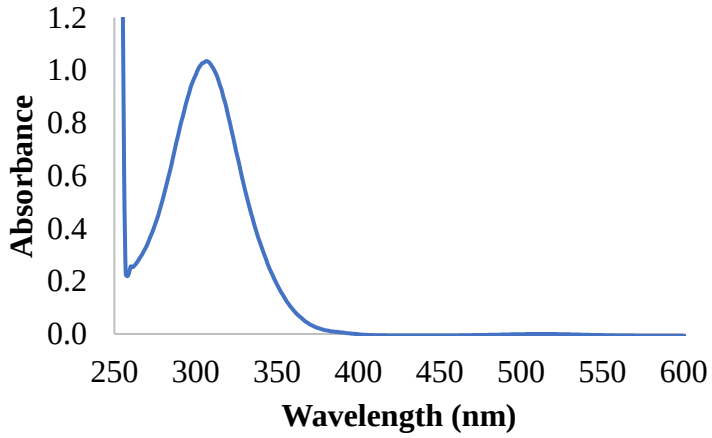

Figure 7.16. UV-Vis spectrum of 4-cyanopentanoic acid dithiobenzoate (CPADB) in DMSO

7.3.2 GPC Analysis

Gel Permeation Chromatography (GPC) was used to obtain molecular weight (M_n and M_w) and polydispersity index (PDI) of polymers using Viscotek GPCMax equipped with 4 columns (T2500, T3000, T4000, and T5000) in a

column oven and differential refractometer (maintained at 40 °C). Tetrahydrofuran (HPLC Grade) was used as the eluent with a flow rate of 1 mL/min. Polystyrene standards (from Polymer Laboratories Inc., 580 Da – 3,150 kDa) were used for calibration. For GPC sample preparation, 2 mg of dry polymer sample was dissolved in 1 mL of THF (HPLC Grade).

7.3.3 Ring Opening Polymerization

Typical procedure for ROP of ε-CL: In a 0.5 dram vial was added ε-CL (0.57 g, 5 mmol), benzyl alcohol (10 μL, 0.1 mmol), 1-tosyloxy-2-methoxyanthraquinone **6.1** (4 mg, 0.01 mmol), and 50 μL of dichloromethane. The solution was photolyzed with the 447 nm CW laser (1W) until full conversion of the PAG. The mixture continued to polymerize in the absence of light until monomer conversion was nearly complete. Conversion was measured by dissolving 10 μL of the polymerization mixture in 0.5 mL of $CDCl_3$ for ^1H NMR and comparing the ratio of the signals corresponding to monomer and polymer. The polymer was isolated by dissolving in chloroform followed by precipitation from cold diethyl ether. The precipitate was vacuum filtered and rinsed with cold diethyl ether.

Typical procedure for ROP of δ-VL: In a 0.5 dram vial was added δ-VL (0.50 g, 5 mmol), benzyl alcohol (10 μL, 0.1 mmol), 1-tosyloxy-2-methoxyanthraquinone **6.1** (4 mg, 0.01 mmol), and 50 μL of dichloromethane. The solution was photolyzed with the 447 nm CW laser (1W) until full conversion of the PAG. The mixture continued to polymerize in the absence of light until monomer conversion was nearly complete. Conversion was

measured by dissolving 10 μL of the polymerization mixture in 0.5 mL of $CDCl_3$ for ^1H NMR and comparing the ratio of the signals corresponding to monomer and polymer. The polymer was isolated by dissolving in chloroform followed by precipitation from cold diethyl ether. The precipitate was vacuum filtered and rinsed with cold diethyl ether.

7.3.4 RAFT Polymerization

Typical procedure for RAFT polymerization of MMA: In a 0.5 dram vial was added MMA (0.25 mL, 2.34 mmol), CPADB (6.5 mg, 0.023 mmol), 1-tosyloxy-2-methoxyanthraquinone **6.1** (1 mg, 0.002 mmol), and 0.25 mL of DMSO. The solution was photolyzed in an RPR-100 Rayonet reactor (16-bulb, 419 nm broadband irradiation, spectral distribution 380 nm-480 nm) for 18 hours. Conversion was measured by dissolving 10 μL of the polymerization mixture in 0.5 mL of $CDCl_3$ for ^1H NMR. The signal corresponding to DMSO was used as the internal standard. The polymer was isolated by precipitating from 1:1 methanol: petroleum ether. The precipitate was vacuum filtered and rinsed with cold 1:1 methanol: petroleum ether.

Typical procedure for RAFT polymerization of HEMA: In a 0.5 dram vial was added HEMA (0.28 mL, 2.31 mmol), CPADB (6.5 mg, 0.023 mmol), 1-tosyloxy-2-methoxyanthraquinone **6.1** (1 mg, 0.002 mmol), and 0.25 mL of DMSO. The solution was photolyzed in the RPR-100 Rayonet reactor (16-bulb, 419 nm broadband irradiation, spectral distribution 380 nm-480 nm) for 18 hours. Conversion was measured by dissolving 10 μL of the polymerization mixture in 0.5 mL of CD_3OD for ^1H NMR. The signal

corresponding to DMSO was used as the internal standard. The polymer was isolated by dissolving in a small amount of methanol and then poured into cold diethyl ether. The resulting suspension was centrifuged and decanted. The polymer was dissolved and precipitated an additional two times.

7.3.5 Brush Copolymerization

In a 0.5 dram vial was added HEMA (56 μL, 0.46 mmol, δ-VL (0.46 g, 4.6 mmol), CPADB (6.5 mg, 0.023 mmol), 1-tosyloxy-2-methoxyanthraquinone **6.1** (6 mg, 0.015 mmol), and 0.175 mL of DMSO. The solution was photolyzed in an RPR-100 Rayonet reactor (16-bulb, 419 nm broadband irradiation, spectral distribution 380 nm-480 nm) for 18 hours. The solution was then photolyzed with the 447 nm CW (1W) laser for 4 hours. Conversion was measured by dissolving 10 μL of the polymerization mixture in 0.5 mL of CD_3OD for ^1H NMR. The signal corresponding to DMSO was used as the internal standard. The polymer was isolated by dissolving in a small amount of methanol and then poured into cold diethyl ether. The resulting suspension was centrifuged and decanted. The polymer was dissolved and precipitated an additional two times.

7.4 Chapter 4 Experimental

7.4.1 Synthesis

9-benzyloxy-9-phenylanthrone (benzyl ether 4.5) was synthesized according to a literature procedure.[123]

10-(4-hydroxyphenyl)-10-(pentyloxy)-9(10*H*)-anthracenone 4.7 was synthesized using the following synthetic route:

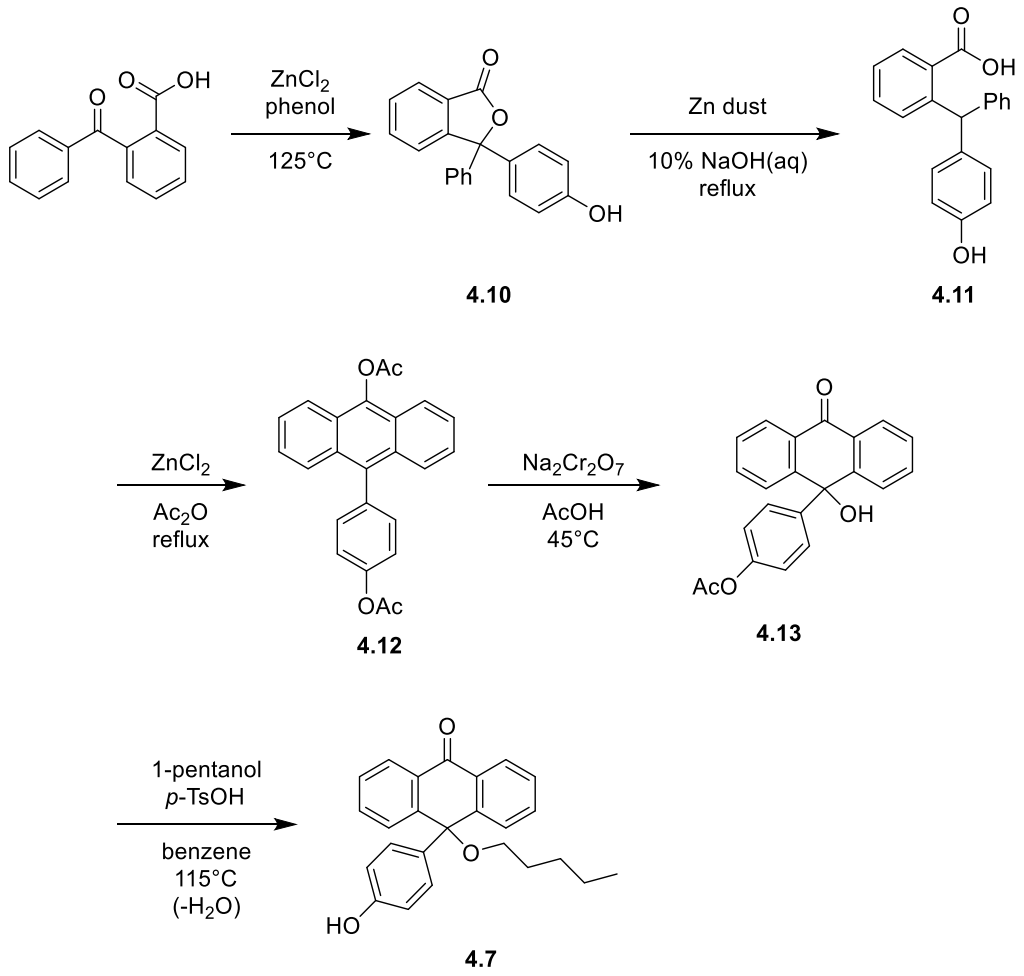

3-Phenyl-3-(4-hydroxyphenyl)phthalide 4.10: Following modified literature procedures,[169, 170] in a 250 mL round bottom flask equipped with a stir bar was added 2-benzoylbenzoic acid (6.9367 g, 30.7 mmol), phenol (3.0873 g, 32.8 mmol), and zinc chloride (4.2408 g, 31.1 mmol). The solid mixture was heated to 125°C and stirred in the melt for 8 hours. Upon completion of the reaction, boiling acetic acid was added until dissolved. Once dissolved, the reaction mixture was poured into approximately 200 mL of deionized water and a white precipitate formed. The water was decanted off and the precipitate was

dissolved in ethyl acetate and washed with 15% aqueous sodium carbonate. The organic layer was dried with magnesium sulfate and the solvent was removed under reduced pressure to yield 5.5278 g (60%) of phthalide.

2-(4'-hydroxybenzhydryl)benzoic acid 4.11 was synthesized following a literature procedure.[170]

9-acetoxy-10-(4-acetoxyphenyl)anthracene 4.12: Following a modified literature procedure,[171] in a 10 mL round bottom flask equipped with a stir bar was added 2-(4'-hydroxybenzhydryl)benzoic acid (1.6283 g, 5.35 mmol) and zinc chloride (0.5 g). To this, acetic anhydride (3.26 mL, 34.5 mmol) was added and the reaction mixture was heated at 99°C for 15 minutes. (Note: this reaction is very time and temperature sensitive). Upon completion of the reaction, the mixture was poured into pH 4 deionized water (acidified with HCl) and a precipitate formed. The water was decanted off and the precipitate was dissolved in dichloromethane, then dried over magnesium sulfate, and then the solvent was removed under reduced pressure to yield 1.9393 g (98%) of 9-acetoxy-10-(4-acetoxyphenyl)anthracene.

10-(4-(acetyloxy)phenyl)-10-hydroxy-9-anthracenone 4.13: Following a literature procedure for the oxidation of 9-phenylanthracene,[123] to a 50 mL round bottom flask equipped with a stir bar, 9-acetoxy-10-(4-acetoxyphenyl)anthracene (1.9534 g, 5.27 mmol) was added to 20 mL of glacial acetic acid. To the slurry solution, sodium dichromate dihydrate (2.3663 g, 7.94 mmol) was added and the mixture was heated at 45°C for 90 minutes with stirring. Soon after the addition of sodium dichromate the solution goes from a

tan/brownish color to dark green. After 90 minutes, the solution was poured into 40 mL of deionized water and vacuum filtered. The precipitate was washed with generous portions of deionized water and placed under vacuum to dry, yielding 1.5935 g (88%) of 10-(4-(acetyloxy)phenyl)-10-hydroxy-9-anthracenone.

10-(4-hydroxyphenyl)-10-(pentyloxy)-9(10*H*)-anthracenone 4.7: Following a literature procedure for synthesizing PTO-ethers,[123] in a 50 mL round bottom flask equipped with a stir bar, 10-(4-acetoxyphenyl)-10-hydroxy-9(10*H*)-anthracenone (0.2303 g, 0.669 mmol), *p*-toluenesulfonic acid monohydrate (48.8 mg, 0.257 mmol) and 1-pentanol (0.20 mL, 1.85 mmol) was added to 25 mL of benzene. The solution was heated at 115°C for 18 hours under reflux equipped with a Dean-Stark trap for the removal of water. Upon completion of the reaction, the solution was left to cool to room temperature and the solvent was removed under reduced pressure. The resulting crude solid was purified using flash chromatography with silica gel and a mobile phase of 80:20 hexanes: ethyl acetate to yield 0.0823 g (33%) of 10-(4-hydroxyphenyl)-10-(pentyloxy)-9(10*H*)-anthracenone. m.p. = 168-172°C, ^{1}H NMR (400 MHz, DMSO-d6) δ = 9.33 (1H, s), 8.19-8.17 (2H, dd), 7.71-7.67 (2H, dt), 7.54-7.50 (2H, dt), 7.47-7.45 (2H, d), 7.03-7.01 (2H, d), 6.62-6.60 (2H, d), 2.95-2.92 (2H, t), 1.56-1.49 (2H, m), 1.35-1.27 (2H, m), 1.24-1.15 (2H, m), 0.85-0.82 (3H, t). ^{13}C NMR (400 MHz, DMSO-d6) δ = 183.43, 156.82, 146.42, 137.65, 135.14, 131.74, 129.09, 127.23, 127.18, 115.93, 78.12, 63.87, 29.87, 28.69, 22.68,

14.70 (1 peak not accounted for and could be overlapping with previous peaks). HRMS (ESI-) Calcd for $C_{25}H_{24}O_3$ [M-H]$^-$: 371.1653, Found: 371.1643

7.4.2 Gas Chromatography Analysis

Gas chromatography analysis was done using a Shimadzu GC-17A, containing a RTX-5 stationary phase column (length = 15 m, inner diameter (i.d.) = 0.25 mm, film thickness = 0.25 μm), equipped with a FID detection system, and using the following method specifications: column temperature = 60°C, injection temperature = 280°C, and detector temperature = 300°C, with a temperature/pressure profile for injection of: 67 kPa, 3.0 minutes, 3.9 mL/minute, 98 kPa, 9.0 minutes, column of: 60°C, 3 minutes, 30 mL/minute, 300°C, 9.0 minutes, injector pressure of 60 kPa, total flow of 31 mL/min., column flow of 1.45 mL/min., and a linear velocity of 39.1 cm/s. For quantifying the yield of benzyl alcohol, a calibration curve was generated (Figure 7.10).

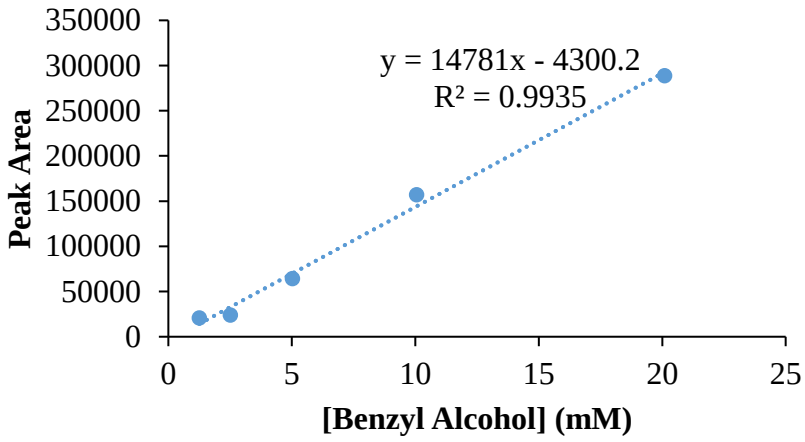

Figure 7.17. Calibration curve for benzyl alcohol **4.6**

7.4.3 Steady-State Photolysis

Benzyl ether **4.5** was photolyzed in an RPR-600 Rayonet reactor (8-bulb, 350 nm max output, spectral distribution 300 nm-400 nm). 1 mL of a 9 mM photolysis solution was placed in a quartz cuvette and purged with nitrogen in both the solution (minimum of 15 minutes) and the headspace (minimum of 3 minutes). The samples were irradiated at 350 nm for up to 3 hours. Upon completion of photolysis, 60 µl of the sample was transferred into a GC vial and then acidified by adding 10 µL of 0.1 M acetic acid. 2 µL of this solution was injected into the GC for analysis.

7.4.4 Pseudo First-Order Analysis

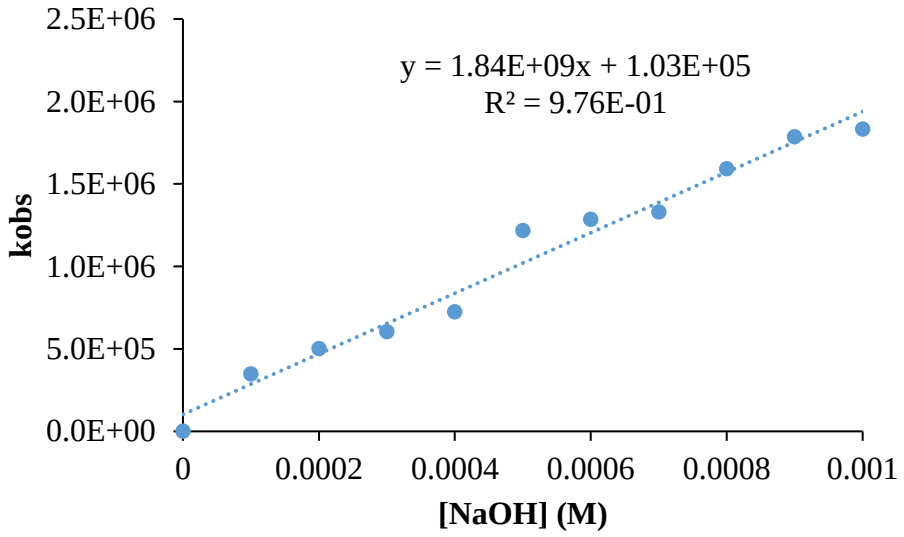

Figure 7.18. Pseudo first-order analysis for determination of second-order rate constant for proton transfer between ketyl radical **4.3** and anion radical **4.2**

7.5 Chapter 5 Experimental

7.5.1 Synthesis

***N*-(4,4'-dibromodiphenyl)-2,4,6-trimethylpyridinium tetrafluoroborate 5.1** was synthesized according to a literature procedure.[146]

7.5.2 Photoproduct Analysis

Guanosine (0.0769 g, 0.272 mmol) was dissolved in 100 mL of water with gentle heating. *N*-(4,4'-dibromodiphenyl)-2,4,6-trimethylpyridinium tetrafluoroborate (0.0708 g, 0.133 mmol) was added and 15 mL of acetonitrile was added for solubility. The reaction mix was photolyzed with a household lamp for 10 hours. Upon completion, the reaction mixture was extracted with chloroform and dried over $MgSO_4$. The solvent was removed under reduced pressure. The resulting residue was rinsed with diethyl ether followed by acetonitrile.

7.5.3 Kinetic Data from LFP

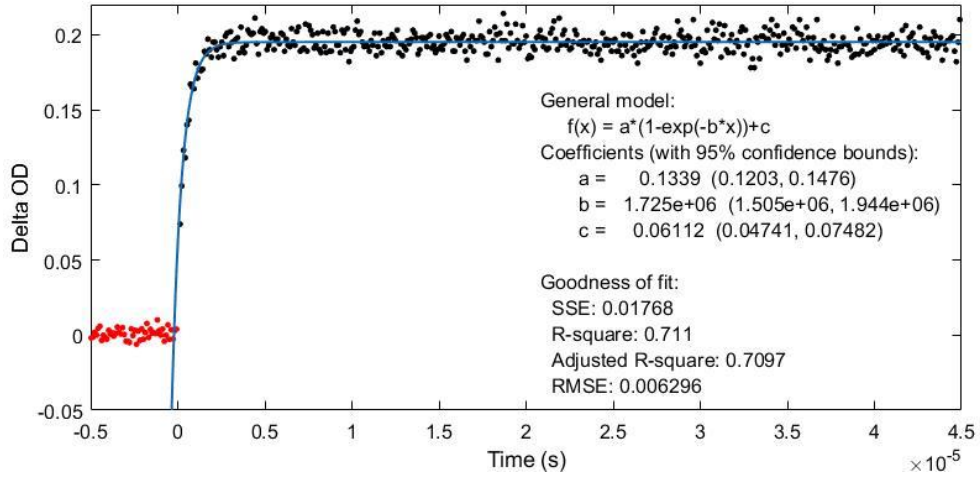

Figure 7.19. Curve fitting for the kinetic growth monitored at 330 nm from the pulsed 355 nm photolysis of *N*-(4,4'-dibromodiphenyl)-2,4,6-trimethylpyridinium tetrafluoroborate **5.1** in 95:5 pH 7.3 water: acetonitrile with 2.22 mM guanosine

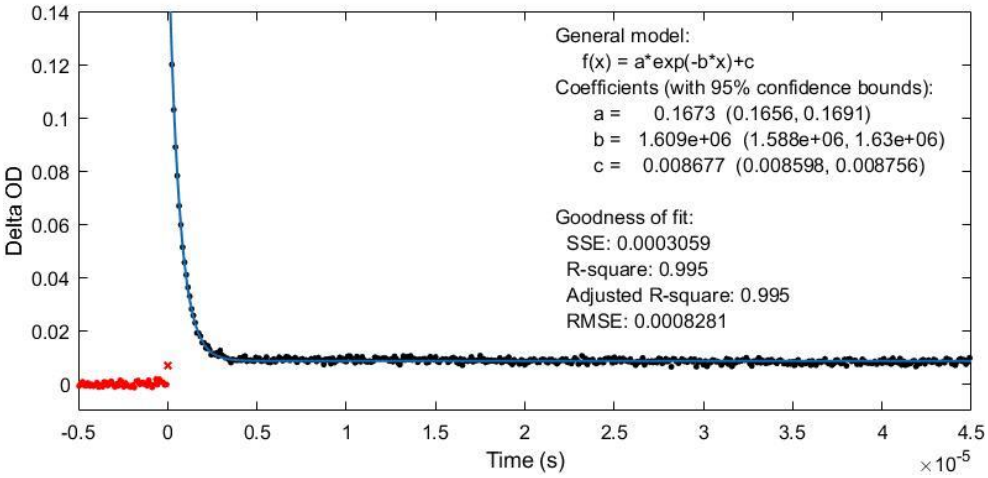

Figure 7.20. Curve fitting for the kinetic decay monitored at 450 nm from the pulsed 355 nm photolysis of *N*-(4,4'-dibromodiphenyl)-2,4,6-trimethylpyridinium tetrafluoroborate **5.1** in 95:5 pH 7.3 water: acetonitrile with 2.22 mM guanosine

7.6.1 Pseudo First-Order Analysis

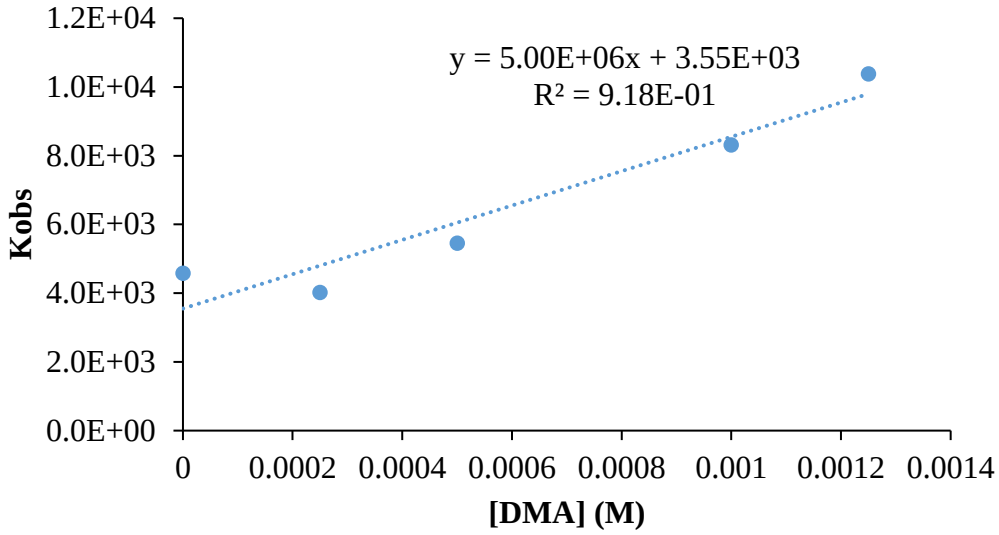

Figure 7.21. Pseudo first-order analysis for determination of second-order rate constant for electron transfer between cation radical **6.3** and *N*,*N*-dimethylaniline (DMA)

7.6.2 Evidence for Ground State Hydrogen Bonding

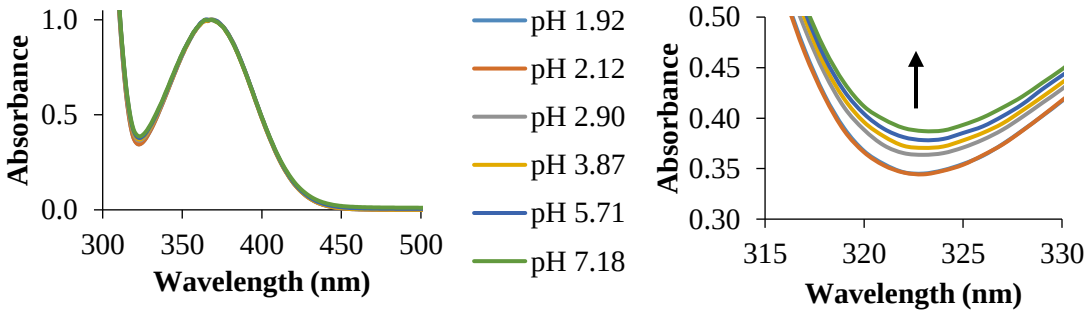

Figure 7.22. UV-Vis spectra of **6.1** (no photolysis) in buffered water at various pHs. Left: Full spectrum normalized at 368 nm. Right: Zoomed in on region of interest

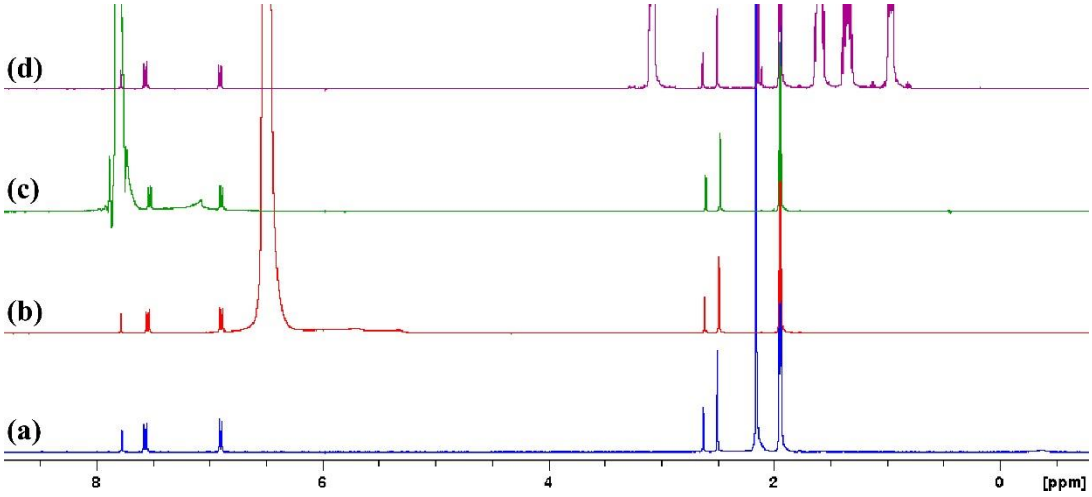

Figure 7.23. ^{1}H NMR spectra of **6.1** in CD_3CN under different conditions. (a) **6.1** only; (b) **6.1** + HBF_4; (c) **6.1** + $HClO_4$; (d) **6.1** + NBu_4ClO_4

Table 7.7. ^{1}H NMR chemical shifts of **6.1** in CD_3CN under different conditions

	6.1	**6.1 + HBF_4**	**Difference**
H_a	2.4979	2.4826	-0.0153
H_b	2.6229	2.6099	-0.0130
H_c	6.8871	6.8793	-0.0078
H_c	6.9097	6.9019	-0.0078
H_d	7.5523	7.5305	-0.0218
H_d	7.5749	7.5529	-0.0220
H_e	7.7728	7.7795	0.0067

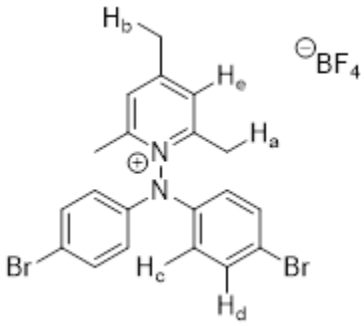

	6.1	**6.1 + $HClO_4$**	**Difference**
H_a	2.4979	2.4731	-0.0248
H_b	2.6229	2.6011	-0.0218
H_c	6.8871	6.8790	-0.0081
H_c	6.9097	6.9015	-0.0082
H_d	7.5523	7.5139	-0.0384
H_d	7.5749	7.5364	-0.0385
H_e	7.7728	under acid	n/a

	6.1	**6.1 + ClO_4^-**	**Difference**
H_a	2.4979	2.5000	0.0021
H_b	2.6229	2.6258	0.0029
H_c	6.8871	6.8907	0.0036
H_c	6.9097	6.9134	0.0037
H_d	7.5523	7.5517	-0.0006

H_d	7.5749	7.5742	-0.0007
H_e	7.7728	7.7795	0.0067

7.6.3 Cartesian Coordinates

Nitrenium Ion **6.2** (Singlet)

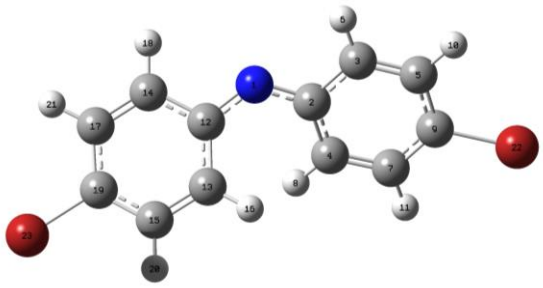

Standard orientation:

Center Number	Atomic Number	Atomic Type	Coordinates (Angstroms) X	Y	Z
1	7	0	0.000000	0.000000	1.659317
2	6	0	-0.037588	1.184460	1.041856
3	6	0	0.353180	2.301488	1.840558
4	6	0	-0.504130	1.417925	-0.290432
5	6	0	0.415228	3.560340	1.299825
6	1	0	0.645382	2.108840	2.866008
7	6	0	-0.488770	2.685654	-0.811270
8	1	0	-0.957608	0.610101	-0.851645
9	6	0	0.000000	3.750107	-0.028241
10	1	0	0.751880	4.405741	1.885384
11	1	0	-0.874644	2.884307	-1.802979
12	6	0	0.037588	-1.184460	1.041856
13	6	0	0.504130	-1.417925	-0.290432
14	6	0	-0.353180	-2.301488	1.840558
15	6	0	0.488770	-2.685654	-0.811270
16	1	0	0.957608	-0.610101	-0.851645
17	6	0	-0.415228	-3.560340	1.299825
18	1	0	-0.645382	-2.108840	2.866008
19	6	0	0.000000	-3.750107	-0.028241
20	1	0	0.874644	-2.884307	-1.802979
21	1	0	-0.751880	-4.405741	1.885384
22	35	0	0.038208	5.461779	-0.749090
23	35	0	-0.038208	-5.461779	-0.749090

Sum of electronic and zero-point Energies= -5664.621358
Sum of electronic and thermal Energies= -5664.608701
Sum of electronic and thermal Enthalpies= -5664.607756
Sum of electronic and thermal Free Energies= -5664.663565

Nitrenium Ion **6.2** (Triplet)

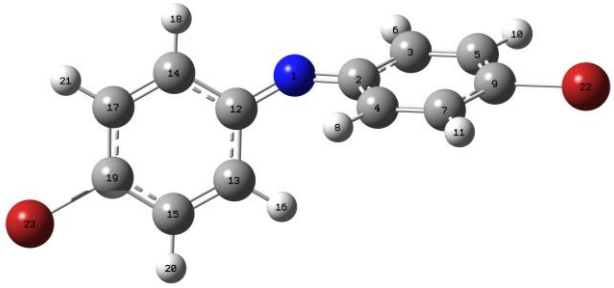

Standard orientation:

Center Number	Atomic Number	Atomic Type	Coordinates (Angstroms) X	Y	Z
1	7	0	0.000000	0.000000	1.200922
2	6	0	0.000000	1.250173	0.790169
3	6	0	-0.771128	2.231350	1.490849
4	6	0	0.821277	1.654926	-0.313970
5	6	0	-0.742995	3.538230	1.086183
6	1	0	-1.369303	1.915351	2.336261
7	6	0	0.828818	2.963117	-0.712781
8	1	0	1.418106	0.907700	-0.823255
9	6	0	0.051587	3.911280	-0.016062
10	1	0	-1.324857	4.289214	1.604982
11	1	0	1.430963	3.278835	-1.555379
12	6	0	0.000000	-1.250173	0.790169
13	6	0	-0.821277	-1.654926	-0.313970
14	6	0	0.771128	-2.231350	1.490849
15	6	0	-0.828818	-2.963117	-0.712781
16	1	0	-1.418106	-0.907700	-0.823255
17	6	0	0.742995	-3.538230	1.086183
18	1	0	1.369303	-1.915351	2.336261
19	6	0	-0.051587	-3.911280	-0.016062
20	1	0	-1.430963	-3.278835	-1.555379
21	1	0	1.324857	-4.289214	1.604982
22	35	0	0.079843	5.687780	-0.563205
23	35	0	-0.079843	-5.687780	-0.563205

Sum of electronic and zero-point Energies= -5664.603347
Sum of electronic and thermal Energies= -5664.590176
Sum of electronic and thermal Enthalpies= -5664.589232
Sum of electronic and thermal Free Energies= -5664.647945

Cation Radical **6.5**

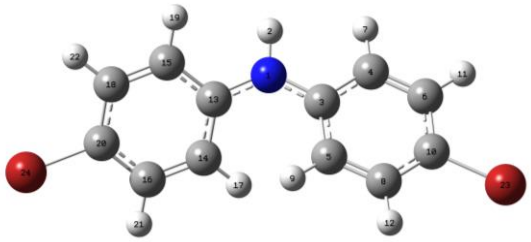

Standard orientation:

Center Number	Atomic Number	Atomic Type	Coordinates (Angstroms) X	Y	Z
1	7	0	0.000000	0.000000	1.617174
2	1	0	0.000000	0.000000	2.633311
3	6	0	0.002909	1.245847	1.029561
4	6	0	-0.443785	2.338740	1.802350
5	6	0	0.492095	1.459846	-0.275697
6	6	0	-0.455098	3.604869	1.265280
7	1	0	-0.805030	2.174489	2.811889
8	6	0	0.485097	2.731457	-0.806699
9	1	0	0.929542	0.644072	-0.836361
10	6	0	0.000000	3.802471	-0.045428
11	1	0	-0.811695	4.445503	1.846027
12	1	0	0.878951	2.909827	-1.799117
13	6	0	-0.002909	-1.245847	1.029561
14	6	0	-0.492095	-1.459846	-0.275697
15	6	0	0.443785	-2.338740	1.802350
16	6	0	-0.485097	-2.731457	-0.806699
17	1	0	-0.929542	-0.644072	-0.836361
18	6	0	0.455098	-3.604869	1.265280
19	1	0	0.805030	-2.174489	2.811889
20	6	0	0.000000	-3.802471	-0.045428
21	1	0	-0.878951	-2.909827	-1.799117
22	1	0	0.811695	-4.445503	1.846027
23	35	0	-0.007610	5.522966	-0.766154

24	35	0	0.007610	-5.522966	-0.766154

Sum of electronic and zero-point Energies= -5665.251299
Sum of electronic and thermal Energies= -5665.238260
Sum of electronic and thermal Enthalpies= -5665.237316
Sum of electronic and thermal Free Energies= -5665.295392

Dication **6.6** (Singlet)

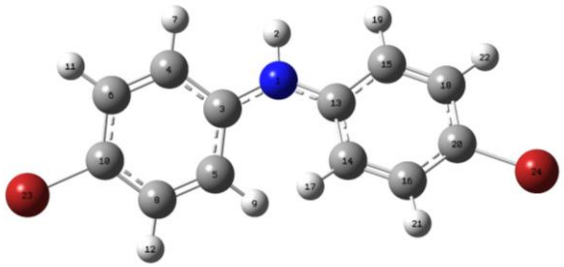

Standard orientation:

Center Number	Atomic Number	Atomic Type	Coordinates (Angstroms) X	Y	Z
1	7	0	0.000000	0.000000	1.519126
2	1	0	0.000000	0.000000	2.542749
3	6	0	0.033871	1.235933	0.968060
4	6	0	-0.315408	2.334234	1.815955
5	6	0	0.450355	1.471893	-0.378144
6	6	0	-0.357327	3.599272	1.309066
7	1	0	-0.594000	2.152228	2.849713
8	6	0	0.429851	2.743213	-0.872730
9	1	0	0.865136	0.668165	-0.973311
10	6	0	0.000000	3.817595	-0.046636
11	1	0	-0.654288	4.437007	1.928193
12	1	0	0.777580	2.950675	-1.877659
13	6	0	-0.033871	-1.235933	0.968060
14	6	0	-0.450355	-1.471893	-0.378144
15	6	0	0.315408	-2.334234	1.815955
16	6	0	-0.429851	-2.743213	-0.872730
17	1	0	-0.865136	-0.668165	-0.973311
18	6	0	0.357327	-3.599272	1.309066
19	1	0	0.594000	-2.152228	2.849713
20	6	0	0.000000	-3.817595	-0.046636
21	1	0	-0.777580	-2.950675	-1.877659
22	1	0	0.654288	-4.437007	1.928193
23	35	0	-0.033450	5.515290	-0.722534

24	35	0	0.033450	-5.515290	-0.722534

Sum of electronic and zero-point Energies= -5664.819323
Sum of electronic and thermal Energies= -5664.806486
Sum of electronic and thermal Enthalpies= -5664.805541
Sum of electronic and thermal Free Energies= -5664.861342

Dication **6.6** (Triplet)

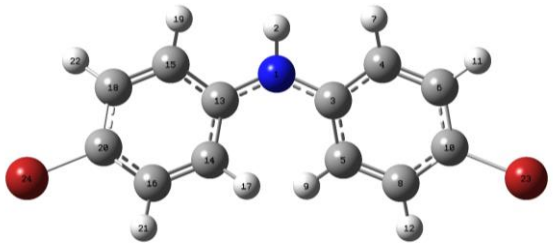

Standard orientation:

Center Number	Atomic Number	Atomic Type	Coordinates (Angstroms) X	Y	Z
1	7	0	0.000000	1.569921	0.000000
2	1	0	0.000000	2.586888	0.000000
3	6	0	1.250348	0.984872	0.005377
4	6	0	2.338733	1.781581	0.455679
5	6	0	1.473993	-0.325535	-0.492434
6	6	0	3.606416	1.273439	0.454644
7	1	0	2.155644	2.785271	0.824237
8	6	0	2.743312	-0.836864	-0.503585
9	1	0	0.661255	-0.899024	-0.918915
10	6	0	3.826247	-0.049803	-0.019406
11	1	0	4.442612	1.862078	0.813077
12	1	0	2.937318	-1.826011	-0.901917
13	6	0	-1.250348	0.984872	-0.005377
14	6	0	-1.473994	-0.325535	0.492434
15	6	0	-2.338733	1.781581	-0.455679
16	6	0	-2.743312	-0.836864	0.503586
17	1	0	-0.661256	-0.899024	0.918915
18	6	0	-3.606416	1.273439	-0.454644
19	1	0	-2.155644	2.785270	-0.824237
20	6	0	-3.826247	-0.049803	0.019406
21	1	0	-2.937318	-1.826011	0.901917
22	1	0	-4.442612	1.862077	-0.813077
23	35	0	5.517249	-0.733618	-0.027524

24 35 0 -5.517249 -0.733618 0.027524

Sum of electronic and zero-point Energies= -5664.808477
Sum of electronic and thermal Energies= -5664.795310
Sum of electronic and thermal Enthalpies= -5664.794366
Sum of electronic and thermal Free Energies= -5664.853016

7.6.4 Calculated UV-Vis Bands & Oscillator Strengths

Table 7.8. Calculated UV-Vis bands and oscillator strengths for nitrenium ion **6.2** (singlet)

State	Energy (kcal/mol)	Excitation Wavelength (nm)	Oscillator Strength
S1	43.2	662.4	0.2829
S2	71.5	399.7	0.6979
S3	71.6	399.5	0.0180
S4	74.3	385.0	0.1923
S5	82.5	346.6	0.0005

Table 7.9. Calculated UV-Vis bands and oscillator strengths for nitrenium ion **6.2** (triplet)

State	Energy (kcal/mol)	Excitation Wavelength (nm)	Oscillator Strength
T1	55.5	515.2	0.0031
T2	56.1	510.0	0.0036
T3	59.6	479.8	0.3867
T4	61.0	468.7	0.0123
T5	69.7	410.1	0.1292
T6	72.0	397.3	0.0001
T7	72.1	396.8	0.0035
T8	76.4	374.0	0.0029
T9	87.6	326.5	0.0004
T10	88.0	324.9	0.0005
T11	94.7	301.9	0.4173
T12	97.3	293.7	0.0062

Table 7.10. Calculated UV-Vis bands and oscillator strengths for cation radical **6.3**

State	Energy (kcal/mol)	Excitation Wavelength (nm)	Oscillator Strength
1	37.5	763.0	0.4431
2	55.3	517.2	0.0018
3	56.9	502.5	0.0017
4	68.1	420.1	0.0223
5	69.6	410.8	0.0001
6	69.7	410.0	0.0000
7	89.2	320.5	0.0250
8	94.4	302.8	0.3937
9	98.4	290.6	0.0021
10	104.1	274.7	0.0138
11	105.4	271.3	0.0104
12	109.4	261.4	0.0000

Table 7.11. Calculated UV-Vis bands and oscillator strengths for dication **6.4** (singlet)

State	Energy (kcal/mol)	Excitation Wavelength (nm)	Oscillator Strength
S1	50.1	570.7	1.1617
S2	56.3	507.9	0.0009
S3	57.0	501.3	0.0081
S4	58.6	487.9	0.0037
S5	59.2	482.8	0.0235

Table 7.12. Calculated UV-Vis bands and oscillator strengths for dication **6.4** (triplet)

State	Energy (kcal/mol)	Excitation Wavelength (nm)	Oscillator Strength
T1	32.9	868.8	0.0003
T2	34.1	838.0	0.0002
T3	34.3	833.9	0.0001
T4	34.4	830.6	0.0002
T5	42.4	674.3	0.4928
T6	61.2	466.9	0.0332
T7	76.4	374.1	0.0017
T8	80.6	354.8	0.0027
T9	81.1	352.4	0.0056
T10	85.0	336.4	0.0463
T11	89.1	321.1	0.3105
T12	90.3	316.5	0.0000

References

1. Bach, T.; Hehn, J. P., Photochemical Reactions as Key Steps in Natural Product Synthesis. *Angewandte Chemie International Edition* **2011,** *50* (5), 1000-1045.

2. Shaw, M. H.; Twilton, J.; MacMillan, D. W. C., Photoredox Catalysis in Organic Chemistry. *The Journal of Organic Chemistry* **2016,** *81* (16), 6898-6926.

3. Romero, N. A.; Nicewicz, D. A., Organic Photoredox Catalysis. *Chemical Reviews* **2016,** *116* (17), 10075-10166.

4. Ravelli, D.; Protti, S.; Fagnoni, M., Carbon–Carbon Bond Forming Reactions via Photogenerated Intermediates. *Chemical Reviews* **2016,** *116* (17), 9850-9913.

5. Skubi, K. L.; Blum, T. R.; Yoon, T. P., Dual Catalysis Strategies in Photochemical Synthesis. *Chemical Reviews* **2016,** *116* (17), 10035-10074.

6. McAtee, R. C.; McClain, E. J.; Stephenson, C. R. J., Illuminating Photoredox Catalysis. *Trends in Chemistry* **2019,** *1* (1), 111-125.

7. LaFratta, C. N.; Fourkas, J. T.; Baldacchini, T.; Farrer, R. A., Multiphoton Fabrication. *Angewandte Chemie International Edition* **2007,** *46* (33), 6238-6258.

8. Zhang, Y.-L.; Chen, Q.-D.; Xia, H.; Sun, H.-B., Designable 3D Nanofabrication by Femtosecond Laser Direct Writing. *Nano Today* **2010,** *5* (5), 435-448.

9. Jung, K.; Corrigan, N.; Ciftci, M.; Xu, J.; Seo, S. E.; Hawker, C. J.; Boyer, C., Designing with Light: Advanced 2D, 3D, and 4D Materials. *Advanced Materials* **2020,** *32* (18), 1903850.

10. Dougherty, T. J.; Gomer, C. J.; Henderson, B. W.; Jori, G.; Kessel, D.; Korbelik, M.; Moan, J.; Peng, Q., Photodynamic Therapy. *JNCI: Journal of the National Cancer Institute* **1998,** *90* (12), 889-905.

11. Lucky, S. S.; Soo, K. C.; Zhang, Y., Nanoparticles in Photodynamic Therapy. *Chemical Reviews* **2015,** *115* (4), 1990-2042.

12. Hoffmann, N., Photochemical Reactions as Key Steps in Organic Synthesis. *Chemical Reviews* **2008,** *108* (3), 1052-1103.

13. Corrigan, N.; Yeow, J.; Judzewitsch, P.; Xu, J.; Boyer, C., Seeing the Light: Advancing Materials Chemistry through Photopolymerization. *Angewandte Chemie International Edition* **2019,** *58* (16), 5170-5189.

14. Klán, P.; Wirz, J., *Photochemistry of Organic Compounds: From Concepts to Practice*. John Wiley & Sons: 2009.

15. Turro, N. J., *Modern Molecular Photochemistry*. University Science Books: 1991.

16. Weller, A., Electron-Transfer and Complex Formation in the Excited State. *Pure and Applied Chemistry* **1968,** *16* (1), 115-124.

17. Rehm, D.; Weller, A., Kinetics of Fluorescence Quenching by Electron and H-Atom Transfer. *Israel Journal of Chemistry* **1970,** *8* (2), 259-271.

18. Dormán, G.; Nakamura, H.; Pulsipher, A.; Prestwich, G. D., The Life of Pi Star: Exploring the Exciting and Forbidden Worlds of the Benzophenone Photophore. *Chemical Reviews* **2016,** *116* (24), 15284-15398.

19. Zeppuhar, A. N.; Wolf, S. M.; Falvey, D. E., Photoacid Generators Activated through Sequential Two-Photon Excitation: 1-Sulfonatoxy-2-alkoxyanthraquinone Derivatives. *The Journal of Physical Chemistry A* **2021,** *125* (24), 5227-5236.

20. Martin, C. J.; Rapenne, G.; Nakashima, T.; Kawai, T., Recent Progress in Development of Photoacid Generators. *Journal of Photochemistry and Photobiology C: Photochemistry Reviews* **2018,** *34*, 41-51.

21. Xia, Y.; Peng, L., Photoactivatable Lipid Probes for Studying Biomembranes by Photoaffinity Labeling. *Chemical Reviews* **2013,** *113* (10), 7880-7929.

22. Yue, X.; Yanez, C. O.; Yao, S.; Belfield, K. D., Selective Cell Death by Photochemically Induced pH Imbalance in Cancer Cells. *Journal of the American Chemical Society* **2013,** *135* (6), 2112-2115.

23. Fadhel, A. A.; Yue, X.; Ghazvini Zadeh, E. H.; Bondar, M. V.; Belfield, K. D., Pegylated and Nanoparticle-Conjugated Sulfonium Salt Photo Triggers Necrotic Cell Death. *International journal of nanomedicine* **2016,** *11*, 6161-6168.

24. Crivello, J. V.; Lam, J., Diaryliodonium Salts. A New Class of Photoinitiators for Cationic Polymerization. *Macromolecules* **1977,** *10* (6), 1307-1315.

25. Crivello, J. V.; Lam, J. H. W., Photoinitiated Cationic Polymerization with Triarylsulfonium Salts. *Journal of Polymer Science: Polymer Chemistry Edition* **1979,** *17* (4), 977-999.

26. Yu, T.; Ober, C. K.; Kuebler, S. M.; Zhou, W.; Marder, S. R.; Perry, J. W., Chemically Amplified Positive Resists for Two-Photon Three-Dimensional Microfabrication. *Advanced Materials* **2003,** *15* (6), 517-521.

27. Crivello, J. V., The Discovery and Development of Onium Salt Cationic Photoinitiators. *Journal of Polymer Science Part a-Polymer Chemistry* **1999,** *37* (23), 4241-4254.

28. Mokbel, H.; Toufaily, J.; Hamieh, T.; Dumur, F.; Campolo, D.; Gigmes, D.; Pierre Fouassier, J.; Ortyl, J.; Lalevée, J., Specific Cationic Photoinitiators for Near UV and Visible LEDs: Iodonium Versus Ferrocenium Structures. *Journal of Applied Polymer Science* **2015,** *132* (46).

29. Zivic, N.; Bouzrati-Zerrelli, M.; Villotte, S.; Morlet-Savary, F.; Dietlin, C.; Dumur, F.; Gigmes, D.; Fouassier, J. P.; Lalevée, J., A Novel Naphthalimide Scaffold Based Iodonium Salt as a One-Component Photoacid/Photoinitiator for Cationic and Radical Polymerization Under LED Exposure. *Polymer Chemistry* **2016,** *7* (37), 5873-5879.

30. Xia, R.; Malval, J.-P.; Jin, M.; Spangenberg, A.; Wan, D.; Pu, H.; Vergote, T.; Morlet-Savary, F.; Chaumeil, H.; Baldeck, P.; Poizat, O.; Soppera, O., Enhancement of Acid Photogeneration Through a Para-to-Meta Substitution Strategy in a Sulfonium-Based Alkoxystilbene Designed for Two-Photon Polymerization. *Chemistry of Materials* **2012,** *24* (2), 237-244.

31. Jin, M.; Wu, X.; Xie, J.; Malval, J. P.; Wan, D., One/Two-Photon-Sensitive Photoacid Generators Based on Benzene Oligomer-Containing D–π–A-Type Aryl Dialkylsulfonium Salts. *RSC Advances* **2015,** *5* (68), 55340-55347.

32. Zivic, N.; Kuroishi, P. K.; Dumur, F.; Gigmes, D.; Dove, A. P.; Sardon, H., Recent Advances and Challenges in the Design of Organic Photoacid and Photobase

Generators for Polymerizations. *Angewandte Chemie-International Edition* **2019,** *58* (31), 10410-10422.

33. Yamaoka, T.; Adachi, H.; Matsumoto, K.; Watanabe, H.; Shirosaki, T., Photochemical Dissociation of p-Nitrobenzyl 9,10-Dimethoxyanthracene-2-sulphonate via Intramolecular Electron Transfer. *Journal of the Chemical Society, Perkin Transactions 2* **1990,** (10), 1709-1714.

34. Andraos, J.; Barclay, G. G.; Medeiros, D. R.; Baldovi, M. V.; Scaiano, J. C.; Sinta, R., Model Studies on the Photochemistry of Phenolic Sulfonate Photoacid Generators. *Chemistry of Materials* **1998,** *10* (6), 1694-1699.

35. Terpolilli, M.; Merli, D.; Protti, S.; Dichiarante, V.; Fagnoni, M.; Albini, A., Cationic and Radical Intermediates in the Acid Photorelease from Aryl Sulfonates and Phosphates. *Photochemical & Photobiological Sciences* **2011,** *10* (1), 123-127.

36. Torti, E.; Della Giustina, G.; Protti, S.; Merli, D.; Brusatin, G.; Fagnoni, M., Aryl Tosylates as Non-Ionic Photoacid Generators (PAGs): Photochemistry and Applications in Cationic Photopolymerizations. *RSC Advances* **2015,** *5* (42), 33239-33248.

37. Arnold, P. A.; Fratesi, L. E.; Bejan, E.; Cameron, J.; Pohlers, G.; Liu, H.; Scaiano, J. C., Evidence of Homolytic and Heterolytic Pathways in the Photodissociation of Iminosulfonates and Direct Detection of the p-Toluenesulfonyloxyl Radical. *Photochemical & Photobiological Sciences* **2004,** *3* (9), 864-869.

38. Malval, J.-P.; Suzuki, S.; Morlet-Savary, F.; Allonas, X.; Fouassier, J.-P.; Takahara, S.; Yamaoka, T., Photochemistry of Naphthalimide Photoacid Generators. *The Journal of Physical Chemistry A* **2008,** *112* (17), 3879-3885.

39. Ikbal, M.; Banerjee, R.; Atta, S.; Dhara, D.; Anoop, A.; Singh, N. D. P., Synthesis, Photophysical and Photochemical Properties of Photoacid Generators Based on N-Hydroxyanthracene-1,9-dicarboxyimide and Their Application toward Modification of Silicon Surfaces. *The Journal of Organic Chemistry* **2012,** *77* (23), 10557-10567.

40. Steidl, L.; Jhaveri, S. J.; Ayothi, R.; Sha, J.; McMullen, J. D.; Ng, S. Y. C.; Zipfel, W. R.; Zentel, R.; Ober, C. K., Non-Ionic Photo-Acid Generators for Applications in Two-Photon Lithography. *Journal of Materials Chemistry* **2009,** *19* (4), 505-513.

41. Shi, Z.; Peng, P.; Strohecker, D.; Liao, Y., Long-Lived Photoacid Based upon a Photochromic Reaction. *Journal of the American Chemical Society* **2011,** *133* (37), 14699-14703.

42. Pawlicki, M.; Collins, H. A.; Denning, R. G.; Anderson, H. L., Two-Photon Absorption and the Design of Two-Photon Dyes. *Angewandte Chemie-International Edition* **2009,** *48* (18), 3244-3266.

43. Kobayashi, Y.; Mutoh, K.; Abe, J., Stepwise Two-Photon Absorption Processes Utilizing Photochromic Reactions. *Journal of Photochemistry and Photobiology C: Photochemistry Reviews* **2018,** *34*, 2-28.

44. Fourkas, J. T.; Petersen, J. S., 2-Colour Photolithography. *Physical Chemistry Chemical Physics* **2014,** *16* (19), 8731-8750.

45. Belfield, K. D.; Schafer, K. J.; Liu, Y.; Liu, J.; Ren, X.; Stryland, E. W. V., Multiphoton-Absorbing Organic Materials for Microfabrication, Emerging Optical Applications and Non-Destructive Three-Dimensional Imaging. *Journal of Physical Organic Chemistry* **2000,** *13* (12), 837-849.

46. Schwärzle, D.; Hou, X.; Prucker, O.; Rühe, J., Polymer Microstructures through Two-Photon Crosslinking. *Advanced Materials* **2017,** *29* (39), 1703469.

47. Cumpston, B. H.; Ananthavel, S. P.; Barlow, S.; Dyer, D. L.; Ehrlich, J. E.; Erskine, L. L.; Heikal, A. A.; Kuebler, S. M.; Lee, I. Y. S.; McCord-Maughon, D.; Qin, J.; Röckel, H.; Rumi, M.; Wu, X.-L.; Marder, S. R.; Perry, J. W., Two-Photon Polymerization Initiators for Three-Dimensional Optical Data Storage and Microfabrication. *Nature* **1999,** *398* (6722), 51-54.

48. Dvornikov, A. S.; Walker, E. P.; Rentzepis, P. M., Two-Photon Three-Dimensional Optical Storage Memory. *The Journal of Physical Chemistry A* **2009,** *113* (49), 13633-13644.

49. Starkey, J. R.; Rebane, A. K.; Drobizhev, M. A.; Meng, F.; Gong, A.; Elliott, A.; McInnerney, K.; Spangler, C. W., New Two-Photon Activated Photodynamic Therapy Sensitizers Induce Xenograft Tumor Regressions after Near-IR Laser Treatment through the Body of the Host Mouse. *Clinical Cancer Research* **2008,** *14* (20), 6564.

50. Schmitt, J.; Heitz, V.; Sour, A.; Bolze, F.; Ftouni, H.; Nicoud, J.-F.; Flamigni, L.; Ventura, B., Diketopyrrolopyrrole-Porphyrin Conjugates with High Two-Photon Absorption and Singlet Oxygen Generation for Two-Photon Photodynamic Therapy. *Angewandte Chemie International Edition* **2015,** *54* (1), 169-173.

51. Tasdelen, M. A.; Kumbaraci, V.; Jockusch, S.; Turro, N. J.; Talinli, N.; Yagci, Y., Photoacid Generation by Stepwise Two-Photon Absorption: Photoinitiated Cationic Polymerization of Cyclohexene Oxide by Using Benzodioxinone in the Presence of Iodonium Salt. *Macromolecules* **2008,** *41* (2), 295-297.

52. Shimizu, M.; Schelper, M.; Mochida, K.; Hiyama, T.; Adachi, M.; Sasaki, Y.; Akiyama, S.; Maeda, S.; Kanbara, H.; Mori, Y.; Kurihara, T., A Novel Strategy for Two-Photon Holographic Recording: Stepwise Two-Photon Absorption of α-Quinquethiophene Followed by Energy Transfer to an Aryl Azide. *Advanced Materials* **2007,** *19* (14), 1826-1829.

53. Thum, M. D.; Falvey, D. E., Photoreleasable Protecting Groups Triggered by Sequential Two-Photon Absorption of Visible Light: Release of Carboxylic Acids from a Linked Anthraquinone-N-Alkylpicolinium Ester Molecule. *Journal of Physical Chemistry A* **2018,** *122* (12), 3204-3210.

54. O'Connor, N. A.; Berro, A. J.; Lancaster, J. R.; Gu, X.; Jockusch, S.; Nagai, T.; Ogata, T.; Lee, S.; Zimmerman, P.; Willson, C. G.; Turro, N. J., Toward the Design of a Sequential Two Photon Photoacid Generator for Double Exposure Photolithography. *Chemistry of Materials* **2008,** *20* (24), 7374-7376.

55. Billone, P. S.; Park, J. M.; Blackwell, J. M.; Bristol, R.; Scaiano, J. C., Two-Photon Acid Generation in Thin Polymer Films. Photoinduced Electron Transfer As a Promising Tool for Subwavelength Lithography. *Chemistry of Materials* **2010,** *22* (1), 15-17.

56. Lamola, A. A.; Hammond, G. S., Mechanisms of Photochemical Reactions in Solution. XXXIII. Intersystem Crossing Efficiencies. *The Journal of Chemical Physics* **1965,** *43* (6), 2129-2135.

57. Herkstroeter, W. G.; Lamola, A. A.; Hammond, G. S., Mechanisms of Photochemical Reactions in Solution. XXVIII.1 Values of Triplet Excitation energies of Selected Sensitizers. *Journal of the American Chemical Society* **1964,** *86* (21), 4537-4540.

58. Guthrie, J. P.; Gallant, R. T., Thermodynamics of Methanesulfonic Acid Revisited. *Canadian Journal of Chemistry* **2000,** *78* (10), 1295-1298.

59. Bertrand, F.; Le Guyader, F.; Liguori, L.; Ouvry, G.; Quiclet-Sire, B.; Seguin, S.; Zard, S. Z., α-Scission of Sulfonyl Radicals: A Versatile Process for Organic Synthesis. *Comptes Rendus de l'Académie des Sciences - Series IIC - Chemistry* **2001,** *4* (7), 547-555.

60. Wang, X.; Ye, Y.; Zhang, S.; Feng, J.; Xu, Y.; Zhang, Y.; Wang, J., Copper-Catalyzed C(sp3)–C(sp3) Bond Formation Using a Hypervalent Iodine Reagent: An Efficient Allylic Trifluoromethylation. *Journal of the American Chemical Society* **2011,** *133* (41), 16410-16413.

61. Hamanoue, K.; Nakayama, T.; Kajiwara, Y.; Yamaguchi, T.; Teranishi, H., The Lowest Triplet States of Anthraquinone and Chloroanthraquinones: The 1-chloro, 2-chloro, 1,5-dichloro, and 1,8-dichloro Compounds. *The Journal of Chemical Physics* **1987,** *86* (12), 6654-6659.

62. van Ramesdonk, H. J.; Bakker, B. H.; Groeneveld, M. M.; Verhoeven, J. W.; Allen, B. D.; Rostron, J. P.; Harriman, A., Ultrafast Intersystem Crossing in 9,10-

Anthraquinones and Intramolecular Charge Separation in an Anthraquinone-Based Dyad. *The Journal of Physical Chemistry A* **2006,** *110* (49), 13145-13150.

63. Yamaji, M.; Itoh, T.; Tobita, S., Photochemical properties of the triplet π,π* state, anion and ketyl radicals of 5,12-naphthacenequinone in solution studied by laser flash photolysis: electron transfer and phenolic H-atom transfer. *Photochemical & Photobiological Sciences* **2002,** *1* (11), 869-876.

64. Choi, J. R.; Jeoung, S. C.; Cho, D. W., Two-Photon-Induced Excited-State Intramolecular Proton Transfer Process in 1-Hydroxyanthraquinone. *Chemical Physics Letters* **2004,** *385* (5), 384-388.

65. Cho, D. W.; Kim, S. H.; Yoon, M.; Jeoung, S. C., Transient Raman Spectroscopic Studies on the Excited-State Intramolecular Reverse Proton Transfer in 1-Hydroxyanthraquinone. *Chemical Physics Letters* **2004,** *391* (4), 314-320.

66. Sun, S.-m.; Zhang, S.; Liu, K.; Wang, Y.-p.; Zhou, M.-m.; Zhang, B., Excited State Intramolecular Proton Transfer of 1-Hydroxyanthraquinone. *Chinese Journal of Chemical Physics* **2015,** *28* (5), 545-551.

67. Jen, M.; Lee, S.; Jeon, K.; Hussain, S.; Pang, Y., Ultrafast Intramolecular Proton Transfer of Alizarin Investigated by Femtosecond Stimulated Raman Spectroscopy. *The Journal of Physical Chemistry B* **2017,** *121* (16), 4129-4136.

68. Yagci, Y.; Jockusch, S.; Turro, N. J., Photoinitiated Polymerization: Advances, Challenges, and Opportunities. *Macromolecules* **2010,** *43* (15), 6245-6260.

69. Chen, M.; Zhong, M.; Johnson, J. A., Light-Controlled Radical Polymerization: Mechanisms, Methods, and Applications. *Chemical Reviews* **2016,** *116* (17), 10167-10211.

70. Michaudel, Q.; Kottisch, V.; Fors, B. P., Cationic Polymerization: From Photoinitiation to Photocontrol. *Angewandte Chemie-International Edition* **2017,** *56* (33), 9670-9679.

71. Lai, H.; Zhang, J.; Xing, F.; Xiao, P., Recent Advances in Light-Regulated Non-Radical Polymerisations. *Chemical Society Reviews* **2020,** *49* (6), 1867-1886.

72. Chatani, S.; Kloxin, C. J.; Bowman, C. N., The Power of Light in Polymer Science: Photochemical Processes to Manipulate Polymer Formation, Structure, and Properties. *Polymer Chemistry* **2014,** *5* (7), 2187-2201.

73. Guy, N.; Giani, O.; Blanquer, S.; Pinaud, J.; Robin, J.-J., Photoinduced Ring-Opening Polymerizations. *Progress in Organic Coatings* **2021,** *153*, 106159.

74. Corrigan, N.; Yeow, J.; Judzewitsch, P.; Xu, J. T.; Boyer, C., Seeing the Light: Advancing Materials Chemistry through Photopolymerization. *Angewandte Chemie-International Edition* **2019,** *58* (16), 5170-5189.

75. Neilson, B. M.; Bielawski, C. W., Photoswitchable NHC-Promoted Ring-Ppening Polymerizations. *Chemical Communications* **2013,** *49* (48), 5453-5455.

76. Barker, I. A.; Dove, A. P., Triarylsulfonium Hexafluorophosphate Salts as Photoactivated Acidic Catalysts for Ring-Opening Polymerisation. *Chemical Communications* **2013,** *49* (12), 1205-1207.

77. Fu, C.; Xu, J.; Boyer, C., Photoacid-Mediated Ring Opening Polymerization Driven by Visible Light. *Chemical Communications* **2016,** *52* (44), 7126-7129.

78. Zhang, X.; Hu, S.; Ma, Q.; Liao, S., Visible Light-Mediated Ring-Opening Polymerization of Lactones Based on the Excited State Acidity of ESPT Molecules. *Polymer Chemistry* **2020,** *11* (22), 3709-3715.

79. Zhang, X.; Ma, Q.; Jiang, Y.; Hu, S.; Li, J.; Liao, S., Visible Light-Regulated Organocatalytic Ring-Opening Polymerization of Lactones by Harnessing Excited State Acidity. *Polymer Chemistry* **2021,** *12* (6), 885-892.

80. Zayas, M. S.; Dolinski, N. D.; Self, J. L.; Abdilla, A.; Hawker, C. J.; Bates, C. M.; Read de Alaniz, J., Tuning Merocyanine Photoacid Structure to Enhance Solubility and Temporal Control: Application in Ring Opening Polymerization. *ChemPhotoChem* **2019,** *3* (6), 467-472.

81. Xia, L.; Zhang, Z.; You, Y.-Z., Visible Light-Induced Living/Controlled Cationic Ring-Opening Polymerization of Lactones. *Polymer Journal* **2020,** *52* (12), 1323-1331.

82. Perrier, S., 50th Anniversary Perspective: RAFT Polymerization—A User Guide. *Macromolecules* **2017,** *50* (19), 7433-7447.

83. Hill, M. R.; Carmean, R. N.; Sumerlin, B. S., Expanding the Scope of RAFT Polymerization: Recent Advances and New Horizons. *Macromolecules* **2015,** *48* (16), 5459-5469.

84. Otsu, T.; Yoshida, M., Role of Initiator-Transfer Agent-Terminator (Iniferter) in Radical Polymerizations: Polymer Design by Organic Disulfides as Iniferters. *Die Makromolekulare Chemie, Rapid Communications* **1982,** *3* (2), 127-132.

85. Xu, J.; Jung, K.; Atme, A.; Shanmugam, S.; Boyer, C., A Robust and Versatile Photoinduced Living Polymerization of Conjugated and Unconjugated Monomers and Its Oxygen Tolerance. *Journal of the American Chemical Society* **2014,** *136* (14), 5508-5519.

86. Xu, J.; Jung, K.; Boyer, C., Oxygen Tolerance Study of Photoinduced Electron Transfer–Reversible Addition–Fragmentation Chain Transfer (PET-RAFT) Polymerization Mediated by Ru(bpy)3Cl2. *Macromolecules* **2014,** *47* (13), 4217-4229.

87. Xu, J. T.; Shanmugam, S.; Duong, H. T.; Boyer, C., Organo-Photocatalysts for Photoinduced Electron Transfer-Reversible Addition-Fragmentation Chain Transfer (PET-RAFT) Polymerization. *Polymer Chemistry* **2015,** *6* (31), 5615-5624.

88. Shanmugam, S.; Xu, J.; Boyer, C., Utilizing the Electron Transfer Mechanism of Chlorophyll a Under Light for Controlled Radical Polymerization. *Chemical Science* **2015,** *6* (2), 1341-1349.

89. Lee, I.-H.; Discekici, E. H.; Anastasaki, A.; de Alaniz, J. R.; Hawker, C. J., Controlled Radical Polymerization of Vinyl Ketones Using Visible Light. *Polymer Chemistry* **2017,** *8* (21), 3351-3356.

90. Quinn, J. F.; Barner, L.; Barner-Kowollik, C.; Rizzardo, E.; Davis, T. P., Reversible Addition−Fragmentation Chain Transfer Polymerization Initiated with Ultraviolet Radiation. *Macromolecules* **2002,** *35* (20), 7620-7627.

91. Corrigan, N.; Xu, J.; Boyer, C., A Photoinitiation System for Conventional and Controlled Radical Polymerization at Visible and NIR Wavelengths. *Macromolecules* **2016,** *49* (9), 3274-3285.

92. Thum, M. D.; Hong, D.; Zeppuhar, A. N.; Falvey, D. E., Visible-Light Photocatalytic Oxidation of DMSO for RAFT Polymerization. *Photochemistry and Photobiology* **2021** https://doi.org/10.1111/php.13468

93. Kishore, K.; Asmus, K.-D., Radical Cations from One-Electron Oxidation of Aliphatic Sulphoxides in Aqueous Solution. A Radiation Chemical Study. *Journal of the Chemical Society, Perkin Transactions 2* **1989,** (12), 2079-2084.

94. Crean, C.; Geacintov, N. E.; Shafirovich, V., Methylation of 2′-Deoxyguanosine by a Free Radical Mechanism. *The Journal of Physical Chemistry B* **2009,** *113* (38), 12773-12781.

95. Serpa, C.; Arnaut, L. G., Does Molecular Size Matter in Photoinduced Electron Transfer Reactions? *The Journal of Physical Chemistry A* **2000,** *104* (47), 11075-11086.

96. Görner, H., Photoreactions of p-Quinones with Dimethyl Sulfide and Dimethyl Sulfoxide in Aqueous Acetonitrile. *Photochemistry and Photobiology* **2006,** *82* (1), 71-77.

97. Zeppuhar, A. N.; Hill-Byrne, K.; Falvey, D. E., Mechanism of the Photorelease of Alcohols from the 9-Phenyl-9-tritylone Protecting Group. *Photochemical & Photobiological Sciences* **2019,** *18* (8), 1990-1995.

98. Greene, T. W.; Wuts, P. G. M., *Protective Groups in Organic Synthesis*. 3rd ed.; Wiley: New York, 1999; p xxi, 779 p.

99. Bochet, C. G., Photolabile Protecting Groups and Linkers. *Journal of the Chemical Society, Perkin Transactions 1* **2002,** (2), 125-142.

100. Pelliccioli, A. P.; Wirz, J., Photoremovable Protecting Groups: Reaction Mechanisms and Applications. *Photochemical & Photobiological Sciences* **2002,** *1* (7), 441-458.

101. Klán, P.; Šolomek, T.; Bochet, C. G.; Blanc, A.; Givens, R.; Rubina, M.; Popik, V.; Kostikov, A.; Wirz, J., Photoremovable Protecting Groups in Chemistry and Biology: Reaction Mechanisms and Efficacy. *Chemical Reviews* **2013,** *113* (1), 119-191.

102. Sun, Y.; Yan, Y.; Wang, M.; Chen, C.; Xu, H.; Lu, J. R., Controlled Release of Hydrophilic Guest Molecules from Photoresponsive Nucleolipid Vesicles. *ACS Applied Materials & Interfaces* **2013,** *5* (13), 6232-6236.

103. Jana, A.; Nguyen, K. T.; Li, X.; Zhu, P.; Tan, N. S.; Ågren, H.; Zhao, Y., Perylene-Derived Single-Component Organic Nanoparticles with Tunable Emission: Efficient Anticancer Drug Carriers with Real-Time Monitoring of Drug Release. *ACS Nano* **2014,** *8* (6), 5939-5952.

104. Venkatesh, Y.; Rajesh, Y.; Karthik, S.; Chetan, A. C.; Mandal, M.; Jana, A.; Singh, N. D. P., Photocaging of Single and Dual (Similar or Different) Carboxylic and Amino Acids by Acetyl Carbazole and its Application as Dual Drug Delivery in Cancer Therapy. *The Journal of Organic Chemistry* **2016,** *81* (22), 11168-11175.

105. Zhao, H.; Sterner, E. S.; Coughlin, E. B.; Theato, P., o-Nitrobenzyl Alcohol Derivatives: Opportunities in Polymer and Materials Science. *Macromolecules* **2012,** *45* (4), 1723-1736.

106. El Zubir, O.; Xia, S. J.; Ducker, R. E.; Wang, L.; Mullin, N.; Cartron, M. L.; Cadby, A. J.; Hobbs, J. K.; Hunter, C. N.; Leggett, G. J., From Monochrome to Technicolor: Simple Generic Approaches to Multicomponent Protein Nanopatterning Using Siloxanes with Photoremovable Protein-Resistant Protecting Groups. *Langmuir* **2017,** *33* (35), 8829-8837.

107. Parasar, B.; Chang, P. V., Chemical Optogenetic Modulation of Inflammation and Immunity. *Chemical Science* **2017,** *8* (2), 1450-1453.

108. Barltrop, J.; Plant, P.; Schofield, P., Photosensitive Protective Groups. *Chemical Communications (London)* **1966,** (22), 822-823.

109. Barth, A.; Hauser, K.; Maentele, W.; Corrie, J. E.; Trentham, D. R., Photochemical Release of ATP From" Caged ATP" Studied by Time-Resolved Infrared Spectroscopy. *Journal of the American Chemical Society* **1995,** *117* (41), 10311-10316.

110. Il'ichev, Y. V.; Schwörer, M. A.; Wirz, J., Photochemical Reaction Mechanisms of 2-Nitrobenzyl Compounds: Methyl Ethers and Caged ATP. *Journal of the American Chemical Society* **2004,** *126* (14), 4581-4595.

111. Givens, R. S.; Matuszewski, B., Photochemistry of Phosphate Esters: An Efficient Method for the Generation of Electrophiles. *Journal of the American Chemical Society* **1984,** *106* (22), 6860-6861.

112. Schade, B.; Hagen, V.; Schmidt, R.; Herbrich, R.; Krause, E.; Eckardt, T.; Bendig, J., Deactivation Behavior and Excited-State Properties of (Coumarin-4-yl)methyl Derivatives. 1. Photocleavage of (7-Methoxycoumarin-4-yl)methyl-Caged Acids with Fluorescence Enhancement. *The Journal of Organic Chemistry* **1999,** *64* (25), 9109-9117.

113. Givens, R. S.; Rubina, M.; Wirz, J., Applications of p-hydroxyphenacyl (pHP) and Coumarin-4-ylmethyl Photoremovable Protecting Groups. *Photochemical & Photobiological Sciences* **2012,** *11* (3), 472-488.

114. Sheehan, J. C.; Umezawa, K., Phenacyl Photosensitive Blocking Groups. *The Journal of Organic Chemistry* **1973,** *38* (21), 3771-3774.

115. Givens, R. S.; Park, C.-H., p-Hydroxyphenacyl ATP1: A New Phototrigger. *Tetrahedron Letters* **1996,** *37* (35), 6259-6262.

116. Jagadesan, P.; Da Silva, J. P.; Givens, R. S.; Ramamurthy, V., Photorelease of Incarcerated Guests in Aqueous Solution with Phenacyl Esters as the Trigger. *Organic Letters* **2015,** *17* (5), 1276-1279.

117. Suzuki, A. Z.; Watanabe, T.; Kawamoto, M.; Nishiyama, K.; Yamashita, H.; Ishii, M.; Iwamura, M.; Furuta, T., Coumarin-4-ylmethoxycarbonyls as Phototriggers for Alcohols and Phenols. *Organic Letters* **2003,** *5* (25), 4867-4870.

118. Hagen, V.; Kilic, F.; Schaal, J.; Dekowski, B.; Schmidt, R.; Kotzur, N., [8-[Bis(carboxymethyl)aminomethyl]-6-bromo-7-hydroxycoumarin-4-yl]methyl Moieties as Photoremovable Protecting Groups for Compounds with COOH, NH2, OH, and C═O Functions. *The Journal of Organic Chemistry* **2010,** *75* (9), 2790-2797.

119. Li, H.; Yang, J.; Porter, N. A., Preparation and Photochemistry of o-Aminocinnamates. *Journal of Photochemistry and Photobiology A: Chemistry* **2005,** *169* (3), 289-297.

120. Duan, X.-Y.; Zhai, B.-C.; Song, Q.-H., Water-Soluble o-Hydroxycinnamate as an Efficient Photoremovable Protecting Group of Alcohols with Fluorescence Reporting. *Photochemical & Photobiological Sciences* **2012,** *11* (3), 593-598.

121. Walton, D. P.; Dougherty, D. A., A General Strategy for Visible-Light Decaging Based on the Quinone Trimethyl Lock. *Journal of the American Chemical Society* **2017,** *139* (13), 4655-4658.

122. Zhou, L.; Yang, H.; Wang, P., Development of Trityl-Based Photolabile Hydroxyl Protecting Groups. *The Journal of Organic Chemistry* **2011,** *76* (15), 5873-5881.

123. Denning, D. M.; Pedowitz, N. J.; Thum, M. D.; Falvey, D. E., Uncaging Alcohols Using UV or Visible Light Photoinduced Electron Transfer to 9-Phenyl-9-tritylone Ethers. *Organic Letters* **2015,** *17* (24), 5986-5989.

124. Barnett, W. E.; Needham, L. L., The Tritylone Protecting Group: Ether Cleavage by Wolff–Kishner Reduction. *Journal of the Chemical Society D: Chemical Communications* **1971,** (3), 170-171.

125. Barnett, W. E.; Needham, L. L.; Powell, R. W., Tritylone Ethers: Cleavage, Stability and Selectivity of Formation. *Tetrahedron* **1972,** *28* (3), 419-424.

126. van der Stouwe, C.; Schäfer, H. J., Cathodic Cleavage of the Tritylone Group from Protected Alcohols Selective Protection of the Primary or Secondary Hydroxyl group in 1,4-Pentane Diol. *Tetrahedron Letters* **1979,** *20* (28), 2643-2646.

127. Ervin, K. M.; DeTuri, V. F., Anchoring the Gas-Phase Acidity Scale. *The Journal of Physical Chemistry A* **2002,** *106* (42), 9947-9956.

128. Kanabus-Kaminska, J.; Gilbert, B.; Griller, D., Solvent Effects on the Thermochemistry of Free-Radical Reactions. *Journal of the American Chemical Society* **1989,** *111* (9), 3311-3314.

129. Berkowitz, J.; Ellison, G. B.; Gutman, D., Three Methods to Measure RH Bond Energies. *The Journal of Physical Chemistry* **1994,** *98* (11), 2744-2765.

130. Buettner, A. V.; Dedinas, J., Photoreduction of Benzophenone in Benzene. II. Flash Photolysis Study of Primary Photochemical Reactions. *The Journal of Physical Chemistry* **1971,** *75* (2), 187-191.

131. Beckett, A.; Porter, G., Primary Photochemical Processes in Aromatic Molecules. Part 9.-Photochemistry of Benzophenone in Solution. *Transactions of the Faraday Society* **1963,** *59* (0), 2038-2050.

132. Timpe, H. J.; Kronfeld, K. P., Light-Induced Polymer and Polymerization Reactions XXXIII: Direct Photoinitiation of Methyl Methacrylate Polymerization by Excited States of Ketones. *Journal of Photochemistry and Photobiology A: Chemistry* **1989,** *46* (2), 253-267.

133. Hammond, G. S.; Moore, W. M., The Role of a Triplet State in the Photoreduction of Benzophenone. *Journal of the American Chemical Society* **1959,** *81* (23), 6334-6334.

134. Land, E.; Porter, G.; Strachan, E., Primary Photochemical Processes in Aromatic Molecules. Part 6.—The Absorption Spectra and Acidity Constants of Phenoxyl Radicals. *Transactions of the Faraday Society* **1961,** *57*, 1885-1893.

135. Falvey, D. E., Nitrenium Ions. In *Reactive Intermediate Chemistry*, Moss, R. A.; Platz, M. S.; Jones Jr., M., Eds. 2003; pp 593-650.

136. Falvey, D. E., Singlet and Triplet States in the Reactions of Nitrenium Ions. *Journal of Physical Organic Chemistry* **1999,** *12* (8), 589-596.

137. Falvey, D. E., Electronic Properties of Nitrenium Ions. In *Nitrenes and Nitrenium Ions*, Falvey, D. E.; Gudmundsdottir, A. D., Eds. 2013; pp 191-216.

138. Novak, M.; Zhang, Y., Chapter Three - Antitumor Drugs and Nitrenium Ions. In *Advances in Physical Organic Chemistry*, Williams, I. H.; Williams, N. H., Eds. Academic Press: 2012; Vol. 46, pp 121-164.

139. McClelland, R. A., Flash Photolysis Generation and Reactivities of Carbenium Ions and Nitrenium Ions. *Tetrahedron* **1996,** *52* (20), 6823-6858.

140. Dipple, A., DNA Adducts of Chemical Carcinogens. *Carcinogenesis* **1995,** *16* (3), 437-441.

141. McClelland, R. A.; Davidse, P. A.; Hadzialic, G., Electron-Deficient Strong Bases. Generation of the 4-Biphenylyl- and 2-Fluorenylnitrenium Ions by Nitrene Protonation in Water. *Journal of the American Chemical Society* **1995,** *117* (14), 4173-4174.

142. McClelland, R. A.; Gadosy, T. A.; Ren, D., 1997 Alfred Bader Award Lecture Reactivities of Arylnitrenium Ions with Guanine Derivatives and Other Nucleophiles. *Canadian Journal of Chemistry* **1998,** *76* (10), 1327-1337.

143. Humphreys, W. G.; Kadlubar, F. F.; Guengerich, F. P., Mechanism of C8 Alkylation of Guanine Residues by Activated Arylamines: Evidence for Initial Adduct Formation at the N7 Position. *Proceedings of the National Academy of Sciences* **1992,** *89* (17), 8278.

144. Kennedy, S. A.; Novak, M.; Kolb, B. A., Reactions of Ester Derivatives of Carcinogenic N-(4-Biphenylyl)hydroxylamine and the Corresponding Hydroxamic Acid with Purine Nucleosides. *Journal of the American Chemical Society* **1997,** *119* (33), 7654-7664.

145. McClelland, R. A.; Ahmad, A.; Dicks, A. P.; Licence, V. E., Spectroscopic Characterization of the Initial C8 Intermediate in the Reaction of the 2-Fluorenylnitrenium Ion with 2‘-Deoxyguanosine. *Journal of the American Chemical Society* **1999,** *121* (14), 3303-3310.

146. Thomas, S. I.; Falvey, D. E., N,N-Di(4-halophenyl)nitrenium Ions: Nucleophilic Trapping, Aromatic Substitution, and Hydrogen Atom Transfer. *The Journal of Organic Chemistry* **2007,** *72* (13), 4626-4634.

147. Moran, R. J.; Falvey, D. E., Photogenerated Diarylnitrenium Ions: Laser Flash Photolysis and Product Studies on Diphenylnitrenium Ion Generated from Photolysis of 1-(N,N-Diphenylamino)pyridinium Ions. *Journal of the American Chemical Society* **1996,** *118* (37), 8965-8966.

148. Du, L.; Yan, Z.; Zhu, Z.; Cheng, S.-C.; Zhang, Y.; Li, X.; Tang, W.; Phillips, D. L., Time-Resolved Spectroscopic Observation of Diphenylnitrenium Ion Reactions with Guanosine. *The Journal of Organic Chemistry* **2020,** *85* (14), 8792-8797.

149. Zeppuhar, A. N.; Falvey, D. E., Generation of N,N-Di(4-bromophenyl)nitrenium Ion under Acidic Conditions: Search for a Nitrenium Dication. *The Journal of Organic Chemistry* **2020,** *85* (14), 8844-8850.

150. McClelland, R. A.; Kahley, M. J.; Davidse, P. A.; Hadzialic, G., Acid−Base Properties of Arylnitrenium Ions. *Journal of the American Chemical Society* **1996,** *118* (20), 4794-4803.

151. Du, L.; Yan, Z.; Bai, X.; Liang, R.; Phillips, D. L., Time-Resolved Spectroscopic Study of N,N –Di(4–bromo)nitrenium Ions in Acidic Aqueous Solution. *International Journal of Molecular Sciences* **2019,** *20* (21), 5512.

152. Wagner, B. D.; Ruel, G.; Lusztyk, J., Absolute Kinetics of Aminium Radical Reactions with Olefins in Acetonitrile Solution1. *Journal of the American Chemical Society* **1996,** *118* (1), 13-19.

153. Zhao, Y.; Truhlar, D. G., Applications and Validations of the Minnesota Density Functionals. *Chemical Physics Letters* **2011,** *502* (1), 1-13.

154. Krishnan, R.; Binkley, J. S.; Seeger, R.; Pople, J. A., Self-Consistent Molecular Orbital Methods. XX. A Basis Set for Correlated Wave Functions. *The Journal of Chemical Physics* **1980,** *72* (1), 650-654.

155. Bordwell, F. G.; Zhang, X. M.; Cheng, J. P., Bond Dissociation Energies of the Nitrogen-Hydrogen Bonds in Anilines and in the Corresponding Radical Anions. Equilibrium Acidities of Aniline Radical Cations. *The Journal of Organic Chemistry* **1993,** *58* (23), 6410-6416.

156. Zweig, A.; Lancaster, J. E.; Neglia, M. T.; Jura, W. H., Cumulative Influence of Dimethylamino Groups on the -System Properties of Aromatic Hydrocarbons. *Journal of the American Chemical Society* **1964,** *86* (19), 4130-4136.

157. Shida, T., *Electronic Absorption Spectra of Radical Ions*. Elsevier: 1988.

158. Fickling, M. M.; Fischer, A.; Mann, B. R.; Packer, J.; Vaughan, J., Hammett Substituent Constants for Electron-Withdrawing Substituents: Dissociation of Phenols, Anilinium Ions and Dimethylanilinium Ions. *Journal of the American Chemical Society* **1959,** *81* (16), 4226-4230.

159. Zweig, A.; Hodgson, W. G.; Jura, W. H., The Oxidation of Methoxybenzenes. *Journal of the American Chemical Society* **1964,** *86* (19), 4124-4129.

160. Wymann, W. E.; Davis, R.; Patterson, J. W.; Pfister, J. R., Selective Alkylations of Certain Phenolic and Enolic Functions with Lithium Carbonate/Alkyl Halide. *Synthetic Communications* **1988,** *18* (12), 1379-1384.

161. Melliou, E.; Magiatis, P.; Mitaku, S.; Skaltsounis, A.-L.; Pierré, A.; Atassi, G.; Renard, P., 2,2-Dimethyl-2H-anthra[2,3-b]pyran-6,11-diones: a new class of cytotoxic compounds. *Bioorganic & Medicinal Chemistry* **2001,** *9* (3), 607-612.

162. Cañeque, T.; Gomes, F.; Mai, T. T.; Blanchard, F.; Retailleau, P.; Gallard, J.-F.; Maestri, G.; Malacria, M.; Rodriguez, R., A Synthetic Study towards the Marmycins and Analogues. *Synthesis* **2017,** *49* (03), 587-592.

163. Zielske, A. G., (Tosyloxy) anthraquinones. Versatile synthons for the preparation of various aminoanthraquinones. *The Journal of Organic Chemistry* **1987,** *52* (7), 1305-1309.

164. Tamura, Y.; Sasho, M.; Nakagawa, K.; Tsugoshi, T.; Kita, Y., Strong Base Induced Cycloaddition of Homophthalic Anhydrides Leading to peri-Hydroxy Polycyclic Compounds. *The Journal of Organic Chemistry* **1984,** *49* (3), 473-478.

165. Park, I. S.; Heo, E.; Nam, Y.-S.; Lee, C. W.; Kim, J.-M., Colorimetric detection of aliphatic primary amines and a molecular logic gate based on a photochromic phenoxyquinone derivative. *Journal of Photochemistry and Photobiology A: Chemistry* **2012,** *238*, 1-6.

166. Perkin, A. G.; Storey, R. C., XXXIV.—The Migration of the Acyl Group in Partly Acylated Phenolic Compounds. Part I. *Journal of the Chemical Society (Resumed)* **1928,** (0), 229-244.

167. Luo, Y. R., *Comprehensive Handbook of Chemical Bond Energies*. CRC Press: 2007.

168. Murov, S. L.; Hug, G. L.; Carmichael, I., *Handbook of photochemistry*. 2nd ed.; M. Dekker: New York, 1993; p viii, 420 p.

169. Gronowska, J.; Miecznik, P., New method of separation of hydroxydiphenylphthalide isomers from their reaction mixture. *Pol. J. Chem.* **1987,** *61* (4-6), 621-2.

170. Gronowska, J.; Dzielendziak, A.; Heldt, J., 9-Acetoxyanthracene derivatives. Part IX. Syntheses and spectral investigations of 9-acetoxy-10-(acetoxyhalogenophenyl)anthracenes. *Acta Phys. Chem.* **1983,** *29* (3-4), 145-56.

171. Blicke, F. F.; Warzynski, R. J., Hydroxy- and Methoxyphenylanthrones. III1. *Journal of the American Chemical Society* **1940,** *62* (11), 3191-3194.